Asymmetric Random Average Processes

vorgelegt von

Frank H. Zielen

aus Oelde

Köln 2002

Abstract. In the present work the asymmetric random average process (ARAP) is considered. This nonequilibrium model is defined on a one-dimensional periodic lattice and equipped with a stochastic nearest neighbour interaction. Its characteristics are continuous and unbounded state variables called masses. The local dynamics is given by asymmetric shifts of mass fragments whereby the transferred mass fragments are determined by an arbitrary probability density function ϕ called fraction density.

We start with a formal definition of the ARAP and show that a lot of stochastic models can be formulated in terms of the ARAP by using suitable fraction densities.

Focused on the ARAP with uniform ϕ-function exact solutions are derived by applying the matrix product ansatz for stochastic processes. We restrict to parallel dynamics, but allow for continuous and discrete masses. In case of continuous state variables we obtain a new kind of matrix algebra given by a functional equation.

Furthermore, we determine analytically the complete set of ARAPs with exact product measure solutions. Here we restrict to state-independent fraction densities. Our results are derived for systems with parallel dynamics of arbitrary system size and adopted to continuous time dynamics. In addition, we establish the connection to the q-model of granular media and present an approximation method for arbitrary state-independent fraction densities.

Finally, a simple truncated ARAP is introduced and studied. Here the transferred mass is restricted by a cutoff. We investigate this model by Monte-Carlo simulations, supplemented by analytical approximations. The phase diagram is derived, featuring a regime of broken ergodicity: the system can either be in a homogeneous high flow phase or in a phase characterized by an infinite aggregate, i.e. a finite fraction of the total mass resides on one lattice site. This phenomenon is very similar to BOSE-EINSTEIN condensation. Furthermore, the deep relation with the KRAUSS traffic model is clarified. We conclude with a comprehensive comparison to other models showing similar effects to emphasize the general relevance of the ARAP.

Contents

1. Introduction

The study of nonequilibrium systems has become an attractive and important research field in modern statistical physics. A lot of interdisciplinary problems are based on nonequilibrium processes, e.g. biological mechanism of protein synthesis, traffic flow theory, diffusion in polymer networks or interface growth. But also traditional physical applications like spin glass relaxations or dissipative transport in thin superconducting wires may obey nonequilibrium dynamics.

In case of equilibrium systems we deal with a well-elaborated theory, valid for both classical and quantum systems. For any kind of ensemble the probability distribution of configurations, namely the BOLTZMANN weight, can be calculated as long as we are equipped with an energy function or hermitian Hamiltonian. However, nonequilibrium systems lack of hermitian Hamiltonians and are generally defined by microscopic dynamics instead. This does not mean that nonequilibrium processes violate NEWTON's or quantum mechanics, but due to missing information about the underlying physics nonequilibrium dynamics are often defined phenomenologically, less restrictive and random based.

Basically one can consider two types of nonequilibrium systems: those relaxing towards thermal equilibrium and those held far from thermal equilibrium, e.g. by an external field. In this work we focus on the latter one. They are given by microscopic dynamics that do not obey the detailed balance condition.[1]

On the one hand, nonequilibrium physics has achieved recent success over the last decades. By introduction of the asymmetric simple exclusion process (ASEP) somewhat like a flexible standard model has been established, even relevant for some applications. Many results and techniques of equilibrium theory, in particular from quantum spin chains, have been adopted like BETHE ansatz, matrix product ansatz or simply the DIRAC notation in the so-called quantum formalism for stochastic systems.

On the other hand, the theory of systems far from equilibrium is still far from completion. This is based mainly on the fact that nonequilibrium systems are less restrictive than equilibrium models of equal dimension. Correspondingly their spectrum of phenomena is richer and principles of equilibrium theory have to be revised or extended,

---

[1]Systems relaxing towards thermal equilibrium are equipped with dynamics obeying the detailed balance condition. One starts with an initial state far from equilibrium and tracks their way towards the (equilibrium) steady state.

e.g. the definitions of phase transitions or universality. In addition, due to the interdisciplinary relevance various applications are associated with nonequilibrium physics and every application comes along with its individual nonequilibrium model.

The bulk of nonequilibrium processes is based on the ASEP and corresponds to driven lattice gases or extended reaction-diffusion models. According to this, the models are defined on discrete space and equipped with discrete and bounded local state variables, e.g. in case of the ASEP lattice sites can be vacant (0) or occupied (1).

In this work we would like to focus on a model that is also defined on a lattice but equipped with continuous and unbounded state variables, called masses. Besides we restrict to a stochastic nearest neighbour interaction given by an asymmetric shift of mass fragments which are determined by a probability density function ϕ. According to this, the model is called asymmetric random average process (ARAP).

We may define the model as general as possible by treating ϕ as an arbitrary function and thus deriving universal properties of the ARAP. In addition, we may focus on a fixed ϕ-function to work out special features of the ARAP that have not been discovered in discrete systems up to now. Both approaches deepen the understanding of nonequilibrium processes defined on continuous state space and in this thesis we will go further into both questions. The following paragraph provides a brief overview of the present work.

Chapter 2: We start with a formal and comprehensive definition of the ARAP including the master equations for discrete and continuous time. The ARAP with discrete state variables is embedded also. Furthermore, we give evidence that the ARAP represents an important subclass of driven nonequilibrium systems, i.e. we prove that a lot of stochastic models and applications can be formulated directly in terms of the ARAP. We conclude this chapter with a presentation of results that have been derived so far and that are relevant in the scope of this work.

Chapter 3: Here we adopt the matrix product technique to ARAPs with continuous and discrete masses. We focus on a uniform ϕ-function and parallel dynamics.

Chapter 4: In case of state-independent fraction densities ϕ we determine analytically the complete set of ARAPs with exact product measure solutions. We restrict on the infinite system with parallel update first and put our results down to finite systems and processes with random sequential dynamics. Furthermore, we consider some simple models explicitly and establish the connection to the q-model of granular media. Finally, we present an approximation method for arbitrary state-independent fraction densities.

Chapter 5: Motivated by road and Internet traffic we introduce several ARAPs with bounded dynamics whereby we focus mainly on a variant called the truncated ARAP (TARAP). Here the transferred mass is restricted by a cutoff. We investigate this model by Monte-Carlo simulations, supplemented by analytical approximations. The phase diagram is derived showing a regime of twofoldly broken ergodicity: the system can either be in a homogeneous high flow phase or in a phase characterized by an infinite aggregate, i.e. a finite fraction of the total mass is kept on one lattice site. This phenomenon is very similar to BOSE-EINSTEIN condensation. Furthermore, we

clarify that the KRAUSS traffic model is strongly related with the TARAP and confirm some findings published recently in context of the KRAUSS model. We conclude with a comprehensive comparison including other models showing similar effects.

Summary and conclusions are presented in chapter 6, whereas the appendices hold advanced and detailed calculations not given in the main text.

2. Basics of the Asymmetric Random Average Process (ARAP)

In this chapter the asymmetric random average process (ARAP) is introduced. We start with a formal definition in section 2.1. After that related applications, mainly from the field of nonequilibrium physics, are given and formulated in terms of the ARAP (section 2.2). We conclude with an overview of the main results derived so far for this interesting stochastic model (section 2.3).

2.1. Definition of the ARAP

In the following section we would like to define a formalized framework of the asymmetric random average process that will be used in the forthcoming parts of this work. Additionally, some variants of the model are presented whereby we focus on versions studied in this or previous works. Introductions to the ARAP are also given in [1,2] and we will refer to this references whenever necessary.

2.1.1. Local Dynamics and Fraction Density ϕ

The ARAP is defined on a one-dimensional (1D) periodic lattice with L sites. Each site i carries a state variable $m_i \in S$ called mass. In the following we distinguish the continuous ARAP and the discrete ARAP defined by $S = \mathbb{R}_0^+$ and $S = \mathbb{N}_0$, respectively. Remember as a common fundamental property of both cases that the local configuration space S is (in principle) unbounded, although it can be explicitly limited which is studied in chapter 5.

The basic ingredient of the dynamics is a local, asymmetric mass transport acting on two adjacent sites i and $i+1$. A random number $r_i \in [0,1]$ is generated from a time- and site-independent probability density function (pdf) ϕ, sometimes called fraction density. This fraction r_i determines the amount of mass $\Delta_i \equiv r_i m_i$ transported from site i to site $i+1$ (here ϕ must ensure $\Delta_i \in S$ which is only important for the discrete ARAP). The transport is completely asymmetric, i.e. no mass moves in the opposite direction $i+1 \rightarrow i$, and we obtain the local update

$$m_{i,i+1} \rightarrow t(r_i)m_{i,i+1} \tag{2.1}$$

with[1] $m_{i,i+1} \equiv (m_i, m_{i+1})$ and the local transfer matrix

$$t(r_i) = \begin{pmatrix} 1 - r_i & 0 \\ r_i & 1 \end{pmatrix} . \tag{2.2}$$

This update conserves mass (columns of t add up to one) and so the total mass $M = \sum_i m_i$ and the density $\rho \equiv \frac{M}{L}$ are fixed quantities. The thermodynamic limit is defined as $M, L \to \infty$ with $\rho = const.$

The free choice of the fraction density ϕ allows the ARAP to be adopted to a variety of problems. Here we restrict ourselves to site-independent densities which ensures (a formal) translational invariance of the dynamics (although it is possible to break this symmetry, see section 5.3.2). In addition, we focus on time-independent pdfs. On the one hand, this simplifies an analytical treatment, on the other hand, most of the applications are based on time-independent densities (see also next section).

In the following we would like to divide the set of ϕ-functions into three groups:

❏ state-independent pdfs $\phi = \phi(r_i)$,

❏ ultralocal state-dependent pdfs $\phi = \phi(r_i, m_i)$ (here m_i is the mass of the site that is broken off) and

❏ local state-dependent pdfs $\phi = \phi(r_i, m_{i-l}, \ldots, m_{i+r})$ with finite boundaries l and r and interaction range $l + r + 1$.

Without loss of generality we assume ϕ-functions to be normalized, i.e.

$$\int_0^1 dr_i \, \phi(r_i, m) = 1 \tag{2.3}$$

for all $m \in S^{\otimes L}$.[2] Sometimes it is more useful to describe the transfer dynamics in terms of absolute shifts Δ_i instead of mass fractions r_i. According to this, we obtain the fragment density

$$f(\Delta_i, m) \equiv \frac{1}{m_i} \phi \left(\frac{\Delta_i}{m_i}, m \right) . \tag{2.4}$$

being normalized on $[0, m_i]$. So f gives the probability density of breaking the mass Δ_i from a stick with height m_i. From (2.3) and (2.4) follows that there are no state-independent fragment densities.

For discrete ARAPs the formalism of fragment densities fits better than the use of fraction densities because there is a built-in unit mass scale missing in the continuous case. Furthermore, state-independent fraction densities do not exist here which is based on the impossibility of finding a non-trivial solution of the normalization conditions

---

[1]We do not distinguish between row and column vectors explicitly.
[2]We use the most general notation $\phi(r_i, m)$ including all kind of fraction densities.

$\sum_{\Delta_i=0}^{m_i} \phi\left(\Delta_i/m_i\right) = 1$ and $\phi(0) = 1$ $(m_i = 0)$ that have to be valid for all $m_i \in \mathbb{N}$. Nevertheless, we can embed the discrete ARAP $\phi^{(\mathrm{d})}$ into the framework of the continuous ARAP $\phi^{(\mathrm{c})}$ by using the relation

$$\phi^{(\mathrm{c})}(r_i, m) = \sum_{\Delta_i=0}^{m_i} \phi^{(\mathrm{d})}(r_i, m)\, \delta\left(r_i - \frac{\Delta_i}{m_i}\right)\ . \tag{2.5}$$

For compactness we introduce the probability measure $\mathrm{d}\psi \equiv \phi\mathrm{d}r_i$. Here ψ is the fraction distribution connected to the fraction density ϕ by $\psi(r_i, m) = \int_0^{r_i} \mathrm{d}r'\phi(r', m)$.[3] In this work we give the same meaning to the terms 'distribution' and 'density' although they represent different objects in a strict mathematical context.

Finally, we would like to mention that the local dynamics is defined slightly different in $[1,2]$ where the ϕ-function merely determines the fraction to transfer. There exists a further parameter p reflecting the probability for executing the shift. However, this external jump rate p can simply be incorporated into the fraction density using $\phi(r_i) \rightarrow p\phi(r_i) + (1-p)\delta(r_i)$.

2.1.2. Update Procedures

The dynamics is completed by the kind of update rules used to evaluate the system over time. In this work we focus mainly on two kinds of updates, the parallel update and the random sequential update.

The parallel update is discrete in time and equipped with a well-defined timescale Δt. In every step $t \rightarrow t + \Delta t$ a set of random numbers $r \equiv (r_1, \ldots, r_L)$ is generated and the local update (2.1) is applied simultaneously to all sites, i.e. all local updates are based on the configuration m at time t and we obtain

$$m_i \rightarrow (1 - r_i)m_i + r_{i-1}m_{i-1} \tag{2.6}$$

for all i. A graphical representation is given in figure 2.1.

For the infinite system $L \rightarrow \infty$ this update is equivalent to the so-called backward sequential update where one starts updating an arbitrary pair of sites $(i, i+1)$ and applies (2.1) moving from right to left under consideration of periodicity until reaching the initial pair. This identity will be used in chapter 3 to solve the ARAP by a matrix product ansatz. However, for finite L the backward sequential update differs from parallel dynamics because the last pair of sites $(i+1, i+2)$ to be updated holds the site $i+1$ that has been updated already. For completeness we also present the forward sequential update that is defined by applying (2.1) from left to right correspondingly, but this kind of dynamics is not related to parallel dynamics and represents an update of its own (because every local update influences the next one). For simplicity we set $\Delta t = 1$ from now on whenever possible.

---

[3]We assume ϕ to be integrable.
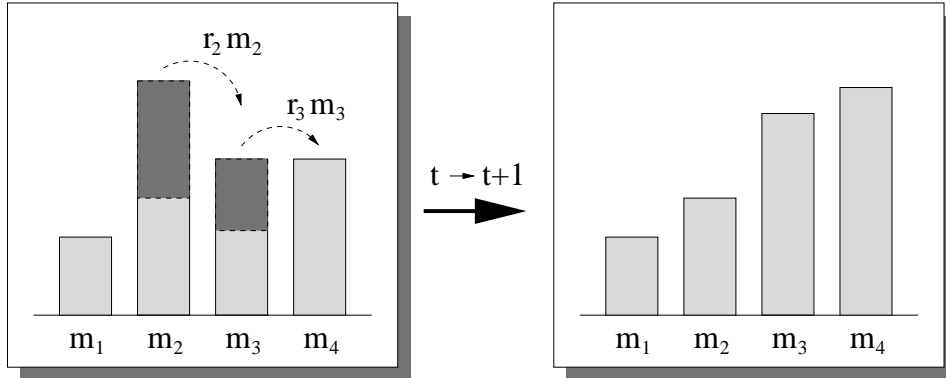
Figure 2.1.: Mass representation of the ARAP with parallel dynamics. The height of a mass stick corresponds to m_i. The fragments $r_i m_i$ are shaded.

For the random sequential update we choose a pair of sites randomly (with uniform probability L^{-1}), apply (2.1) and repeat the procedure. This update corresponds to a continuous time dynamics with t real valued as we will see in subsection 2.1.4 where an interpolation between the continuous time ARAP and the parallel ARAP is presented.

2.1.3. Master Equation for Parallel Dynamics

Now the ARAP is written in terms of the so-called quantum formalism for stochastic processes, e.g. used in [3]. We switch to this representation whenever useful. Furthermore, we restrict ourselves to the continuous ARAP first and deduce the discrete case afterwards.

The orthonormal state space $\mathcal{S}$ is spanned by the continuous ket basis $\{|m\rangle\}$ with configuration vectors $m \in S^{\otimes L}$ and equipped with the inner product $\langle m_1 | m_2 \rangle \equiv \delta(m_1 - m_2)$ (here δ represents the δ-function). Correspondingly states of the ARAP at time t are given by

$$|P(t)\rangle = \int_0^\infty \mathrm{d}^L m P(m, t) |m\rangle \tag{2.7}$$

whereby $\mathrm{d}^L m P(m, t)$ is a non-negative probability measure and the normalization

$$\langle s | P(t) \rangle = \int_0^\infty \mathrm{d}^L m P(m, t) = 1 \tag{2.8}$$

with $\langle s | \equiv \int_0^\infty \mathrm{d}^L m \langle m |$ holds.[4] Additionally, the abbreviated form $\int_I \mathrm{d}^n x \equiv \int_I \ldots \int_I \mathrm{d}^n x$ with $I \subset \mathbb{R}$ has been introduced.

So $P(m, t)$ gives the probability (density) of finding the system in the configuration m at time t and our main aim is to calculate the function P which corresponds to the

---

[4]The normalization (2.8) can be achieved due to probability conserving dynamics. According to this, the state space is concentrated to the surface of the unit ball $\langle s | P \rangle = 1$.

solution of the problem. Please note that we do not work with explicit time depending state variables $m(t)$ here which would lead to stochastic differential equations.

In case of the parallel update we obtain the following $t \to t + 1$ map of the basis:

$$|m\rangle \to T\,|m\rangle \equiv \int_0^1 \mathrm{d}^L r \phi(r, m)\,|T(r)m\rangle \qquad (2.9)$$

with $\phi(r, m) \equiv \prod_i \phi(r_i, m)$ and

$$T_{i,j}(r) = (1 - r_i)\delta_{i,j} + r_{i-1}\delta_{i-1,j}\,. \qquad (2.10)$$

Here $T(r)$ represents an $L \times L$ matrix with diagonal elements $1 - r_i$ and lower band entries r_i. Based on periodic boundary conditions the top right entry is also unequal to zero, i.e., $T_{1,L}(r) = r_L$. So $m \to T(r)m$ is the compact matrix formulation of (2.6). Note that $T(r)$ operates on the space of configuration vectors S, whereas T operates on the state space $\mathcal{S}$.

In the limit $L \to \infty$ the relation $T(r) = t(r_1)t(r_2)\ldots$ holds whereby the local transfer matrices $t(r_i)$ are embedded in the space of $T(r)$-operators, i.e.

$$t(r_i) \to 1 \otimes \ldots \otimes 1 \otimes t(r_i) \otimes \ldots\,. \qquad (2.11)$$

Here 1 is the unit operator acting on one site. In the following we assume all operators being embedded suitably without explicit mention. Note that adjacent local operators $t(r_i)$ and $t(r_{i+1})$ do not commute which implies difference of forward and backward sequential update. For completeness we give the definition of the operator T_i which performs a local update of the sites i and $i + 1$:

$$|m\rangle \to T_i\,|m\rangle \equiv \int_0^1 \mathrm{d}r_i \phi(r_i, m)\,|t(r_i)m\rangle \qquad (2.12)$$

Therefore, the associated transfer operators for forward and backward sequential update are $\ldots T_{i+1}T_iT_{i-1}\ldots$ resp. $\ldots T_{i-1}T_iT_{i+1}\ldots$.

Using (2.7),(2.9) and (2.10) we obtain

$$P(m', t + 1) = \langle m'\,|TP(t)\rangle = \int_0^\infty \mathrm{d}^L m \int_0^1 \mathrm{d}^L r\; \phi(r, m)\delta(m' - T(r)m)P(m, t)\,. \quad (2.13)$$

This is the master equation of the continuous ARAP with parallel update, the basis of all forthcoming calculations. The expression $\phi(r, m)\delta(m' - T(r)m)$ represents the transition probability density from state $|m\rangle$ into state $|m'\rangle$.

The L-dimensional δ-function can be rewritten using

$$\delta(m' - T(r)m) = |\det T(r)|^{-1}\,\delta(T^{-1}(r)m' - m) \qquad (2.14)$$

(easily derived by FOURIER-transformation) and we obtain an alternative representation of the master equation:

$$P(m', t+1) = \int_0^1 \mathrm{d}^L r \frac{\phi(r, T(r)^{-1} m')}{|\det T(r)|} P(T(r)^{-1} m', t) \ . \tag{2.15}$$

The master equation (2.13) simplifies even more by LAPLACE-transformation, exemplified in chapter 4.

2.1.4. Master Equation for Continuous Dynamics

Now we will formulate the corresponding master equation for continuous time dynamics which yields the SCHRÖDINGER-like master equation

$$\partial_t |P(t)\rangle = -H |P(t)\rangle \quad \text{with} \quad H = \sum_{i=1}^L h_i \ . \tag{2.16}$$

The local dynamics leads to a decomposition of H whereby h_i acts on site i and $i+1$. Furthermore, (2.16) misses a definite time scale (compared to the discrete time updates), i.e. $t \to \lambda t$ implies $H \to \lambda H$. This rescaling allows us to change from probabilities to rates in the "Hamiltonian" that do not have to be normalized.

The change of a state $|P(t)\rangle$ in time is given by the sum of win and loss terms because we deal with a MARKOV process on continuous time [4]. So the matrix representation

$$\langle m | -h_i | P(t)\rangle = \int_0^{m_{i+1}} \mathrm{d}\Delta \, f(\Delta, m(i, \Delta)) P(m(i, \Delta), t) - \int_0^{m_i} \mathrm{d}\Delta \, f(\Delta, m) P(m, t) \tag{2.17}$$

with

$$m(i, \Delta) \equiv (\dots, m_i + \Delta, m_{i+1} - \Delta, \dots) \tag{2.18}$$

is derived.[5] The second expression on the r.h.s. of (2.17) represents the ways of leaving the configuration m, while the first term consists of configurations that may end in m. Note that the normalization of the fragment density simplifies (2.17):

$$\langle m | -h_i | P(t)\rangle = \int_0^{m_{i+1}} \mathrm{d}\Delta \, f(\Delta, m(i, \Delta)) P(m(i, \Delta), t) - \langle m | P(t)\rangle \ . \tag{2.19}$$

Now we would like to present a formula that interpolates between parallel and random sequential update in case of state-independent ϕ-functions. For a given fraction density $\phi(r_i)$ we define the p-dependent function

$$\phi_p(r_i) = p\phi(r_i) + (1-p)\delta(r_i) \quad \text{with} \quad p \in [0, 1] \ . \tag{2.20}$$

---

[5]From now on we neglect the index of scalar vector components like Δ_i, r_i or m_i, if there is no risk of confusion with the associated vectors Δ, r or m. In general the integral measure indicates the dimensionality of the variables.

We use (2.20) with the discrete master equation (2.13) only. For $p = 1$ the parallel update is obtained and we will sketch that $p \to 0$ yields the case of continuous time.

For the complete ϕ-function we obtain

$$\phi_p(r) = \prod_i \delta(r_i) + p \sum_i [\phi(r_i) - \delta(r_i)] \prod_{j \neq i} \delta(r_j) + O(p^2) . \qquad (2.21)$$

Inserting (2.21) into (2.13) by using (2.10) and carefully evaluating all δ-functions, we finally achieve

$$P(m, t + \Delta t) = P(m, t) + p \sum_i \left[\int_0^{\frac{m_{i+1}}{m_i + m_{i+1}}} \mathrm{d}r \frac{\phi(r)}{1 - r} P\left(m\left(i, \frac{rm_i}{1 - r} \right), t \right) - P(m, t) \right] + O(p^2) .$$
$$(2.22)$$

Assuming $\Delta t = p$ and performing $p \to 0$ we get

$$\langle m \left| -h_i \right| P(t) \rangle = \int_0^{\frac{m_{i+1}}{m_i + m_{i+1}}} \mathrm{d}r \frac{\phi(r)}{1 - r} P\left(m\left(i, \frac{rm_i}{1 - r} \right), t \right) - P(m, t) . \qquad (2.23)$$

By the substitution $\Delta_i = \frac{rm_i}{1-r}$ and (2.4) the representation (2.19) is derived after all.

Thus, the random sequential update can be regarded as a special case of the parallel update. Instead of using the continuous time dynamics (2.19) we may apply the interpolated fraction density (2.20) to parallel dynamics and perform the limit $p \to 0$.

2.1.5. Master Equations of the Discrete ARAP

The next step is to derive the master equations for the discrete ARAP. This can easily be done by using (2.5) and the relation $P^{(c)}(m, t) = \sum_{\{m'\}} P^{(d)}(m', t) \delta(m - m')$.[6,7] Here $P^{(d)}(m, t)$ corresponds to the probability of finding the configuration m at time t in the discrete ARAP, embedded via $P^{(c)}$ into the continuous ARAP. Inserting in (2.13) we obtain for the parallel update

$$\sum_{\{m\}} P^{(d)}(m, t + 1) \delta(m - m') = \sum_{\{m\}} \sum_{\{\triangle\}}^m \phi^{(d)}(r, m) \delta(m' - T(r)m) P^{(d)}(m, t) \Big|_{r_i = \frac{\Delta_i}{m_i}} \quad (2.24)$$

with $\phi^{(d)}(r, m) = \prod_i \phi^{(d)}(r_i, m)$. Now applying the identity $\delta(x - ay) = \sum_z \delta(x - z) \delta_{z, ay}$ (with $x, y, ay \in \mathbb{N}_0^L$ and KRONECKER delta $\delta_{i,j}$) results in

$$P^{(d)}(m', t + 1) = \sum_{\{m\}} \sum_{\{\triangle\}}^m \phi^{(d)}(r, m) \delta_{m', T(r)m} P^{(d)}(m, t) \Big|_{r_i = \frac{\Delta_i}{m_i}} , \qquad (2.25)$$

---

[6] $\sum_{\{m\}} = \sum_{m_1=0}^{\infty} \cdots \sum_{m_L=0}^{\infty}$ and $\sum_{\{\triangle\}}^m = \sum_{\Delta_1=0}^{m_1} \cdots \sum_{\Delta_L=0}^{m_L}$

[7] Instead of embedding the discrete into the continuous state space, we could also work directly with the discrete space.

the discrete master equation for parallel update.[8]

According to (2.19) we derive the continuous time update for the discrete ARAP:

$$\partial_t P^{(\mathrm{d})}(m,t) = \sum_i \left[\sum_{\Delta=0}^{m_{i+1}} f^{(\mathrm{d})}\left(\Delta, m(i,\Delta)\right) P(m(i,\Delta),t) - P^{(\mathrm{d})}(m,t) \right] . \qquad (2.26)$$

Here the identity $f^{(\mathrm{d})}\left(\Delta_i, m\right) \equiv \phi^{(\mathrm{d})}(\frac{\Delta_i}{m_i}, m)$ has been used, obtained by evaluating (2.4) with (2.5).

2.1.6. Steady States

In the forthcoming parts of this work we will mainly focus on steady state dynamics, i.e. we look for time-independent solutions $|P\rangle$ of (2.13), (2.17), (2.25) and (2.26). This simplifies the corresponding master equations to eigenvalue problems: in case of parallel dynamics we obtain $|P\rangle = T\,|P\rangle$ while the continuous time equations read $H\,|P\rangle = 0$. For ergodic ARAPs, defined by dynamics that allow the the system to evolve from any given initial state to any final state in a finite time, the steady state is equal to the infinite time limit, so $|P\rangle = \lim_{t\to\infty} |P(t)\rangle$. This property enables us to measure steady state properties by long time Monte-Carlo simulations.

2.1.7. Variants

We finish this section by discussing possible extensions and variants of the ARAP that are not discussed in the present work:

❏ symmetric processes or, more general, biased processes: after choosing the fraction that should be transferred, the mass is added with probability $p_r = p$ to the right and with probability $p_l = 1 - p$ to the left stick. This yields a 3-site interaction. The symmetric ARAP ($p = \frac{1}{2}$) with state-independent fraction density $\phi = 1$ has been discussed (and partially solved) in [2].[9]

❏ open boundaries: the ARAP could also be defined with open boundaries, but unbounded (and even uncountable) state variables offer a lot of freedom for implementing injection and removal rules. Furthermore, it seems to be difficult to achieve boundary induced phase transitions – well known from the asymmetric simple exclusion process [5,6] – because there is no explicit mass exclusion and so it is possible to put an arbitrary amount of mass on one site.

❏ local defects: Introducing site-dependent fraction densities $\phi = \phi_i$ makes it possible to study the influence of local defects.

---

[8]For $m_i = 0$ the expression $r_i = \frac{\Delta_i}{m_i}$ has to be replaced by $r_i = 0$.

[9]There the mass also could stay at the original site with probability q, i.e. we have $p_r + p_l + q = 1$.

2.2. Applications of the ARAP

In this section we would like to present a brief overview of applications based on the ARAP. Especially a huge class of interdisciplinary problems can be mapped onto the asymmetric random average process. We point out the relationship with the q-model that describes force distributions in granular materials [7–11]. Furthermore, a particle representation of the ARAP is presented and its close relation to traffic flow models, in particular a continuous NAGEL-SCHRECKENBERG model, is emphasized [12–16]. After that we briefly work out the parallels with processes of aggregation and fragmentation [17–22] and conclude with deriving the asymmetric simple exclusion process (ASEP), the standard model of nonequilibrium physics, as a special case of the ARAP [5, 23–27].

All models and processes mentioned above are rewritten in terms of fraction (ϕ) or fragment (f) densities to exemplify their connections with the ARAP. However, a detailed presentation of application specific results is omitted because this would go beyond the scope of this work and can be found elsewhere (see references above).

2.2.1. Granular Materials: q-model

The study of granular materials represents an attractive research field for experimental and theoretical physics. Here we focus on the important question how stress is distributed in a granular medium when external forces are exerted. For a brief introduction and an experimental realization of this problem we refer to [7] while the corresponding analytically treatable model, the so-called q-model, is introduced in [8].

In the following we consider identical, regularly piled up beads, forming a multi-layer construction (refer to figure 2.2 whenever necessary). The layers, labelled by $t \in \mathbb{N}_0$, are given by one-dimensional periodic lattices of length L holding the beads $i = 1, \ldots, L$. This setup formally preserves the connection with the ARAP, but it is straightforward to extend the framework to d-dimensional layers with arbitrary lattice geometries [9].
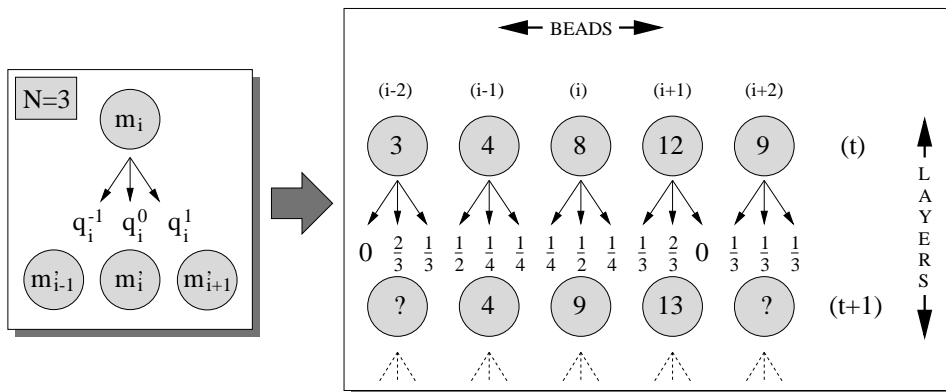

Figure 2.2.: A visualization of the q-model with 3-successor interaction.

Now we assume the beads in the top layer $t = 0$ to experience an external force given by the distribution $P(m, t = 0)$ with $m = (m_1, \dots)$ and m_i representing the force in the downward direction on the bead i. Every particle i transmits the force to exactly N successors $i + \alpha$ in the layer below with $\alpha \in \mathcal{D}$. Due to translational invariance the set of displacement vectors $\mathcal{D}$ is independent of beads and layers and we denote the fraction of transmitted stress to site $i + \alpha$ by q_i^α satisfying the constraint

$$\sum_{\alpha \in \mathcal{D}} q_i^\alpha = 1 \ . \tag{2.27}$$

So the weight m_i' is determined by the composed forces $m_{i-\alpha}$ one layer above:

$$m_i' = \sum_{\alpha \in \mathcal{D}} q_{i-\alpha}^\alpha m_{i-\alpha} \ . \tag{2.28}$$

Supposing that inhomogeneities of the packing lead to fluctuation driven distributions of the weights on the descendant beads we obtain forces that propagate stochastically to the bottom of the system and according to this, the q_i^α are random variables. They obey the fraction density

$$\rho\left(q_i\right) \equiv \rho\left(q_i^{\alpha_1}, \dots, q_i^{\alpha_N}\right) \equiv \frac{1}{Z} \prod_{\alpha \in \mathcal{D}} g(q_i^\alpha) \, \delta\left(\sum_{\alpha' \in \mathcal{D}} q_i^{\alpha'} - 1\right) \tag{2.29}$$

with normalization

$$Z \equiv \int_0^1 \mathrm{d}^N q_i \prod_{\alpha \in \mathcal{D}} g(q_i^\alpha) \, \delta\left(\sum_{\alpha' \in \mathcal{D}} q_i^{\alpha'} - 1\right) \ . \tag{2.30}$$

Here the function g is a free parameter that has to be adjusted to the physical problem (see below). Applying $\prod g(q_i^\alpha)$ instead of a general ansatz $g(q_i^{\alpha_1}, \dots, q_i^{\alpha_N})$ ensures symmetry in the arguments of $\rho(q_i)$. In [7] it has been shown that the choice $g(q) = 1$, i.e. all assortments of suitable q's are equiprobable, reproduces experimental data very well. Nevertheless, other choices are possible, e.g. for $g(q) = \lambda\delta(q) + (1 - \lambda)\delta(1 - q)$ we obtain the critical phase of the q-model (here the total mass is transmitted to exactly one neighbour in a layer below).[10] After all we are able to formulate the evolution equation for the force distribution from one layer to the next layer. Using (2.28), (2.29) and the definition $\rho(q) = \prod_i \rho(q_i)$ neglecting correlations between q-values at different sites, we derive[11]

$$P(m', t + 1) = \int_0^\infty \mathrm{d}^L m \int_0^1 \mathrm{d}^L q \, \rho(q) \prod_j \delta\left(m_j' - \sum_{\alpha \in \mathcal{D}} q_{j-\alpha}^\alpha m_{j-\alpha}\right) P(m, t) \ . \tag{2.31}$$

---

[10]In the critical phase the force distribution obeys a power law in the limit $t \to \infty$ compared to exponential behaviour in the non-critical phase.

[11]$\int d^L q = \prod_i \int d^N q_i = \prod_i \prod_{\alpha \in \mathcal{D}} \int dq_i^\alpha$

The stationary state $\lim_{t\to\infty} P(m,t)$ has been calculated for some g-functions [8]. In recent investigations the relaxation behaviour of the q-model is also studied, i.e. time-dependent quantities are considered and calculated, e.g. the second moments for general q-distributions on a triangular lattice [10] or the full distribution for the uniform g-density for arbitrary lattices [11]. Recently even the set of all factorizing stationary states has been calculated [9] which is similar to the approach presented in chapter 4.

Relation (2.31) bears a strong resemblance to the master equation of the continuous ARAP with parallel update (2.13). Nevertheless, the transition density includes N-site interaction which is more complex than the two-site mass shift of the ARAP. However, for $N = 2$ and $\mathcal{D} = \{0, 1\}$ the q-model reduces to an ARAP with state-independent and symmetric fraction density $\phi(r) = \phi(1 - r)$. We calculate for the inner integral expression of (2.31)

$$
\int_0^1 \mathrm{d}^L q \, \rho(q) \prod_j \delta \left(m_j' - \sum_{\alpha \in \mathcal{D}} q_{j-\alpha}^{\alpha} m_{j-\alpha} \right)
$$

$$
\overset{(2.29)}{=} \prod_{i=1}^L \int_0^1 \mathrm{d}q_i^1 \, \frac{1}{Z} g \left(1 - q_i^1 \right) g \left(q_i^1 \right) \prod_j \delta \left(m_j' - \left[(1 - q_j^1) m_j + q_{j-1}^1 m_{j-1} \right] \right)
$$

$$
\overset{r_i = q_i^1}{=:} \int_0^1 \mathrm{d}^L r \prod_i \phi(r_i) \, \delta \left(m' - T(r) m \right) \quad (2.32)
$$

with

$$
\phi(r_i) = \left[\int_0^1 \mathrm{d}r g(r) g(1 - r) \right]^{-1} g(r_i) g(1 - r_i) \quad (2.33)
$$

and T as given in (2.10). Thus, results derived in the context of the $N = 2$ q-model can be projected onto the ARAP and vice versa. This will be done in section 4.3. In addition, we show that there also exists a close relation to the N-dimensional[12] q-model because for uniform g-functions the steady state of the q-model is identical to appropriately chosen ARAPs.

2.2.2. Traffic Flow Theory: Krauss Model

Traffic flow theory represents an important branch of interdisciplinary research in physics. In the last decade a lot of models have been developed or adopted, and studied analytically or numerically. In general we distinguish macroscopic and microscopic models. While the first class is based on hydrodynamic approaches, the latter systems represent interacting particle systems with explicitly given dynamics. For a comprehensive overview we refer to [12].

The ARAP, defined by lattice size L, density ρ and fraction density ϕ, can be mapped onto a particle model easily: Consider a ring of length $L\rho$ with L particles positioned

---

[12]In the q-model the expression 'dimension' is also used for the number of successors.

anticlockwise at $x_i \in [0, L\rho)$. By identifying the masses in the stick picture with the particle gaps in the particle picture, i.e.

$$x_{i+1} = x_i + m_i \mod L\rho \, , \tag{2.34}$$

we obtain an asymmetric clockwise movement with conserved order, i.e. the particles cannot overtake each other (figure 2.3). In general the jump distance of the particles ranges from zero ($r_i = 0$) to the full headway (=distance to the preceding car, $r_i = 1$). So the range of interaction is a priori unlimited (at least in the infinite system) and it is possible that particles occupy the same place. However, features like particle exclusion or a maximum hopping length can be included by a straightforward adjustment of the fraction densities.
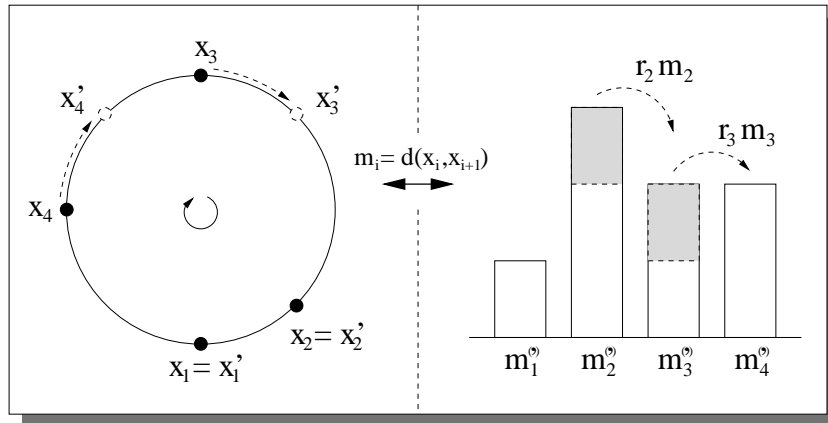
Figure 2.3.: Representation of the ARAP in the particle (left) and mass (right) picture. The state variables x_i, m_i and x_i', m_i' correspond to the times t and $t+1$, respectively. The function $d(x_i, x_{i+1})$ represents the distance between the particles i and $i+1$ measured anticlockwise.

A famous example of traffic models is the NAGEL-SCHRECKENBERG (NaSch) cellular automaton defined on a one-dimensional lattice in discrete time [13]. Here particles represent cars and carry an additional internal velocity parameter v_i, determining the distance covered per update step, i.e. $x_i \rightarrow x_i + v_i$. However, v_i is not fixed in general. The cars increase their velocity by one in every update step until they reach the maximal velocity $v_{\max}$ or the headway (to avoid collisions). Furthermore, cars may decrease their velocity by one with a given fixed probability. This reflects a non-perfect driveability of road users including fluctuations in speed, over-reactions or retarded accelerations. The underlying dynamics is fully parallel. Although defined by simple rules this model can reproduce many phenomena of one-lane traffic [12].

In general it is not possible to represent the NaSch model in the framework of the ARAP because we are confronted with an additional state variable v_i. In the mass picture of the ARAP the velocity v_i corresponds to the mass shifted in the previous

timestep. Thus, the ARAP would be equipped with a short-time memory. Nevertheless, there are two limiting cases which can be modelled in the context of the ARAP:

❑ the asymmetric simple exclusion process (ASEP) which is obtained for $v_{\max} = 1$ and discussed in section 2.2.4 and

❑ the so-called KRAUSS model [14] defined in the next paragraph.

The KRAUSS model represents a continuous version of the Nagel-Schreckenberg cellular automaton for traffic flow. Particles with real valued positions $x_i(t)$ and velocities $v_i(t)$ move on a ring according to the following dynamics:

$$
\begin{aligned}
v_i(t+1) &= \max \left\{ 0, \underbrace{\min \left\{ v(t) + a_{\max}, v_{\max}, x_{i+1}(t) - x_i(t) \right\}}_{\text{destinated } v_i(t+1)} - \sigma \xi_i(t) \right\} \\
x_i(t+1) &= x_i(t) + v_i(t) .
\end{aligned}
\tag{2.35}
$$

Drivers accelerate by $a_{\max}$, but drive collision free, i.e. $v_i(t+1) \leqslant x_{i+1}(t) - x_i(t)$, and do not exceed the maximum velocity $v_{\max}$. The maximum deceleration σ is coupled with a uniformly distributed random parameter $\xi_i(t)$ between zero and one (reflecting a probabilistic individual driving behaviour).

We would like to mention that (2.35) represent the simplest form of the KRAUSS model. In later publications the particle gap $x_{i+1}(t) - x_i(t)$ is replaced by a more complex expression determined by the requirement that a car moves with a velocity that allows a complete stop just in time [15]. This condition reads as $d(v_i) + v_i \tau \leqslant d(v_{i+1}) + x_{i+1} - x_i$ with reaction time τ and braking distance $d(v)$ at velocity v.

For accelerations $a_{\max} \geqslant v_{\max}$ the update (2.35) is independent of the velocity v_i of cars. So we can rewrite the dynamics using m_i as defined in (2.34) and obtain

$$
\Delta(m_i, \xi_i) = \max \left\{ 0, \min \left\{ v_{\max}, m_i \right\} - \sigma \xi_i \right\} .
\tag{2.36}
$$

Here Δ represents the fragment shifted from a site i to the right and $\xi_i \in [0, 1]$ is a random number generated from a uniform distribution. In Monte-Carlo simulations the parameters $a_{\max}$ and $v_{\max}$ are set to values that differ only weakly [14,16]. So the ansatz $a_{\max} = v_{\max}$, leading to (2.36), is justified. It represents a model where cars accelerate instantaneously to maximum velocity[13]. For the following work we rewrite (2.36) in terms of the fragment density. After some algebra we obtain the expression

$$
\begin{aligned}
f(\Delta_i, m_i) = {}& \left(1 - \sigma^{-1} \min \left\{ \sigma, v_{\max}, m_i \right\} \right) \delta(\Delta_i) \\
& + \sigma^{-1} \theta \left(\min \left\{ v_{\max}, m_i \right\} - \Delta_i \right) \theta \left(\Delta_i - \left(\min \left\{ v_{\max}, m_i \right\} - \min \left\{ \sigma, m_i \right\} \right) \right)
\end{aligned}
\tag{2.37}
$$

---

[13]This represents a rescaling of time.

with $\theta(x)$ representing the continuous HEAVISIDE step function. In section 5.5 we will discuss a simplified version of (2.37) into detail.

Recently the KRAUSS model has become of interest because numerical investigations point to a new regime in its phase diagram [16]. In chapter 5 we present and study a truncated version of the ARAP that is much simpler than (2.37), but shares a lot of properties with the KRAUSS model. In particular, this ARAP can give support for the occurrence of the new phase (section 5.5).

2.2.3. Aggregation and Fragmentation: Zero-Range Processes

The most intuitive approach to the ARAP is via driven aggregation and fragmentation: parts of the sticks are broken off (fragmentation) and the shifted mass is recombined with the next neighbour (aggregation). Especially for one-dimensional discrete systems a lot of work has been done (see below). Those processes can be mapped onto the ARAP without difficulty as long as the underlying local dynamics is totally asymmetric and include only nearest neighbour interactions.

An interesting model of aggregation and fragmentation is the so-called chipping model (CM) [17, 18]. It is defined on discrete state space and equipped with random sequential dynamics. The CM-dynamics consists of two competing processes:

❏ diffusion, i.e. transfer of an entire stick with rate 1 (maximal shift). The mass update reads $m_i \to 0$ and $m_{i+1} \to m_{i+1} + m_i$.

❏ chipping, i.e. transfer of the unit mass 1 with rate $w \geqslant 0$ (minimal shift). The mass update reads $m_i \to m_i - 1$ and $m_{i+1} \to m_{i+1} + 1$ (for $m_i \geqslant 1$).

Note that the CM can be considered as a toy model for one-dimensional polymerization: the mass sticks correspond to polymers of length m_i that are driven through a tube. If two polymers collide, they stick together. On the other hand, polymers may dissolve successively by the separation of single monomers.

It is clear that configurations containing one large stick (polymer) are very stable as long as w is small enough, because huge columns (polymers) cannot be reduced by chipping and are moved by diffusion only. Note that configurations with several large sticks (polymers) are not stable and will completely coalesce due to diffusion. Since the occurrence of large sticks is linked to the mass density, the w-ρ ratio determines if condensed configurations are stable. For the symmetric CM the critical density

$$\rho_c(w) = \sqrt{w + 1} - 1 \tag{2.38}$$

has been calculated exactly [19]. For $\rho > \rho_c$ the system is in a singular phase given by an infinite mass aggregate and algebraic decaying mass densities for small m, whereas for $\rho < \rho_c$ the CM resides in a homogeneous phase with exponential decaying mass distributions.

Note that the CM can be interpreted as an ARAP with fragment density

$$f(\Delta, m) = \frac{w}{1+w}\delta_{\Delta,1} + \frac{1}{1+w}\delta_{\Delta,m} \tag{2.39}$$

for $m \in \mathbb{N}$. In section 5.6 we will discuss similarities and differences between CM and the truncated ARAP introduced and studied in chapter 5.

Another interesting class of fragmentation models is given by zero-range processes initially introduced into the mathematical literature by SPITZER [20]. They have a lot of physical applications and have often appeared incognito in a wide range of different contexts. In particular, a lot of interacting particle systems are based on zero-range processes, e.g. the ASEP (section 2.2.4). For an introductory overview we refer to [21].

Consider a one-dimensional finite lattice with L sites and periodic boundary conditions. Each site can hold an integer number of indistinguishable particles[14], so the configuration of the system is specified by the occupation number m_i of each site i. The local dynamics of the system is given by the probabilities (or rates) at which a particle leaves a site i and moves to the right nearest neighbour site $i + 1$. The hopping probabilities (rates) $p(m_i)$ depend only on the number of particles at the site of departure.

Thus, the zero-range process corresponds to an ultralocal ARAP that allows for the transfer of one (or no) particle only. The fragment density of the zero-range process is given by

$$f(\Delta, m) = (1 - p(m))\,\delta_{\Delta,0} + p(m)\delta_{\Delta,1} \tag{2.40}$$

for $m \geqslant 1$. The zero-range process has been expanded to inhomogeneous dynamics, i.e. site-dependent f-functions, or arbitrary networks, i.e. the range of interaction exceeds the nearest neighbour restriction, see [21], but here we would like to focus on homogeneous systems with nearest neighbour shifts only. The remarkable property of the zero-range process is that the stationary state is given by a product measure for any system size (even in the thermodynamic limit) and for any kind of update. Correspondingly its mass correlations are zero ranged. So we have

$$P(m) = \frac{1}{Z(L,M)}\prod_{i=1}^{L} h(m_i) \quad \text{with} \quad Z(L,M) = \sum_{\sum_i m_i = M}\prod_{i=1}^{L} h(m_i)\,. \tag{2.41}$$

In case of the random sequential update the h-function reads

$$h(m) = \begin{cases} 1 & m = 0 \\ \prod_{n=1}^{m} \frac{1}{p(n)} & m > 0 \end{cases} \tag{2.42}$$

while

$$h(m) = \begin{cases} 1 - p(1) & m = 0 \\ \frac{1-p(1)}{1-p(m)}\prod_{n=1}^{m} \frac{1-p(n)}{p(n)} & m > 0 \end{cases} \tag{2.43}$$

---

[14]These particles do not correspond to the particles presented in the particle picture of section 2.2.2.

is derived for parallel dynamics, e.g. [21]. These states are unique as long as the system is ergodic which is valid for irreducible transition matrices. The proof of stationarity is rather simple and works by inserting (2.41) with (2.42) or (2.43) into the corresponding stationary master equations. Nevertheless, it is also possible to obtain the solution constructively [21, 22].[15]

In chapter 4 we give evidence that the class of product measure solutions related to the continuous ARAP with state independent ϕ-function is also valid for arbitrary system sizes as in case of the zero-range process. And according to (2.41) we define a kind of grand-canonical partition sum for an adequate normalization, see section 4.4.

Furthermore, every zero-range process can be mapped onto an equilibrium zero-range process [21], i.e. it is possible to construct a new zero-range process (with different dynamics) with identical steady state, but that steady state is an equilibrium state in the new model! This mapping makes it possible to transfer principles of equilibrium statistics to a special class of nonequilibrium problems. This mapping is similar to the relation between N-dimensional q-models and ARAPs with monomial ϕ-densities (section 4.3).

Finally, we briefly discuss the occurrence of condensation effects in zero-range processes that are strongly related to the truncated ARAP (chapter 5) as mentioned above. As an important tool one can identify $Z(L, M)$ as a grand-canonical partition sum and correspondingly determine a fugacity z by help of a saddle point method [21]:

$$\rho = \frac{zF'(z)}{F(z)} \quad \text{with} \quad F(z) = \sum_{m=0}^{\infty} z^m h(m) . \tag{2.44}$$

The question comes up whether for every density ρ a valid saddle point value of z can be found by (2.44). From (2.44) we extract that $\rho = \rho(z)$ is monotonically increasing in z with $\rho(0) = 0$. If we assume the r.h.s. of (2.44) to possess a finite radius of convergence R with $\rho(R) < \infty$ we cannot solve (2.44) for $z > R$. This corresponds to a so-called condensation transition, i.e. a finite fraction of the total mass is held by a spontaneously selected site i (even in the thermodynamic limit!). This effect is the same as in the model (2.39) defined above.

As an example we present a zero-range process with a sharp crossover phenomenon given by

$$p(m) = \begin{cases} 1 & m < C \\ \beta & m \geqslant C \end{cases} \tag{2.45}$$

with $\beta < 1$ and continuous dynamics. By the help of (2.42) and (2.44) we evaluate the fugacity z in dependence of ρ. In the $C \to \infty$ limit we obtain two phases: for $\rho < \rho^\star$ with $\rho^\star = \beta(1 - \beta)^{-1}$ the particles are evenly spread between all sites (homogeneous phase) while there is a condensation effect for $\rho > \rho^\star$. Intuitively this phase separation

---

[15]The solution of arbitrary networks can also be given explicitly. Here one has to solve only the corresponding one particle problem whose solution is simply fed in a general formula.

is clear because in case of high densities, i.e. high occupations in average, the transfer rate for high columns is reduced (only β) so that condensates become very stable. The bigger R the sharper is the crossover between low and high density regime. Please note that the system is not critical (no phase transition) if we perform the C-limit first, i.e. use $p(m) = 1$.

2.2.4. A Standard Model: ASEP

The asymmetric simple exclusion process (ASEP), e.g. [23] or [24], has achieved the status of a standard model in nonequilibrium physics. A lot of interesting phenomena like boundary-induced phase transitions [5] or one-dimensional symmetry breaking [25] have been studied first in the framework of the ASEP. New analytical approaches for stochastic systems like the matrix product technique [26] or the BETHE ansatz [27] have been applied successfully to this simple toy model. Finally, it represents a basic system for a lot of interdisciplinary applications.

The ASEP is defined on a one-dimensional integer lattice. A lattice site can be empty or occupied by exact one particle (principle of exclusion). The local dynamics is defined rather simply: a particle hops to the right with probability p if the right nearest neighbour site is empty.

However, the ASEP can also be described in a mass picture by assigning the number of vacant sites between two particles i and $i + 1$ to a new state variable m_i. That way we obtain a zero-range process with state-independent hopping probability $p(m_i) = p$. Hence the fragment density of the ASEP is given by

$$f(\Delta, m) \equiv \delta_{m,0}\delta_{\Delta,0} + \theta_{m-1}\left\{(1-p)\delta_{\Delta,0} + p\delta_{\Delta,1}\right\} . \qquad (2.46)$$

Here we have also included the term for $m = 0$ which has been omitted in the previous sections.

Now we verify (2.46) by showing that the known steady state distribution for the ASEP on a ring with continuous time fulfills the master equation (2.26). In the particle picture the steady state is given by a BERNOULLI measure, which is a product measure with $P(\tau_i) = (1 - \bar\rho)(1 - \tau_i) + \bar\rho\tau_i$, $\tau_i \in \{0, 1\}$ and particle density $\bar\rho = \frac{1}{\rho}$ [24]. In the stick representation the steady state is also given by product measure and we derive $P(m_i) = \bar\rho(1 - \bar\rho)^{m_i}$, e.g. from (2.42). By using (2.46) and the relation $P(m(i, \Delta)) = P(m)$ we finally obtain

$$\sum_i \sum_{\Delta=0}^{m_{i+1}} f(\Delta, m_i + \Delta)P(m(i, \Delta))$$

$$= \sum_i \left\{\delta_{m_i,0} + \theta_{m_{i-1}} + p\left(\theta_{m_{i+1}-1} - \theta_{m_i-1}\right)\right\}P(m) = \sum_i P(m) , \quad (2.47)$$

the steady state condition of (2.26).

2.3. Properties of the ARAP

In this section the most important results are brought together which have been derived for the ARAP so far. While the last chapter gave a crude overview of related models and problems only, we present ARAP specific conclusions here and go into detail a little bit more. We focus on exact solutions, discuss the correlation functions in space and summarize some miscellaneous findings.

2.3.1. The Free ARAP

In literature the free ARAP defined by

$$\phi(r_i) = 1 \tag{2.48}$$

has been studied intensively. Here the notation "free" is used to emphasize the absence of truncation (see chapter 5). Regarding the master equation (2.13), reflecting parallel dynamics, this obviously seems to be the most simply defined ARAP on continuous state space. It has been shown that the steady state distribution factorizes in the infinite limit, i.e. $P(m) = \prod_i P(m_i)$, and the corresponding single-site distribution is

$$P(m) = \frac{4m}{\rho^2}\, \mathrm{e}^{-2\frac{m}{\rho}}\; . \tag{2.49}$$

Here we use the relaxed notation m instead of m_i. This result has been derived first in context of the q-model [8] and has been reproved several times in the following [1,2,18]. We will present the derivation of (2.49) briefly because some of the following ideas are used in chapter 4.

Assuming that product measure holds, the stationary master equation for the single-site mass density reads

$$P(m_2') = \int_0^\infty \mathrm{d}m_1 \int_0^\infty \mathrm{d}m_2 \int_0^1 \mathrm{d}r_1 \int_0^1 \mathrm{d}r_2\, \delta\left(m_2' - [r_1 m_1 + (1-r_2)m_2]\right) P(m_1)P(m_2)\; , \tag{2.50}$$

where we made use of (2.13) and (2.48). By LAPLACE-transforming (2.50), i.e. introducing $Q(s) = \int_0^\infty \mathrm{d}m\, P(m)\exp(-ms)$, the compact functional equation

$$Q(s) = \left[\int_0^1 \mathrm{d}r\, Q(sr)\right]^2 =: V^2(s) \tag{2.51}$$

is obtained. Note that LAPLACE-transforming allows for a factorization of the δ-function into site specific terms, i.e. the (formal) interaction between m_1 and m_2 disappears. Additionally, we are equipped with a symmetric fraction density $\phi(r) = \phi(1-r)$ enabling the substitution $1 - r_2 \to r_2$ without formal changes. Finally, the uniform structure of ϕ yields the simple relation $\frac{\mathrm{d}}{\mathrm{d}s}(sV(s)) = Q(s)$ and (2.51) transforms into a nonlinear

differential equation of first order. This can be solved easily with respect to the boundary conditions

$$Q(0) = 1 \quad \text{and} \quad Q'(0) = -\rho \tag{2.52}$$

reflecting normalization and mass conservation. Inverting the LAPLACE-transform yields (2.49). We skip the proof of exactness of product measure and refer to the general approach in chapter 4.

It has been shown that a product measure ansatz is not exact for random sequential dynamics, both for finite systems [1] and infinite systems [2]. Nevertheless, the mean field equation can be solved exactly, e.g. in the same way as above, and we get

$$P(m) = \frac{1}{\sqrt{2\pi\rho m}} e^{-\frac{1}{2}\frac{m}{\rho}} . \tag{2.53}$$

Although this distribution is not exact the results are in excellent agreement with Monte-Carlo simulations [1,2]. On the one hand, this is not surprising because 2-point (and 3-point) correlations vanish for every ARAP with (symmetric) state-independent fraction density (see below), so deviations to mean field approximations occur first in fourth order moments. On the other hand, the non-exactness of product measures does not imply that the mean field single-site density (2.53) is wrong!

Furthermore, we would like to point out another difference between continuous and discrete time dynamics demonstrated in the particle picture. While in case of a random sequential update the particles tend to bunch ($P(m) \to \infty$ for $m \to 0$), it is vice versa for the parallel update ($P(0) = 0$).

Above calculations can easily be adapted to the discrete ARAP, but as mentoined before the fraction density is now ultralocal:

$$f(\Delta, m) = \frac{1}{1+m} . \tag{2.54}$$

Nevertheless, the results obtained are very similar: A mean field ansatz turns out to be exact in case of a parallel update and breaks down for random sequential dynamics. The corresponding single-site mass distributions are [2]

$$P(m) = 4(m+1)\frac{\rho^m}{(2+\rho)^{m+2}} \quad \text{(parallel)} \tag{2.55}$$

and

$$P(m) = \frac{(2m)!}{2^m(m!)^2}\frac{\rho^m}{(1+2\rho)^{m+1/2}} \quad \text{(continuous)} . \tag{2.56}$$

Again the single-site distribution (2.56) matches the numerical data perfectly although the mass density does not factorize.

For completeness we mention that the symmetric variants of the free ARAP have been studied also [1,2] and the behaviour is totally different. Now for continuous time the exact solution factorizes while the mean field ansatz breaks down for parallel update. It cannot even be given in a closed form and does not fit well with the Monte-Carlo results.

2.3.2. Correlations

We present the 2-point mass moments of the continuous ARAP in the thermodynamic limit in case of state independent fraction densities $\phi(r)$. For both kinds of updates correlations are absent [1,2] which suggests the good convergence of a mean field ansatz. The n-site moments can be calculated directly without determining the mass density $P(m)$. From a simple set of linear equations one derives exactly $C_k \equiv \langle m_i m_{i+k} \rangle$ (the index i is suppressed due to translation invariance):[16]

$$C_0 = \frac{\mu_1(1 - \mu_1)}{\mu_1 - \mu_2}\rho^2 \ , \quad C_{k \geqslant 1} = \rho^2 \quad \text{(parallel)} \tag{2.57}$$

and

$$C_0 = \frac{\mu_1}{\mu_1 - \mu_2}\rho^2 \ , \quad C_{k \geqslant 1} = \rho^2 \quad \text{(continuous).} \tag{2.58}$$

Here we have introduced the moments of the fraction density

$$\mu_n \equiv \int_0^1 \mathrm{d}r \ r^n \phi(r) \ . \tag{2.59}$$

In the context of the q-model it has been additionally proven that also the 3-point correlations vanish for $\phi(r) = \phi(1 - r)$ [9]. However, for general $\phi(r)$ 3-point moments do not factorize and third order correlations occur.[17]

2.3.3. Miscellaneous

We complete this introduction by a list of further interesting results from publications also dealing with the ARAP:

❏ For the free continuous ARAP with random sequential dynamics the tracer diffusion coefficient, describing the movement of a tagged particle, has been calculated exactly [28]. This is in agreement with a heuristic approach, also applicable to other updates, presented in [1].

❏ The correlations between the positions of tagged particles have been studied analytically for the symmetric and asymmetric random average process with state-independent fraction densities [29].

---

[16]This is the representation in the thermodynamic limit. For finite systems $C_{k \neq 0}$ is constant but differs from ρ^2.

[17]Private communication with J.M.J. van Leeuwen and J. Snoeijer.

3. Matrix Product Ansatz (MPA) for the Free ARAP

In this chapter we solve both the continuous and the discrete free ARAP, (2.48) and (2.54), with parallel dynamics by using a matrix product ansatz (MPA). This technique has been initially introduced for calculating exact ground states of quantum spin chains [30, 31]. Shortly after, DERRIDA and coworkers have successfully applied the MPA to a nonequilibrium system, namely the ASEP with random sequential dynamics [26]. Meanwhile the MPA has been evolved to a standard tool for one-dimensional stochastic models, e.g. [6, 24, 32, 33] and references therein. However, its field of application is basically restricted to variants of the ASEP (different updates, local defects or two species of particles).

In general the MPA is applied to systems defined on a two-dimensional local state space, i.e. sites can be vacant or occupied. Corresponding to this, manageable sets of algebraic objects (corresponding to the local states) and algebraic relations (reflecting the local dynamics) are obtained. For example the ASEP defined in section 2.2.4 provides one condition, $pDE = D + E$, where the objects E and D correspond to holes and particles. Nevertheless, it is rather complicated to find representations of that poorly defined algebra [24]. An extension to a model with an arbitrary but still finite number of local states is given in [34].

Here we apply the MPA to the free ARAP in case of discrete and continuous state variables. In both cases mean field is exact (section 2.3.1), i.e. the corresponding algebras have one-dimensional representations. However, we are confronted with an infinite number of algebraic objects and conditions in case of the discrete ARAP, while the matrix algebra of the continuous ARAP is given by a functional equation!

We derive solutions for both ARAPs in agreement with the results given in section 2.3.1. So the scope of the MPA is extended to unbounded and continuous state spaces.

3.1. Matrix Product Solution of the Discrete ARAP

In this section we reproduce the product measure solution of the discrete free ARAP with parallel dynamics (2.55) by the matrix product technique for the case $L \to \infty$. A related calculation has been presented in [35] for the ASEP with parallel update.

We start with the "defect" matrix product ansatz for backward sequential dynamics [6], i.e. we assume the local interaction to obey

$$t\left(A \otimes \bar{A}\right) = \bar{A} \otimes A \tag{3.1}$$

with

$$A = \sum_{m=0}^{\infty} D_m \left|m\right\rangle \quad \text{and} \quad \bar{A} = \sum_{m=0}^{\infty} \bar{D}_m \left|m\right\rangle . \tag{3.2}$$

Here $\left|m\right\rangle$ spans the infinite-dimensional local state space of a single site and the tensor product is defined as usual, i.e.

$$A \otimes \bar{A} = \sum_{m,m'} D_m \bar{D}_{m'} \left|m, m'\right\rangle , \tag{3.3}$$

whereby we have used the notation $\left|m, m'\right\rangle \equiv \left|m\right\rangle \otimes \left|m'\right\rangle$. In general D_m and $\bar{D}_m$ are arbitrary algebraic objects, but here we assume a matrix representation of arbitrary dimension. It is easy to see that

$$\left|P\right\rangle_L = \text{tr}\left(\bar{A} \otimes \underbrace{A \otimes A \otimes \cdots \otimes A}_{L-1 \text{ terms}} \right) \tag{3.4}$$

represents a steady state of the local dynamics (3.1) under terms of backward sequential dynamics (section 2.1.2).[1,2] In the thermodynamic limit the parallel update corresponds to the backward sequential update (section 2.1.2 again). The defect can be neglected and we obtain

$$\left|P\right\rangle = \lim_{L \to \infty} \left|P\right\rangle_L = \text{tr}\left(A \otimes A \otimes \dots\right) . \tag{3.5}$$

Now we give the explicit definition of the local dynamics by using (2.54):

$$t\left|m_1, m_2\right\rangle = \sum_{\Delta=0}^{m_1} \frac{1}{m_1 + 1} \left|m_1 - \Delta, m_2 + \Delta\right\rangle . \tag{3.6}$$

Using (3.6) with (3.1) and (3.2) yields the matrix algebra

$$\sum_{i=0}^{l} \frac{1}{k+i+1} D_{k+i} \bar{D}_{l-i} = \bar{D}_k D_l \quad \text{with} \quad k, l \in \mathbb{N}_0 . \tag{3.7}$$

A non-trivial one-dimensional representation[3] of (3.7) is given by

$$D_m = \frac{1+m}{2^m} D_0 \left(\frac{D_1}{D_0}\right)^m \quad \text{and} \quad \bar{D}_m = \frac{1}{2^m} \bar{D}_0 \left(\frac{D_1}{D_0}\right)^m \tag{3.8}$$

---

[1]Note that trace operator tr and time evolution operator T commute.

[2]The trace operator ensures translational invariance of the steady state.

[3]In this case the trace operator is redundant.

with free parameters D_0, D_1 and $\bar{D}_0$. This is shown directly by inserting (3.8) into (3.7). From (3.5) we see that $P(m) = D_m$. Taking into account that the boundary conditions $\sum_m P(m) = 1$ and $\sum_m m P(m) = \rho$ have to be satisfied, equation (2.55) is reproduced easily.

Since a one-dimensional representation exists we have also shown that mean field is exact here. This proof is quite elegant and appears from nowhere while in [2] the exactness of product measure has been shown by proving that all joint probabilities factorize.

3.2. Matrix Product Solution of the Continuous ARAP

The product measure solution of the continuous ARAP is given by (2.49) and reproduced by the MPA in this section. Hereby we fall back on some definitions of the previous section.

We start again with the "defect" matrix product ansatz for sequential dynamics (3.1). However, the single-site vectors A and $\bar{A}$ are defined slightly different now:

$$A = \int_0^\infty \mathrm{d}m D(m) \left| m \right\rangle \quad \text{and} \quad \bar{A} = \int_0^\infty \mathrm{d}m \bar{D}(m) \left| m \right\rangle . \tag{3.9}$$

Here $\left| m \right\rangle$ spans the infinite and continuous local state space of a single site. Note that the algebraic objects D and $\bar{D}$ depend on a continuous parameter m. Dynamics and steady state are given according to the discrete case.

Now we give the explicit definition of the local dynamics. First we change notation (or more formal: the basis) uniquely in the following way

$$\left| m_1, m_2 \right\rangle \rightarrow \left| m_1 + m_2, m_1 \right\rangle \tag{3.10}$$

because the local interaction is mass conserving. So the mapping

$$t \left| s, m \right\rangle = \int_0^m \mathrm{d}\Delta f(\Delta, m) \left| s, m - \Delta \right\rangle = \int_0^m \mathrm{d}\Delta \frac{1}{m} \left| s, m - \Delta \right\rangle \tag{3.11}$$

is obtained. Here the relation (2.4) has been used.

Using (3.11) and (3.10) with (3.1) and (3.9) yields after some calculation the matrix algebra in form of a functional equation:

$$\int_0^{s-m} \mathrm{d}\Delta \frac{1}{s - \Delta} D(s - \Delta) \bar{D}(\Delta) = \bar{D}(m) D(s - m) . \tag{3.12}$$

Assuming a one-dimensional representation of the algebraic objects, we have to determine the functions D and $\bar{D}$ (which we suppose to be real valued) by the use of (3.12). Please note that we are confronted with one condition and two objects only, whereas we face an infinite number of conditions and objects in the discrete case (3.7).

Differentiating (3.12) with respect to m generates

$$-\frac{1}{m}D(m)\bar{D}(s-m) = \bar{D}'(m)D(s-m) - \bar{D}(m)D'(s-m) \,, \qquad (3.13)$$

a differential equation with two functions (defined on $\mathbb{R}_0^+$) and two variables. For $s = 2m$ (3.13) reduces to

$$\left(\ln\frac{D(m)}{\bar{D}(m)}\right)' = \frac{1}{m} \qquad (3.14)$$

and we obtain the relation

$$D(m) = Cm\bar{D}(m) \,. \qquad (3.15)$$

Inserting this solution in (3.13) results in

$$\frac{\bar{D}'(m)}{\bar{D}(m)} = \frac{\bar{D}'(s-m)}{\bar{D}(s-m)} \qquad (3.16)$$

which has to be valid for all $0 \leqslant m \leqslant s < \infty$. So (3.16) has to be constant and we get $\bar{D}(m) = \tilde{C}e^{\lambda m}$. Under respect of (3.15), the identity $P(m) = D(m)$ and the conditions $\int_0^\infty \mathrm{d}m P(m) = 1$ and $\int_0^\infty \mathrm{d}m P(m)m = \rho$, we reproduce (2.49). And again the proof of exactness is delivered for free!

4. Product Measure Solutions for State-Independent ARAPs

In this chapter we extend our considerations to ARAPs with arbitrary state-independent fraction densities $\phi = \phi(r)$. This is basically motivated by reasons of practical relevance, e.g. the q-model is given by this kind of ϕ-functions. Furthermore, state-independent ARAPs may represent suitable approximants for ARAPs that are defined by more complex density functions. Finally, our investigations deepen the general understanding of the underlying dynamics.

In the following we focus on the fully parallel update and calculate the set of all ϕ-functions leading to product measure solutions. This is done for finite systems and for systems in the thermodynamic limit as well. By the interpolation formula (2.20) we also derive results for continuous time dynamics.

Several parts of this chapter can be found in [36, 37].[1] Furthermore, the set of product measure solutions has been determined recently by a similar approach for the q-model [9].

The chapter is divided as follows: in section 4.1 a functional equation acting on the LAPLACE space of the single-site mass distributions $P(m)$ is derived. Product measure holds if a mean field ansatz is a solution of this condition. In section 4.2 we determine the set $\mathcal{M}$ of all fraction densities $\phi(r)$ yielding product measure states. Although this construction incorporates a conjecture based on high order calculations, it is proven rigorously. We discuss the structure of $\mathcal{M}$ and show that the class of exact mean field solutions covers a wide range of dynamics including almost critical fraction densities. The explicit form of the mass distributions $P(m)$ is also derived.

As an example we study ARAPs with monomial ϕ-function which belong to the class $\mathcal{M}$ as well (section 4.3). However, we calculate $P(m)$ and prove the exactness of mean field explicitly. Due to the fact that the N-dimensional q-model with uniform distributed q's leads to the same mass distributions [8], its relationship with the ARAP is also discussed briefly.

In section 4.4 finite systems are considered, whereas the results for continuous time dynamics are presented in section 4.5. Finally, we demonstrate that the results of the previous sections can be used to obtain very accurate approximations for ARAPs which

---

[1]Basically parts of the sections 4.1, 4.2, 4.3 and 4.6.

do not lead to solutions of product measure form (section 4.6).

4.1. A Functional Equation of Exact Mean Field Solutions

In this section we derive a functional equation (see eq. (4.7) below) for determining and testing mean field solutions.

The fundamental element of all upcoming considerations is the master equation. For the single-site stationary mass distribution $P(m)$ it reads

$$
\begin{aligned}
P(m_2') &= \int_0^\infty \mathrm{d}m_1 \int_0^\infty \mathrm{d}m_2 \, P(m_1, m_2) \int_0^1 \mathrm{d}r_1 \int_0^1 \mathrm{d}r_2 \, \phi(r_1)\phi(r_2) \\
&\quad \times \delta\left(m_2' - [r_1 m_1 + (1 - r_2)m_2]\right) \ .
\end{aligned} \tag{4.1}
$$

as can be seen from (2.13). By the mean field ansatz $P(m_1, m_2, \ldots) = \prod_i P(m_i)$ equation (4.1) determines the single-site distribution $P(m)$. The resulting product measure is exact if the mean field ansatz holds for all joint probabilities, too, i.e. $P(m)$ has to satisfy

$$
\prod_{i=2}^k P(m_i') = \left\{ \prod_{i=1}^k \int_0^\infty \mathrm{d}m_i \, P(m_i) \int_0^1 \mathrm{d}r_i \, \phi(r_i) \right\} \prod_{i=2}^k \delta\left(m_i' - [r_{i-1}m_{i-1} + (1 - r_i)m_i]\right) \tag{4.2}
$$

for all $k \in \mathbb{N}_{\geqslant 2}$ in case of $L \to \infty$. For $k = 2$ this equation reduces to (4.1). This appears to be an infinite set of conditions, but LAPLACE-transforming $P(m_1, m_2, \ldots)$ reduces (4.2) to just one functional equation. By introducing the $k-$dimensional LAPLACE-transform

$$
Q(s_1, \ldots, s_k) \equiv \int_0^\infty \mathrm{d}^k m \, P(m) e^{-(m,s)}, \tag{4.3}
$$

where $(m, s) = \sum_{i=1}^k m_i s_i$, and using the map

$$
F_Q(s, \tilde{s}) \equiv \int_0^1 \mathrm{d}r \, \phi(r) \, Q\left((1 - r)s + r\tilde{s}\right) \tag{4.4}
$$

equation (4.2) reads in LAPLACE space

$$
\prod_{i=1}^k Q(s_i) = F_Q(0, s_1) \cdot \prod_{i=1}^{k-1} F_Q(s_i, s_{i+1}) \cdot F_Q(s_k, 0) \tag{4.5}
$$

for $k \in \mathbb{N}$.[2] Note that the factorization property of P carries over to Q.

---

[2] Note that there is no strict one-to-one correspondence between the indices in (4.2) and (4.5).

By a straightforward proof we now show that the conditions for $k \neq 2$ are redundant. The $k = 1$-equation

$$Q(s) = F_Q(s, 0) \cdot F_Q(0, s) \qquad (4.6)$$

is used to determine Q. We rewrite the $k = 2$-criterion using (4.6) and obtain

$$F_Q(s_1, s_2) = F_Q(s_1, 0) \cdot F_Q(0, s_2) . \qquad (4.7)$$

Applying (4.6) and (4.7) proves the validity of (4.5) for all $k \geqslant 3$ and using the identity $Q(s) = F_Q(s, s)$ equation (4.6) becomes a special case of (4.7). So (4.7) is the only necessary equation to determine a mean field solution ($s_1 = s_2$) and check its accuracy ($s_1 \neq s_2$).

The mean field criterion (4.7) has been derived under the assumption $L = \infty$, but it is also valid for closed finite systems: by LAPLACE-transformation of the master equation for $P(m_1, \ldots, m_L)$ we obtain (using the same techniques as before)

$$\prod_{i=1}^{L} Q(s_i) = \prod_{i=1}^{L} F_Q(s_i, s_{i+1}) . \qquad (4.8)$$

Then projection on the $s_2 = \ldots = s_L = 0$ surface yields (4.6) while (4.7) is achieved by $s_3 = \ldots = s_L = 0$ and use of (4.6). On the other hand, (4.7) ensures validity of (4.8).[3]

In addition, we deal with a grand-canonical representation for finite systems, i.e. we have not included the constraint of fixed mass yet. In general product measures allocate a probability density $\prod_i P(m_i)$ for every configuration m. However, a priori the support of these solutions[4] is not restricted to the hyperplane $\sum_i m_i = \rho L$ which represents a necessary condition for finite systems. In section 4.4 we will present the constructive mapping onto finite systems into detail.

4.2. Exact Mean Field Solutions

In this section we explicitly derive the set of density functions $\phi(r)$ that result in product measure steady states. This yields a more useful criterion for determining the exactness of a mean field solution without calculating and verifying $Q(s)$ by condition (4.7). In addition, we derive the mass distribution $P(m)$ and discuss the class of mean field solutions.

4.2.1. Implicit Form of $\mathcal{M}$

We start by proving that equation (4.6) always has a unique solution in the space of functions that are analytical in the origin. Intuitively one supposes holomorphicity at

---

[3] For $L = 2$ one can prove only (4.7) $\Rightarrow$ (4.8), but not the opposite direction.

[4] The support of a function f is the smallest open subset A of the domain D so that $f|_{D \setminus A} = 0$.

zero because the mass moments

$$m_n \equiv \langle m^n \rangle_{P(m)} = \int_0^\infty \mathrm{d}m \, m^n P(m) \tag{4.9}$$

are (formally) generated by $m_n = (-1)^n Q^{(n)}(0)$. But a priori we do not know if all derivatives $Q^{(n)}$ of the moment function $Q(s)$ exist or ensure convergence. The moments $m_0 = 1$ and $m_1 = \rho$ are determined by the normalization and the density ρ, respectively.

We first represent the moment function as a (formal) power series[5], i.e.

$$Q(s) = \sum_n a_n s^n \,. \tag{4.10}$$

The coefficients a_n are related to the moments (4.9) by $a_n = (-1)^n \frac{m_n}{n!}$ and thus we have $a_0 = 1$ and $a_1 = -\rho$, see (2.52). The remaining coefficients are determined with help of a recurrence relation obtained by inserting the series representation into (4.6):

$$a_n = \frac{1}{1 - \mu_{n,0} - \mu_{0,n}} \sum_{k=1}^{n-1} \mu_{k,0} \, \mu_{0,n-k} \, a_k \, a_{n-k} \qquad (\forall n \geqslant 2). \tag{4.11}$$

Here $\mu_{n,m}$ are generalized moments of the fraction density ϕ defined by

$$\mu_{n,m} \equiv \langle r^n (1-r)^m \rangle_{\phi(r)} = \int_0^1 \mathrm{d}r \phi(r) r^n (1-r)^m \,. \tag{4.12}$$

We assume $\mu_{n,m} > 0$ in the following which is equivalent to $\phi(r) \neq 0$ for at least one $r \in (0,1)$, e.g. $\mu_{n,m} = 0$ does not occur for continuous distributions. The only class of functions including non-positive generalized moments are densities that are supported on $r = 0$ and $r = 1$ only, e.g.

$$\phi_p^{\mathrm{crit}}(r) = p\delta(r) + (1-p)\delta(1-r) \,. \tag{4.13}$$

This ARAP is trivial for $p = 0$ or $p = 1$ and critical for $0 < p < 1$ [8]. Correspondingly it is not solvable under mean field assumptions. We will revisit (4.13) in subsection 4.2.4. From

$$1 - \mu_{n,0} - \mu_{0,n} \stackrel{(4.12)}{=} \sum_{k=1}^{n-1} \binom{n}{k} \mu_{k,n-k} > 0 \qquad (\forall n \geqslant 2) \tag{4.14}$$

we conclude that all a_n are well-defined and the solution of (4.6) is unique. By the formula of Cauchy-Hadamard we then show that Q is holomorphic in $s = 0$: We start by proving the lemma

$$|a_n| \leqslant D^{n-1} c_n \rho^n \qquad (\forall n \geqslant 1) \tag{4.15}$$

---

[5]In case of formal power series we do not care about convergence or absolute convergence. Operations like adding or multiplying are allowed because we are interested in power counting only [38].

with $D \equiv \frac{1}{1-\mu_{2,0}-\mu_{0,2}}$ and density ρ. Here $\{c_n\}_{n\in\mathbb{N}}$ are the CATALAN numbers [38] fulfilling the equations

$$c_1 = 1 \quad \text{and} \quad c_n = \sum_{k=1}^{n-1} c_k c_{n-k} = \frac{1}{n}\binom{2(n-1)}{n-1} \quad (\forall n \geqslant 2). \tag{4.16}$$

Inserting (4.15) into (4.11) using (4.16), the relation $a_n = (-1)^n |a_n|$ and the fact that $\mu_{n,m} > \mu_{n+k_1,m+k_2}$ for all $k_i \in \mathbb{N}$ shows inductively the validity of the lemma (4.15). From[6]

$$\sqrt[n]{c_n} = \left(\frac{1}{n}\right)^{\frac{1}{n}} \exp\left\{\frac{1}{n}\ln\binom{2(n-1)}{n-1}\right\} \approx \left(\frac{1}{n}\right)^{\frac{1}{n}} \exp\left\{2\ln(2)\frac{n-1}{n}\right\} \xrightarrow[n\to\infty]{} 4 \tag{4.17}$$

we conclude that the series expansion $Q(s) = \sum_n a_n s^n$ has a positive radius of convergence.

After proving that mean field solutions are always representable as power series we now try to express the exact solutions in terms of the density function ϕ. Inserting (4.10) into (4.7) yields an infinite set of conditions

$$\binom{n}{k}\mu_{k,n-k}\, a_n = \mu_{k,0}\,\mu_{0,n-k}\, a_k\, a_{n-k} \quad (\forall n \in \mathbb{N}_0, \;\; \forall k \in \{0,\dots,n\}). \tag{4.18}$$

In the following we refer to a special equation of (4.18) as (n,k)-condition or equation of order n. Summing over $k = 1, \dots, n-1$ in (4.18) yields condition (4.11). This shows again that (4.7) includes formula (4.6) and implies convergence of $Q(s)$.

Now we are confronted with the problem that a_n is determined by $n+1$ equations. Since the $(n,0)$- and (n,n)-conditions match identities there are effectively $n-1$ equations to be fulfilled for $n \geqslant 2$. Thus, for $n \geqslant 3$ the occurrence of inconsistencies is possible and for arbitrary ϕ or moments $\mu_{n,m}$ we see by explicit calculation contradictions in order $n = 3$ already. Is it possible to find a set of moments $\{\mu_{n,m}\}$ such that (4.18) is satisfied for all (n,k)?

Assuming that all (n,k)-conditions yield the same a_n we see from (4.18) that the function

$$f(n,k) \equiv \frac{\mu_{k,0}\,\mu_{0,n-k}\, a_k\, a_{n-k}}{\binom{n}{k}\mu_{k,n-k}} \tag{4.19}$$

is independent of k. Therefore, $n-2$ consistency equations

$$f(n,1) = f(n,2) = \dots = f(n,n-1) \equiv a_n \tag{4.20}$$

have to be satisfied. The definition (4.12) implies that $\mu_{n,m}$ can be expressed by $\mu_{j,0}$ only:

$$\mu_{n,m} = \sum_{j=0}^{m}\binom{m}{j}(-1)^j \mu_{n+j} \quad \text{with} \quad \mu_j \equiv \mu_{j,0}. \tag{4.21}$$

---

[6]We have used STIRLING's formula $\ln N! \approx N(\ln N - 1)$ for large N.

Together with (4.18) it follows inductively that $a_n = a_n(\mu_0, \ldots, \mu_n)$. This leads to a successive constructive approach in n: We try to find a μ_n (depending on $\mu_0, \ldots, \mu_{n-1}$) that solves all conditions (4.20) of order n starting with $n = 3$ and repeat this for all upcoming orders $n = 4, 5, \ldots$.

The $n - 2$ equations (4.20) are linear in μ_n. This ensures uniqueness of a possible solution. For arbitrary $k, \tilde{k} = 1, \ldots, n-1$ with $k \neq \tilde{k}$ we obtain

$$\mu_n = \frac{\binom{n}{k} h_{n,k}\, g_{n,\tilde{k}} - \binom{n}{\tilde{k}} h_{n,\tilde{k}}\, g_{n,k}}{\binom{n}{\tilde{k}}(-1)^{n-\tilde{k}}\, g_{n,k} - \binom{n}{k}(-1)^{n-k}\, g_{n,\tilde{k}}} \, . \tag{4.22}$$

Here $g_{n,k} \equiv \mu_{k,0}\, \mu_{0,n-k}\, a_k\, a_{n-k}$ and $h_{n,k} \equiv \sum_{j=0}^{n-k-1} \binom{n-k}{j}(-1)^j\, \mu_{k+j}$ only depend on $\mu_1, \ldots, \mu_{n-1}$. Thus, (4.22) gives us the desired recursion relation to determine all moments μ_n. However, we have to check whether the r.h.s. of (4.22) is independent of k and $\tilde{k}$. We have done this successfully up to order $n = 10$ by computer algebra and our results furthermore lead us to conjecture the following form of the solution of the density moments:

$$\mu_{n+1} = \frac{n + \tilde{\lambda}}{n + \lambda} \mu_n \quad \text{with} \quad \mu_0 = 1 \tag{4.23}$$

or explicitly

$$\mu_n = \prod_{l=0}^{n-1} \frac{l + \tilde{\lambda}}{l + \lambda} = \frac{\Gamma(n + \tilde{\lambda})}{\Gamma(\tilde{\lambda})} \frac{\Gamma(\lambda)}{\Gamma(n + \lambda)} \tag{4.24}$$

with

$$\tilde{\lambda} = \mu_1 \frac{\mu_1 - \mu_2}{\mu_2 - \mu_1^2} \, , \qquad \lambda = \frac{\mu_1 - \mu_2}{\mu_2 - \mu_1^2} \, , \tag{4.25}$$

which again has been checked up to μ_{10}. Note that μ_1 and μ_2 are free parameters that only have to be chosen with respect to the general moment properties

$$1 > \mu_1 > \mu_2 \geqslant \mu_1^2 \, . \tag{4.26}$$

The special case $\mu_1^2 = \mu_2$ yields $\mu_n = \mu_1^n$ representing $\phi(r) = \delta(r - \mu_1)$ which leads to $Q(s) = \exp(-\rho s)$ and thus to the mass distribution $P(m) = \delta(m - \rho)$. So we assume $\mu_2 > \mu_1^2$ in the following. Under these restrictions $\mu_{n \geqslant 3}$ is pole-free and satisfies $0 < \mu_{n+1} < \mu_n$ as demanded.

So (4.24)-(4.26) define the set $\mathcal{M}$ of all fraction densities $\phi(r)$ yielding product measure steady-state distributions and equations (4.24-4.25) represent a powerful criterion for determining the exactness of a mean field ansatz: We only have to calculate the moments μ_n of the fraction density (if they are not already given) and check consistency with (4.24) and (4.25) - without even calculating the mean field mass distribution or its LAPLACE-transform!

Note that the parametrization of $\mathcal{M}$ in terms of μ_1 and μ_2 is arbitrary and a consequence of our construction - other parametrizations are possible. For symmetric densities $\phi(r) = \phi(1 - r)$ the space $\mathcal{M}$ reduces to one dimension because $\mu_1 = \frac{1}{2}$ is fixed.

Nevertheless, the results obtained so far are a little bit unsatisfying. First the representation (4.24)-(4.26) is very bulky and it would be nice to work with an explicit functional form which would allow a detailed discussion and comparison with arbitrary chosen densities. Second our result is not strictly proven. To verify the validity of $\mathcal{M}$ we have to calculate the associated distributions $P(m)$ and insert everything in the mean field criterion (4.7).

4.2.2. Explicit Form of $\mathcal{M}$

In this subsection we derive an explicit representation of the fraction densities ϕ that are spanning $\mathcal{M}$. We start from the recurrence relation of ϕ-moments (4.23). In addition, the moments μ_n could be obtained by differentiating the characteristic function[7] of ϕ:

$$F(s) \equiv \int_0^1 \phi(r) \mathrm{e}^{rs} \mathrm{d}r = \sum_n \frac{1}{n!} \mu_n s^n \; . \tag{4.27}$$

From $\mu_{n+1} \leqslant \mu_n$ we easily prove the analyticity of F at zero. By (4.23) and (4.27) the differential equation

$$sF''(s) + (\lambda - s)F'(s) - \tilde{\lambda}F(s) = 0 \tag{4.28}$$

is derived which is nothing else than KUMMER's equation [39]. For a second order differential equation there are two independent solutions. Here only one of them, the so-called KUMMER M-function $M(\tilde{\lambda}, \lambda, s)$[8], is analytical in $s = 0$, in fact as long as $\tilde{\lambda} \notin \mathbb{Z}\backslash\mathbb{N}_0$. However, the positivity of $\tilde{\lambda}$ is ensured by (4.25) and (4.26) ($\mu_2 = \mu_1^2$ excluded).

Consulting [39] yields for the special case $\mathrm{Re}\,\lambda > \mathrm{Re}\,\tilde{\lambda}$, which is satisfied here, the unique integral representation

$$M(\tilde{\lambda}, \lambda, s) = \int_0^1 \underbrace{\frac{\Gamma(\lambda)}{\Gamma(\tilde{\lambda})\Gamma(\lambda - \tilde{\lambda})} r^{\tilde{\lambda}-1}(1-r)^{\lambda-\tilde{\lambda}-1}}_{=\phi(r)} \mathrm{e}^{rs} \mathrm{d}r \; . \tag{4.29}$$

which gives an explicit representation of ϕ by comparison with (4.27).

Nevertheless, equation (4.29) can also be derived by inserting (4.27) in (4.28) which yields a linear first order differential equation in ϕ after some algebra[9]. This is solved completely by the boundary condition $F(0) = 1$ and the useful formula

$$\int_0^1 dx\, x^\alpha (1-x)^\beta = \frac{\Gamma(\alpha+1)\Gamma(\beta+1)}{\Gamma(\alpha+\beta+2)} \; . \tag{4.30}$$

---

[7]In general the function $F(is)$ is called characteristic function in statistics.

[8]The KUMMER M-function is also denoted as $_1F_1$ sometimes.

[9]One simply uses the identity $se^{rs} = \frac{\mathrm{d}}{\mathrm{d}r}\mathrm{e}^{rs}$ and partial integration to obtain $r(1-r)\phi'(r) + \left[(\lambda-2)r - (\tilde{\lambda}-1)\right]\phi(r) = 0$.

Now the solution is rewritten in parameters a and b instead of $\tilde{\lambda}$ and λ to simplify representation. Therefore, we start with a brief discussion of the parameter range of λ_i. By defining the set

$$A \equiv \left\{ (\mu_1, \mu_2) \, \middle| \, 1 > \mu_1 > \mu_2 > \mu_1^2 > 0 \right\} \tag{4.31}$$

and the map

$$\sigma : A \to W \, , \quad \sigma(\mu_1, \mu_2) = \begin{pmatrix} \tilde{\lambda}(\mu_1, \mu_2) \\ \lambda(\mu_1, \mu_2) \end{pmatrix} \tag{4.32}$$

with $W = \left\{ (\tilde{\lambda}, \lambda) \, \middle| \, 0 < \tilde{\lambda} < \lambda < \infty \right\}$ we can prove that σ is one-to-one by elementary tools.[10] Transforming the parameters via

$$\begin{pmatrix} a \\ b \end{pmatrix} = \begin{pmatrix} 1 & 0 \\ -1 & 1 \end{pmatrix} \begin{pmatrix} \tilde{\lambda} \\ \lambda \end{pmatrix} \, , \tag{4.33}$$

which conserves one-to-one correspondence to A, yields a more symmetric representation of the mean field class

$$\mathcal{M} = \mathcal{M}_{\text{cont}} \cup \mathcal{M}_\delta \tag{4.34}$$

with

$$\mathcal{M}_{\text{cont}} = \left\{ \phi_{a,b}(r) = \frac{\Gamma(a+b)}{\Gamma(a)\Gamma(b)} r^{a-1}(1-r)^{b-1} \, \middle| \, a, b \in \mathbb{R}^+ \right\} \tag{4.35}$$

and

$$\mathcal{M}_\delta = \left\{ \delta(r - \mu_1) \, \middle| \, \mu_1 \in (0, 1) \right\} \, . \tag{4.36}$$

The set of symmetric densities represents an interesting subclass of (4.35):

$$\mathcal{M}_{\text{cont}}^{\text{s}} = \left\{ \phi_a(r) = \frac{\Gamma(2a)}{\Gamma(a)^2} \left[r(1-r) \right]^{a-1} \, \middle| \, a \in \mathbb{R}^+ \right\} \, . \tag{4.37}$$

A discussion of the mean field models will be given after deriving the associated mass distributions.

4.2.3. Explicit Form of $P(m)$

After determining the class $\mathcal{M}$ of fraction densities leading to a product measure we now like to calculate the single-site mass distributions $P(m)$ for these $\phi \in \mathcal{M}$. From the $(n+1, n)$-condition (4.18) we derive the recurrence relation

$$\lambda \, (n+1)a_{n+1} + \rho \, (n+\lambda)a_n = 0 \tag{4.38}$$

---

[10]From (4.25) the relations $\lambda_i(A) = \mathbb{R}^+$ and $\tilde{\lambda}(\mu) < \lambda(\mu)$ for all $\mu \in A$ are derived which prove $\sigma(A) \subseteq W$. Furthermore, $\sigma(\mu)$ can be inverted in a unique way ensuring injectivity. By $\sigma^{-1}(W) \subseteq A$ we complete the proof of surjectivity.

that is valid for all $n \in \mathbb{N}_0$ and where we used the relation

$$\lambda = a + b \;, \tag{4.39}$$

see (4.33). Equation (4.38) corresponds to a first order differential equation for the moment function $Q(s) = \sum_n a_n s^n$:

$$(\lambda + \rho s)\, Q'(s) + \lambda \rho\, Q(s) = 0 \;. \tag{4.40}$$

Using the boundary condition $Q(0) = 1$ we obtain

$$Q(s) = \frac{1}{\left(1 + \frac{\rho}{\lambda} s\right)^\lambda} \tag{4.41}$$

or, by calculating the inverse LAPLACE-transform,

$$P_\lambda(m) = \frac{\lambda^\lambda}{\Gamma(\lambda)} \frac{1}{\rho} \left(\frac{m}{\rho}\right)^{\lambda - 1} e^{-\lambda \frac{m}{\rho}} \;. \tag{4.42}$$

In contrast to (4.35) depending on both a and b, $P(m)$ is a function of $\lambda = a + b$ only. So ARAPs with λ fixed, but arbitrary a (or b), have identical mass distributions (4.42).

4.2.4. Classification of the Mean Field Models

Although the mean field models are parameterized by a two-dimensional manifold, the associated mass distributions (4.42) are connected to a one-dimensional parameter space only. However, we have to keep in mind that this conclusion concerns only the steady state, i.e. the way how two systems reach the infinite time limit could differ completely.

From (4.42) we could divide the (a, b)-models given by (4.35) into three classes whereby a few representative distributions are given in figure 4.1 for illustration:

1. $\lambda > 1$: The probability density $P(m)$, defined for all m, is determined by the algebraic part for small and by the exponential part for large masses. So we obtain $P(0) = 0$ while the peak of the distribution can be found at $m^\star = (1 - \frac{1}{\lambda})\rho < \rho$. For $\lambda \to \infty$ the curve sharpens and $P_\infty(m) = \delta(m - \rho)$ is obtained because we get

$$P_\lambda(m^\star) = \frac{1}{\rho} \frac{\lambda^\lambda e^{-\lambda}}{\Gamma(\lambda)} \underbrace{\left(1 + \frac{(-1)}{\lambda}\right)^\lambda}_{\to 1 \text{ for large } \lambda} \frac{\lambda}{\lambda - 1} e \approx \frac{1}{\rho} \frac{e^{(\ln\lambda - 1)\lambda}}{\Gamma(\lambda)} \approx \frac{1}{\rho} \frac{\Gamma(\lambda + 1)}{\Gamma(\lambda)} \to \infty \quad (4.43)$$

by STIRLING's formula and[11] $P(m) = 0$ for $m \neq m^\star$ with $\int P_\lambda(m)\mathrm{d}m = 1$ for all λ. In the particle picture these mass distributions correspond to configurations where particles do not glue together and arrange themselves with non-zero distances. So $\lambda > 1$ corresponds to a so-called free flow phase.

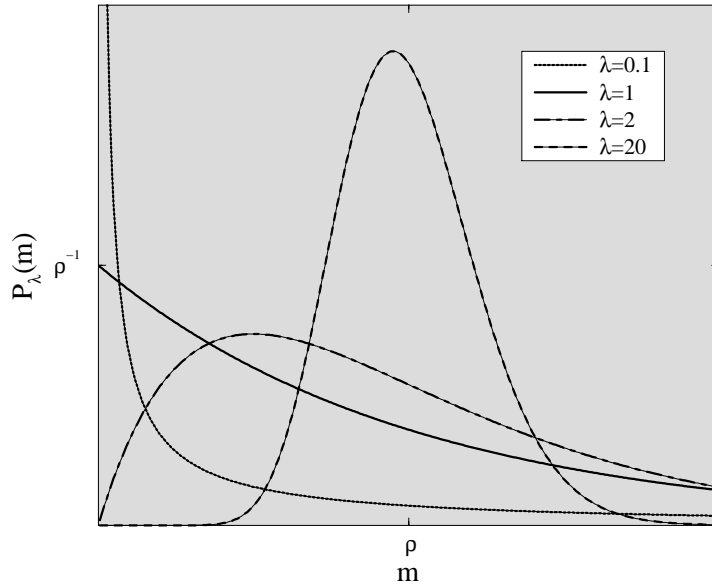[11] This result has been verified by computer algebra only.

Figure 4.1.: Exact mass distributions $P_\lambda(m)$ for different values of λ.

2. $\lambda = 1$: Here the mass distribution decays exponentially with vanishing algebraic corrections. It is $P(0) = \frac{1}{\rho}$ and particle bunching becomes more possible.

3. $\lambda < 1$: The density $P(m)$ diverges for $m \to 0$ and particles tend to bunch. So a lot of particles stick together forming jams while a few of them move freely. In the limit $\lambda \to 0$ we reach the set of critical fraction densities $\phi_p^{\mathrm{crit}}(r)$ defined in (4.13) where the mean field assumption fails. Correspondingly the result $P_{-1}(m) = \delta(m)$ is obtained which contradicts the law of mass conservation because $\langle m \rangle_{P_{-1}} = 0 \neq \rho$. But this discrepancy can be solved if we assume that the total mass is distributed on a finite number of sites only. Thus, a site is vacant with probability one in the thermodynamic limit which corresponds to $\delta(m)$. So we should better write $P_{-1}(m) = \delta(m) + \text{finite shares}$.

Now we consider the associated class $\mathcal{M}_{\mathrm{cont}}$ of ϕ-functions. The parameters a and b separately control the behaviour of ϕ at the domain borders and weigh the influence of "no shift" ($r = 0$) and "complete shift" ($r = 1$) dynamics in the fraction density. These processes seem to be completely different and compete each other. But a and b contribute to λ in the exact same manner (it is just a sum) and so processes focussing on rejection of mass transfers ($r = 0$) may yield the same steady state mass distribution as processes primarily shifting whole sticks ($r = 1$).

This symmetry becomes clearer if we compare the deterministic dynamics $\delta(r)$ and $\delta(1 - r)$. While the first one does not change the state of the system, i.e. $P(m, t + 1) =$

$P(m, t)$, the latter one only shifts the actual configuration to the right, i.e. $m \to \mathcal{R}m$[12].
If we assume translational invariance of the initial state, i.e $P(m, 0) = P(\mathcal{R}^n m, 0)$ for
all n, we derive the relation $P(m, t + 1) = P(m, t)$ like in the $\delta(r)$ case.

Nevertheless, we would like to remark that the
simple interpolation ϕ_p^{crit} between $\delta(r)$ and $\delta(1-r)$
given in (4.13) results in a critical behaviour for
$p \in (0, 1)$ because a stick may stay on its site or
hop and coalesce. So the total mass is located on
one site in the steady state and moves through the
system which corresponds to a critical state (see
figure 4.2), e.g. in case of the q-model this would
mean that the force exerted on the surface of a
granular material sums up and presses on one bead
only. This corresponds to an enormous stress lead-
ing to structural displacements or destruction. In
the steady state the finite system corresponds to
a one particle asymmetrically driven random walk
with hopping probability $1 - p$ and the mass dis-
tribution reads $P(m) = \sum_{i=0}^{L-1} \delta\left(\mathcal{R}^i \tilde{m} - m\right)$ with
$\tilde{m} = (M, 0, 0, \ldots)$. We derive for the single-site
density $P(m_i) = \frac{L-1}{L} \delta(m_i) + \frac{1}{L} \delta(M - m_i)$ which
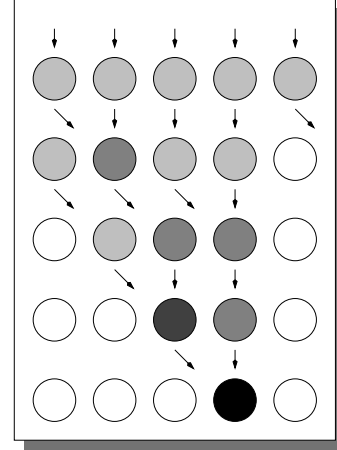fails in the limit $L \to \infty$.

Figure 4.2.: Force propagation in layers of beads modelled by ϕ_p^{crit}. The stress is visualized by the darkness of the marbles.

Back to the set $\mathcal{M}_{\text{cont}}$: For almost critical systems defined by $\lambda \leqslant 1$ the associated
ϕ-functions diverge for $r \to 0$ and $r \to 1$ because $a, b < 1$. Furthermore, the shape
of the ϕ graphs does not vary strongly. However, for $\lambda > 1$ the behaviour is more
diversified. Figure 4.3 shows that a lot of different fraction densities may lead to the
same P_λ. In general there are four classes of ϕ densities: continuous functions with
$\phi(0), \phi(1) \in \{0, 1\}$, single peak functions with $\phi(0) = \infty$ or $\phi(1) = \infty$ and double peak
functions with $\phi(0) = \phi(1) = \infty$. All four classes contribute to the $\lambda > 1$ regime (fig.
4.4). It is interesting that continuous and single peak densities, resp. single and double
peak densities, may lead to identical mass distributions. However, this is impossible in
case of continuous and double peak ARAPs.

4.2.5. Completion of the Proof

In this subsection we close the small gap still contained in the argumentation.

We have shown that a mean field ansatz always provides a unique solution for ar-
bitrary non-critical ϕ-functions. This solution should be exact if ϕ is an element of $\mathcal{M}$.
We have proven that the construction of $\mathcal{M}$ is unique in a sense that for given first and
second moments the corresponding fraction density leading to an exact product measure

---

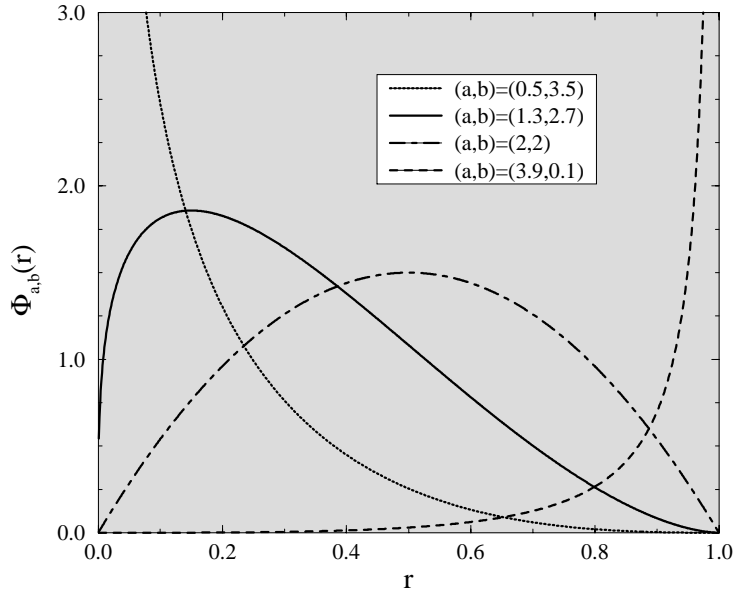[12]$\mathcal{R}m = (m_L, m_1, \ldots, m_{L-1})$, so $\mathcal{R} = T(1, 1, \ldots, 1)$.

Figure 4.3.: Several $\phi_{a,b}$ functions yielding the same stationary state defined by $\lambda = 4$.

state is unique. The first and second moments are only restricted to general moment properties, so $\mathcal{M}$ spans the whole set of "exact" fraction densities. But we have not given strict evidence that all elements of $\mathcal{M}$ really lead to exact factorized solutions because $\mathcal{M}$ has been derived as a conjecture of high order calculations only.

But this can be made up easily by inserting (4.35) resp. (4.36) and (4.41) in (4.7) and simple arithmetics lead us to $F_Q(s_1, 0) = \left(1 + \frac{s_1}{\lambda}\right)^{-b}$, $F_Q(0, s_2) = \left(1 + \frac{s_2}{\lambda}\right)^{-a}$ and $F_Q(s_1, s_2) = \left(1 + \frac{s_1}{\lambda}\right)^{-b} \left(1 + \frac{s_2}{\lambda}\right)^{-a}$ (with ρ set to one) completing the proof. We would like to add that these calculations could also be done by the help of FEYNMAN parameters introduced below.

Nevertheless, there is an alternative approach of finding a set of exact mean field solutions. It has been used in the context of the q-model [8, 9] and can be adopted without efforts to the ARAP. While the constructive ansatz given before provides an explicit representation of $\mathcal{M}$ as the final result, we will obtain functional forms of ϕ and Q directly in the following calculations. But there remains the outstanding task of proving that there are no other solutions which has been done as first step in the presented constructive approach.

The following considerations are based mainly on FEYNMAN parameters which is nothing else than the formula

$$\prod_{i=1}^{n} x_i^{-\alpha_i} = \Gamma\left(\sum_{i=1}^{n} \alpha_i\right) \prod_{i=1}^{n} \left(\Gamma(\alpha_i)\right)^{-1} \int_0^\infty \mathrm{d}^L r \delta\left(\sum_{i=1}^{n} r_i - 1\right) \prod_{i=1}^{n} r_i^{\alpha_i - 1} \left(\sum_{i=1}^{n} r_i x_i\right)^{-\sum_{i=1}^{n} \alpha_i}.$$
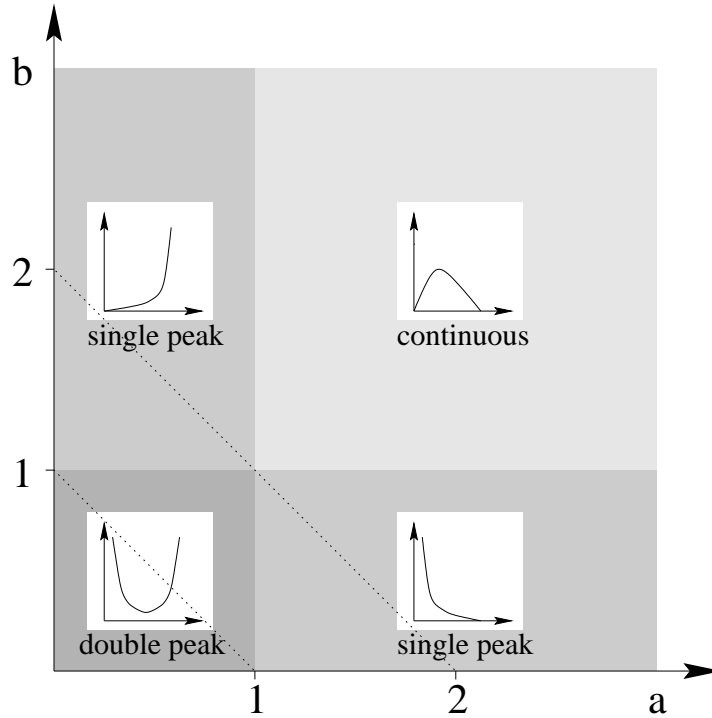
$$(4.44)$$

Figure 4.4.: Classes of ϕ-functions in dependence of a and b. The dotted lines correspond to $\lambda = 1$ and $\lambda = 2$.

A derivation of (4.44) is given in [40] where it is used for the calculation of FEYNMAN diagrams. It includes a nice substitution that introduces and integrates out an additional variable.

In [8] (4.44) has been used to show the exactness of solutions belonging to density generators $g(q) = q^n$ with $n \in \mathbb{N}_0$. For an explanation of g please refer to (2.29) again. Six years later it was noticed [9] that the FEYNMAN parameters are also defined for positive real exponents α_i which enables an enlargement of the scope to $n \in \mathbb{R}^+$. Ultimately a last upgrade of (4.44) is given by switching from symmetric (q-model) to antisymmetric (ARAP) density functions which we will present in more detail now.

In the last subsections equation (4.7) was the origin of all forthcoming considerations but here we will work with the equivalent representation (4.8). Using the set of parameters

$$n = 2 \quad , \quad x_i = (1 + \omega s_i) \quad , \quad \alpha_1 = b \quad \text{and} \quad \alpha_2 = a \tag{4.45}$$

with ω as a free parameter, equation (4.44) rereads

$$\frac{1}{(1 + \omega s_i)^a} \frac{1}{(1 + \omega s_{i+1})^b} = \int_0^1 \mathrm{d}r \frac{\Gamma(a + b)}{\Gamma(a)\Gamma(b)} \frac{r^{a-1}(1 - r)^{b-1}}{(1 + \omega\left[(1 - r)s_i + rs_{i+1}\right])^{a+b}} \ . \tag{4.46}$$

Multiplying over i, rearranging the left side and comparing with (4.8) yields (4.41) and

(4.35) immediately. The free parameter ω is determined by the boundary conditions (2.52).

Finally, the most enfolding application of FEYNMAN parameters is an antisymmetric q-model (which reduces to a state independent ARAP for two dimensions).[13]

4.3. Explicit Solution for Monomial ϕ-Function

In this section we derive the solution of the ARAP with density function

$$\phi_n(r) = (n-1)r^{n-2} \qquad (\forall n \in \mathbb{N}_{\geqslant 2}) \tag{4.47}$$

in a closed form ($n-1$ is the normalization constant) and prove the exactness of the product measure $\prod_k P(m_k)$ explicitly. It is clear from (4.35) that (4.47) is a subset of $\mathcal{M}_{\text{cont}}$, so the following calculations act mainly as an example. Additionally, a brief comparison between ARAP and the q-model is presented.

We start by constructing the analytic solution of the functional equation (4.6) explicitly. For $n = 2$, where ϕ_n reduces to a constant distribution, we refer to [1, 2, 8] and find

$$Q_2(s) = \frac{1}{\left(1 + \frac{\varrho}{2}s\right)^2} \ . \tag{4.48}$$

To solve the problem for $n = 3$ we generalize the method used in [1, 2, 8] and presented in section 2.3. Defining the functions

$$V(s) = \int_0^1 \mathrm{d}r \, Q_3(rs) \quad \text{and} \quad W(s) = \int_0^1 \mathrm{d}r \, r \, Q_3(rs) \tag{4.49}$$

the functional equation (4.6) transforms into

$$Q_3(s) = 4W(s)\left(V(s) - W(s)\right) \ . \tag{4.50}$$

From (4.49) we derive

$$sV'(s) + V(s) = Q_3(s) = sW'(s) + 2W(s) \tag{4.51}$$

which implies the following relation between V and W:

$$V(s) = W(s) + \frac{1}{s}\int W(s)\mathrm{d}s \ . \tag{4.52}$$

Defining the anti-derivative $f(s) \equiv \int W(s)\mathrm{d}s$ and inserting (4.52) and (4.51) into (4.50) yields the nonlinear differential equation

$$s^2 f''(s) + 2s f'(s) - 4f'(s)f(s) = 0 \tag{4.53}$$

---

[13]Private conversation with Prof. van Leeuwen and Jacco Snoeijer.

with boundary conditions $f'(0) = \frac{1}{2}$ and $f''(0) = -\frac{1}{3}\rho$. This results in $f(s) = \frac{s}{2}\left(1 + \frac{\rho}{3}s\right)^{-1}$, e.g. solved by a power series ansatz, and we get

$$Q_3(s) = \frac{1}{\left(1 + \frac{\rho}{3}s\right)^3} \ . \tag{4.54}$$

The results (4.48) and (4.54) suggest the assumption

$$Q_n(s) = \frac{1}{\left(1 + \frac{\rho}{n}s\right)^n} \ , \tag{4.55}$$

for general n. Q_n fulfills the initial conditions (2.52). By a straightforward induction in n (using partial integration) we are able to prove

$$F_{Q_n}(s, 0) = \frac{1}{1 + \frac{\rho}{n}s} \quad \text{and} \quad F_{Q_n}(0, s) = \frac{1}{\left(1 + \frac{\rho}{n}s\right)^{n-1}} \tag{4.56}$$

and see with (4.55) that (4.6) is valid.

The next step is to verify the functional equation (4.7). This is again done straightforwardly by induction in n. So (4.55) represents the exact solution of the ARAP with fraction density (4.47).

Additionally, we rederive (4.55) using the mean field criterion in moment representation (4.24-4.25). Calculating the moments of ϕ_n exactly is an easy task and yields

$$\mu_k = \frac{n-1}{n-1+k} \ . \tag{4.57}$$

In particular, we have $\mu_1 = \frac{n-1}{n}$ and $\mu_2 = \frac{n-1}{n+1}$ and, using (4.25), we obtain $\tilde{\lambda} = n - 1$ and $\lambda = n$.

The exact form (4.57) of the moments is reproduced by taking into account (4.24). Thus, the monomial density functions ϕ_n are elements of $\mathcal{M}$. Using $\lambda = n$ after all, shows the equivalence of (4.41) and (4.55).

For completeness we also give the explicit form of the single-site mass distribution for the monomial density functions (4.47):

$$P_n(m) = \frac{n^n}{(n-1)!} \frac{m^{n-1}}{\rho^n} e^{-n\frac{m}{\rho}} \ . \tag{4.58}$$

Finally, we like to mention that Q_n also satisfies the relation

$$Q_n(s) = (F_{Q_n}(0, s))^n = \left[\int_0^1 dr \ \phi_n(r) Q_n(rs)\right]^n \ . \tag{4.59}$$

This functional equation represents the master equation of the n-ancestor q-model with uniform distributed q's and was explicitly solved in [8]. Because of the formal difference

of the underlying equations (4.6) and (4.59) the coincidence of the corresponding solution (4.55) is remarkable. On the other hand, this result is pointing to the deeper relationship between the n-dimensional q-model and the ARAP.

As already noticed in section 2.2.1 the two-ancestors q-model ($n = 2$) corresponds to an ARAP with symmetric density function $\phi(r) = \phi(1 - r)$. COPPERSMITH *et al.* [8] identified a set of mean field solutions generated by monomial distributions, i.e. $g(q) = q^m$. By using (2.33) this result is translated into the language of the ARAP and we obtain $\phi(r) = \frac{(2m+1)!}{(m!)^2} r^m (1 - r)^m$. Comparing with (4.37) we notice that this class of fraction densities is a subset of $\mathcal{M}_{\text{cont}}^{\text{s}}$.

However, in [9] all densities leading to product measures have been identified for the q-model. They are given by $g(q) = q^m$ with $m \in \mathbb{R}^+$. Rewriting this result for the two-dimensional q-model, $n = 2$, in terms of ϕ-functions, we obtain the solution space $\mathcal{M}_{\text{cont}}^{\text{s}}$. Surprisingly, the same set of mass distributions is obtained for any dimension n, i.e. we do not obtain new kinds of solutions by increasing the range of interaction. Actually, the set of solutions is even identical to the class (4.42). However, the underlying master equations differ marginally.

4.4. Finite Systems

In this section we present the exact product mass distributions for finite systems.

For $L < \infty$ the configuration space can be restricted to

$$F_L(M) \equiv \left\{ m \in S^{\otimes L} \, \middle| \, \sum_i m_i = M \right\} \tag{4.60}$$

due to mass conserving dynamics. Renormalization of the mass density completes this procedure and we obtain

$$P_\lambda^{(L)}(m_1, \ldots, m_L) = \begin{cases} \frac{1}{Z} \prod_{i=1}^{L} P_\lambda(m_i) & m \in F_L(\rho L) \\ 0 & \text{else} \end{cases} \tag{4.61}$$

with

$$Z = Z(\lambda, \rho, L, \rho L) \equiv \int_{F_L(\rho L)} \mathrm{d}^L m \prod_{i=1}^{L} P_\lambda(m_i) = \frac{1}{\rho L} \frac{(\lambda L)^{\lambda L}}{\Gamma(\lambda L)} \mathrm{e}^{-\lambda L} . \tag{4.62}$$

Thus, projection onto the $F_L(\rho L)$ surface, i.e. fixing the total mass, corresponds to reducing our focus from grand-canonical to a canonical point of view whereby Z corresponds to the canonical partition sum. A detailed calculation of Z is given in appendix A.2.

One should keep in mind that the exact solutions (4.61) are still of product measure form if restricted on $F_L(\rho L)$. However, this coincidence with the $L = \infty$ case is only formal, e.g. the one-site mass density is *not* simply given by $Z^{-\frac{1}{L}} P(m)$. One has to take

into account the additional interaction induced by the restriction $m \in F_L(\rho L)$. So we derive by using the relation (A.5) again:

$$P_\lambda^{(L)}(m_i) = \int\limits_{F_{L-1}(\rho L - m_i)} \mathrm{d}^{L-1}\tilde{m} \, \frac{1}{Z} P_\lambda(m_i) \prod_{i=1}^{L-1} P_\lambda(\tilde{m}_i) = \frac{Z(\lambda, \rho, L-1, \rho L - m_i)}{Z(\lambda, \rho, L, \rho L)} P_\lambda(m_i) \,.$$

(4.63)

In figure 4.5 we compare our results for the single-site distribution with numerical data and find excellent agreement. Furthermore, the $L = \infty$ result is given, exemplifying the influence of finite-size effects.

Finally, we would like to add that $P_\lambda^{(L)}(m_i) \sim (L\rho - m_i)^{\lambda(L-1)-1} m_i^{\lambda-1}$. So the mass density may diverge or tend to zero at the boundaries $m_i = 0$ and $m_i = L\rho$. The limits depend on λ and L and may differ for both boundaries.
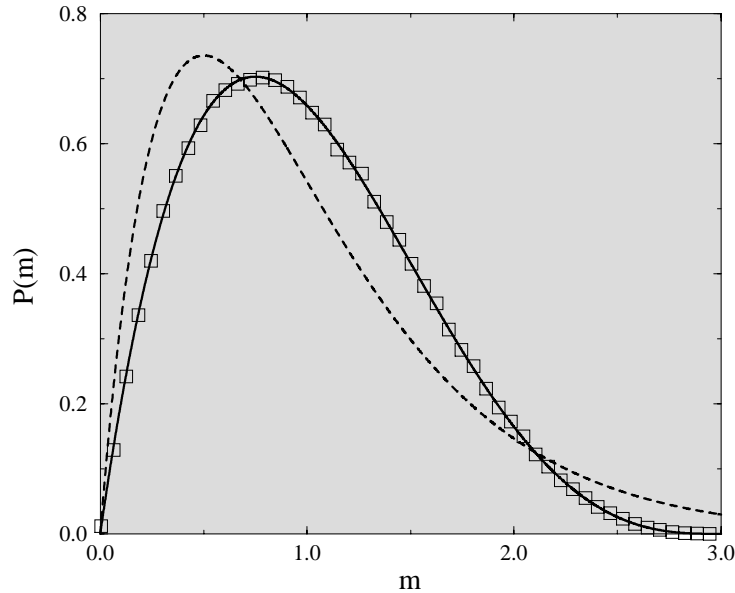

Figure 4.5.: Exact analytical (line) and numerical ($\square$) single-site mass densities $P_\lambda(m)$ for $\lambda = 2$ (free ARAP), $\rho = 1$ and $L = 3$. The dashed line shows the corresponding values for $L = \infty$.

4.5. Continuous Time Dynamics

In this section we derive the set of all exact solutions with product measure form for the random sequential update by using the "interpolation formula" (2.20), i.e. we look for fraction densities ϕ where the interpolated functions ϕ_p are elements of $\mathcal{M}$ in the limit $p \to 0$.

Hereby taking the interpolation limit is the crucial point of the procedure. If we perform $p \to 0$ at the beginning, we obtain the trivial result $\phi_0(r) = \delta(r)$ which is of course not an element of $\mathcal{M}$ unless we redefine $\mathcal{M} \to \mathcal{M} - \delta(r)$ for the continuous time dynamics which corresponds to a non-normalized (and thus unphysical) set of fraction densities.

We start by deriving the mean field criterion for the random sequential update. Using (2.20) with (4.7) and performing the interpolation limit $p \to 0$, the condition

$$Q(s_1) = F_Q(s_1, 0) + Q(s_1)F_Q(0, s_2) - F_Q(s_1, s_2) \tag{4.64}$$

is obtained. By setting $s_1 = s_2 = s$ we are also able to calculate mean field approximations from

$$2Q(s) = F_Q(s, 0) + Q(s)F_Q(0, s) \ . \tag{4.65}$$

These equations correspond to (4.6) and (4.7) derived for the parallel update. However, we do not solve these lines explicitly as done in section 4.2, but use the results derived so far together with the interpolation formula (2.20).

So we directly attack the problem at the level of moments. The interpolated moments are given by

$$\mu_n^{(p)} := \langle r^n \rangle_{\phi_p} = \begin{cases} 1 & n = 0 \\ p\mu_n & n > 0 \end{cases} . \tag{4.66}$$

Calculating the p depending parameters $\tilde{\lambda}^{(p)}$ and $\lambda^{(p)}$ according to (4.25), inserting everything into the recursive formulation (4.23) and performing $p \to 0$, we obtain the conditions to be satisfied for an exact mean field solution. It is $\tilde{\lambda}^{(0)} = 0$ and $\lambda^{(0)} = \frac{\mu_1 - \mu_2}{\mu_2}$. So we get

$$\mu_{n+1} = \frac{n}{n + \lambda^{(0)}} \mu_n \tag{4.67}$$

and for $n \geqslant 1$ everything is fine. However, for $n = 0$ (4.67) reduces to $\mu_1 = 0$ which yields $\mu_n = 0$ for $n \geqslant 1$ and combined with μ_0 we derive the trivial result $\delta(r)$ again.

But we have to keep in mind that (4.23) resp. (4.24) determine moments of order three and higher only, while the equations for μ_1 and μ_2 reduce to tautologies and are included in the formulas for cosmetic reasons only. For $n = 2$ this redundancy is even reproduced by (4.67), while it breaks down for $n = 1$, so we neglect the relation for the free parameter μ_1. Therefore, the moment representation of $\mathcal{M}$ is given by (4.67) restricted to $n \geqslant 1$ with $\mu_0 = 1$ and $(\mu_1, \mu_2) \in A$.

Now the question arises if there exists a ϕ-function or a distribution ψ reproducing these moments. This task is well known in the world of mathematics as the "Hausdorff's moment problem" or the "little moment problem" and HAUSDORFF was the first to obtain necessary and sufficient conditions for a sequence to be a moment sequence [41] and research is still active in this corner of statistics.

It is easy to see that (4.23) defines a strict monotonous sequence which is necessary. Furthermore, it is clear that the moment problem cannot be solved by using the values

$\tilde{\lambda}^{(0)}$ and $\lambda^{(0)}$ with (4.35) because we obtain a singularity in $r = 0$ due to $a = 0$. So let us work with the moment generator as defined in (4.27) again. F has to be an entire function because $\mu_n \leqslant 1$. Using (4.67) for $n \geqslant 1$ we obtain after some algebra the inhomogeneous differential equation

$$sF''(s) + \left(\lambda^{(0)} - s\right) F'(s) = \mu_1 \lambda^{(0)} \tag{4.68}$$

which can be rewritten as a KUMMER equation by differentiating once again (see also section 4.2.2):

$$sF'''(s) + \left(\lambda^{(0)} + 1 - s\right) F''(s) - F'(s) = 0 . \tag{4.69}$$

The solution is given by the holomorphic KUMMER M-function and considering the boundary condition $F'(0) = \mu_1$ we obtain $F'(s) = \mu_1 M\left(1, 1 + \lambda^{(0)}, s\right)$.

In general the relation between a KUMMER function and its derivative is given by the relation $M'(a, b, z) = \frac{a}{b} M(a + 1, b + 1, z)$ which is easily derived from the series presentation. But the formula cannot be applied here because of a formal singularity, so we cannot give a closed representation of F. But the comparison of the integral representation of F', see (4.29), and the alternative representation $F'(s) = \int_0^1 r\phi(r)e^{rs}dr$ yields a diverging ϕ-function again. So the detour via KUMMER functions does not give any new insight and we stay with a moment representation of $\mathcal{M}$ only.

Nevertheless, we would like to gain awareness of the shape of the fraction densities ϕ connected to (4.67). So an approximative fraction density $\phi^{(n)}$ is constructed for given moments $\mu_0, \ldots, \mu_n$, fulfilling the restrictions

$$\left\langle r^k \right\rangle_{\phi^{(n)}} = \mu_k, \quad k = 0, \ldots, n . \tag{4.70}$$

There are a lot of constructive approaches, e.g. [42] and references therein, but here we prefer a simple polynomial ansatz $\phi^{(n)}(r) = \sum_{l=0}^{n} a_l^{(n)} r^l$. Although this approach does not guarantee positivity in general, the curves $\phi^{(n)}$ will tend to the real curve ϕ for large n under the assumption that ϕ is (at least approximatively) representable by a series. However, the relation $\lim_n \phi^{(n)} = \phi$ is not mandatory, e.g. the polynomial ansatz could fail if ϕ involves δ functions.

So the construction of $\phi^{(n)}$ under (4.70) means solving the matrix equation

$$H^{(n)} a^{(n)} = \mu^{(n)} \tag{4.71}$$

with

$$a^{(n)} = \left(a_0^{(n)}, \ldots, a_n^{(n)}\right), \ \mu^{(n)} = \left(\mu_0^{(n)}, \ldots, \mu_n^{(n)}\right) \ \text{and} \ H^{(n)} = \left(\frac{1}{1 + k + l}\right)_{0 \leqslant k, l \leqslant n} . \tag{4.72}$$

Here $H^{(n)}$ are so-called HILBERT matrices [43]. They are symmetric and positive definite, so it follows $\det H^{(n)} > 0$. Thus, (4.71) has a unique solution for all n. Although $H^{(n)}$ is close to singular (the determinant is smaller than every matrix entry and strongly

decreasing with n), an explicit representation of the inverse exists[14] and (4.71) can be solved directly.

In figure 4.6 we have plotted several ϕ approximants of different orders n. Although the shape of $\phi^{(n)}$ seems to be rather reasonable for small n, the curves do not tend to a fixed function for large n. Oscillations arise with upcoming order n and the functional values explode: while $\phi^{(n)}(0)$ is negative and decreases weakly for increasing n (which seems to be in accordance with $\delta(r)$ derived before), we face $\phi^{(n)}(1) \to \infty$ at the other side of the domain whereby the divergence is much stronger here. But also in $(0, 1)$ the behaviour is far away from normal, e.g. the peaks of the oscillations are very large and seem to be quenched in direction of the left boundary of the domain.
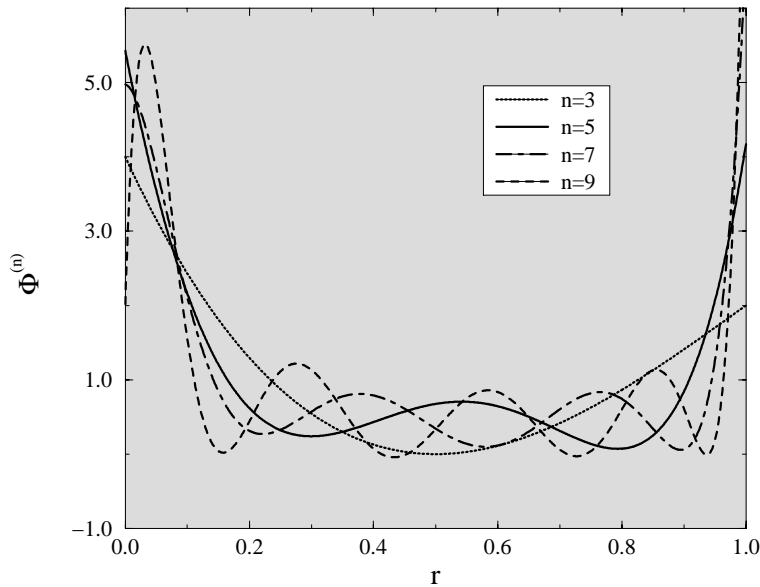

Figure 4.6.: Approximants $\phi^{(n)}$ for small orders n. The trends for $n \to \infty$ mentioned in the text can be read out already. However, $\phi^{(n)}$ is still positive here but this alters for larger n.

Beside of numerical problems occurring for high orders of n, this behaviour suggests that ϕ-functions leading to exact product states either are of pathological definition or cannot be given, i.e. they can be expressed on the level of moments only.

However, this constructive approach even fails if we feed in moments generated by double peak densities taken from $\mathcal{M}$![15] So the monomial basis r^l represents a poor choice and it may be possible that the construction of ϕ converges (better) for another basis.

Finally, we face the question if there has to be a generating ϕ-function for any given set of moments. It would be also possible to treat the sequence of moments as the

---

[14]The inverse $\hat{H}^{(n)} = (-1)^{k+l}(k + l + 1)\binom{n+k+1}{n-l}\binom{n+l+1}{n-k}\binom{k+l}{k}^2$ has integer entries only.

[15]Private communication with J. Snoeijer.

fundamental object instead of the probability density. On the other hand, we have to set up and verify conditions ensuring a reasonable set of moments, e.g. the moments may not contradict general moment inequalities like $\langle (r^2 - \mu_1)^2 \rangle \geqslant 0$ for example.[16]

4.6. Approximative Mass Distributions for Arbitrary Density Functions

In this section we present a heuristically motivated approximation method for state independent density functions. Additionally, we compare this ansatz with ordinary mean field solutions.

4.6.1. $\mathcal{M}$-Approximants

An appropriate approximant is chosen from the class $\mathcal{M}$ for arbitrary state independent fraction densities. This is done by calculating the parameter $\lambda = \lambda(\phi)$ with the help of (4.25) (using the exact moments μ_1 and μ_2 of ϕ) and taking the corresponding mean field solution (4.42) as an approximation. To illustrate this method and estimate its quality we consider two examples and discuss the quality of our ansatz briefly.

Our discussion starts with density functions being convex combinations of elements of $\mathcal{M}$. Here we restrict ourselves to the special case

$$\phi_c = (1 - c)\phi_2 + c\phi_3 \,, \quad c \in [0, 1] \tag{4.73}$$

with the monomial density functions ϕ_n defined in (4.47) whereby the extension to arbitrary ϕ_n is straightforward. This convex combination of probability densities conserves their basic properties like normalization or positivity. Calculating the first and second moment of ϕ_c yields

$$\lambda = \lambda_c = \frac{6}{3 - c^2} \,. \tag{4.74}$$

Inserting this result into (4.42) generates c-dependent approximations P_c.

Comparing the distribution P_c with numerical data shows an excellent agreement between approximation and the results of Monte-Carlo simulations for all values of c (see figure 4.7). Only for small masses m systematical differences occur.

Furthermore, one can prove that $\phi_c \notin \mathcal{M}$ for all $0 < c < 1$. This is most easily seen by comparing the third moment μ_3 of (4.73) with the corresponding mean field expression (4.24) or by verifying that it is impossible to rewrite ϕ_c as an element of (4.35). So the excellent agreement of the data match is far from trivial. Nevertheless, ϕ_c is an interpolation between exact mean field solutions and may inherit some of their properties.

---

[16]Added in proof: this condition is fulfilled by (4.67). Express μ_4 by μ_2, use $\mu_2 = (1 - \lambda^{(0)})\mu_1$ and show by simple arithmetics that the resulting inequality holds for all $\mu_1, \lambda^{(0)} \in (0, 1)$.
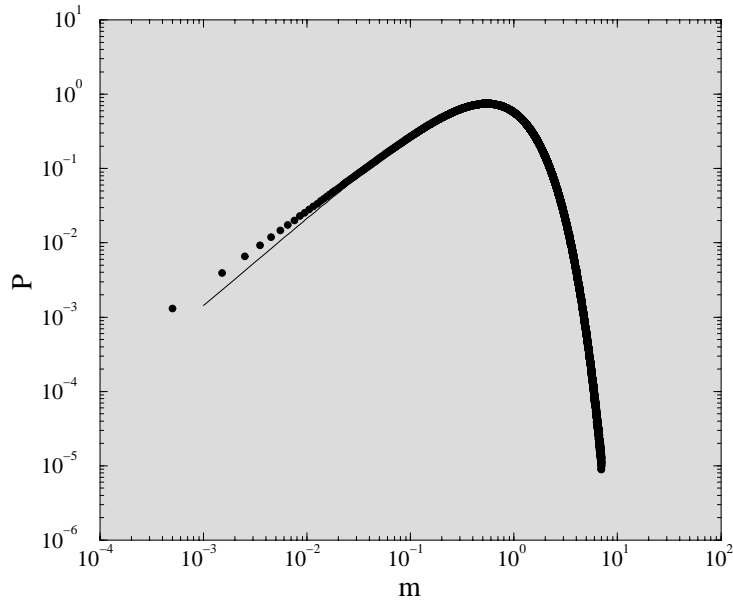
Figure 4.7.: Analytical ($-$) and numerical ($\bullet$) mass distributions $P(m)$ of the convex combined ARAP with $c = 0.5$. The analytical curves are appropriate approximants taken from the mean field class $\mathcal{M}$. The numerical results are obtained by Monte-Carlo simulations of systems with size $L = 1000$ and random initial condition. After 10^4 steps the distribution was measured for 10^7 timesteps. A log-log plot is used to exhibit the deviations for small masses m which can hardly be seen in a conventional representation.

Our second example represents the simplest version of an ARAP with cutoff. It is based on the model with uniform fraction density, but enhanced by an additional parameter $R \in [0, 1]$. The cut-off R controls the movement in the following way: A stick fragment $r_i m_i$ - whereby r_i is distributed uniformly - is only transferred if $r_i \leqslant R$. The corresponding density function takes the form:

$$\phi_R(r_i) = (1 - R)\delta(r_i) + \theta(R - r_i) \, . \tag{4.75}$$

A detailed discussion of several truncated ARAPs can be found in chapter 5.

If $R = 1$ we obtain the free ARAP which is exactly solvable by product measure ansatz (2.49). For $0 < R < 1$ one can show that $\phi_R \notin \mathcal{M}$. In the case $R = 0$, where no motion is possible, the mean field condition (4.7) reduces to an identity - so any distribution represents an exact mean field solution. In this sense (4.75) interpolates between ARAPs with product measure steady state as in the first example, but the construction is not a convex combination.

The approximants P_R are calculated as described above with

$$\lambda = \lambda_R = \frac{1}{R}\frac{6 - 4R}{4 - 3R} \tag{4.76}$$

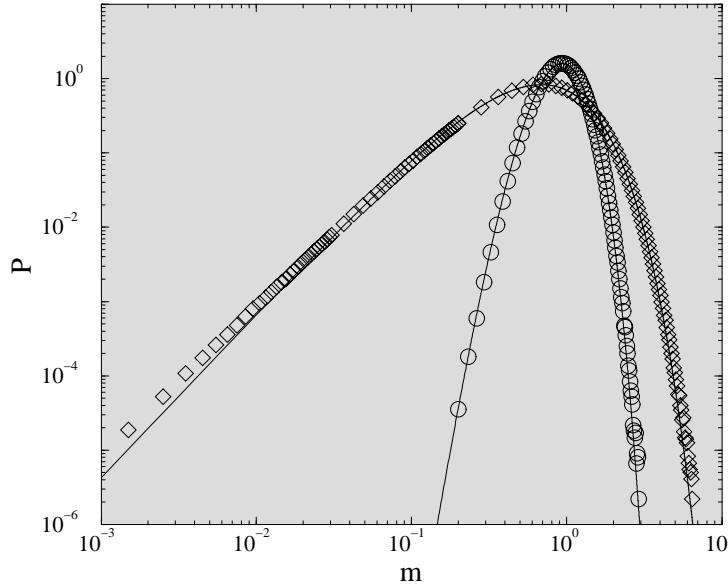and match the Monte-Carlo simulation data perfectly again except deviations for small m (see figure 4.8).

Figure 4.8.: Analytical $(-)$ and numerical $(\diamond, \circ)$ mass distributions $P(m)$ of the truncated ARAP with $R = 0.5$ $(\diamond)$ and $R = 0.1$ $(\circ)$. Setup for simulations as mentioned in figure 4.8.

It is interesting that our ansatz does not seem to take into account similarities between the given fraction density ϕ and the class $\mathcal{M}$, i.e. we do not study the relation to the set of $\phi_{a,b}$-functions, but work directly with the mass distributions P_λ. So it has to be discussed if the choice $\lambda = \lambda(\phi)$ filters the most appropriate approximant. Furthermore, we have to clarify how the quality of an approximation should be measured.

Finally, our method looks for the density $\phi_{a,b}$ that shares first and second moment with the given density ϕ. So we do not compare the shape of ϕ with $\phi_{a,b}$ but the information which is contained in the moments, and of course the low order moments have to fit primarily. So for arbitrary ϕ with moments μ_1 and μ_2 we have to pick $\phi_{a,b}$ with $a = \mu_1 \frac{\mu_1 - \mu_2}{\mu_2 - \mu_1^2}$ and $b = (1 - \mu_1) \frac{\mu_1 - \mu_2}{\mu_2 - \mu_1^2}$ which follows from (4.25) and (4.33) ensuring (4.39).

We have already seen that completely different ϕ-functions end up in the same P_λ distribution. So it is unreasonable to compare the shape of fraction densities. But $\phi_{a,b}$ densities lying on the line $a + b = \text{const}$ have completely different first and second order moments which contradicts the heuristic argument that the information is mainly stored in μ_1 and μ_2. So the interaction between μ_1 and μ_2 also plays an important role.

Now let us formalize the task: For given density ϕ we look for the most suitable approximation lying in the class $\mathcal{M}$. Keep in mind that this candidate does not have to

be the best approximant in general, not even the best approximant of product measure form. Furthermore, we do not know what kind of solution a mean field calculation of the problem would provide.

By using the metric induced by the 1-norm $\|P\|_1 = \int |P(m)| \mathrm{d}m$ we can define the following criterion: For a given fraction density ϕ the subset of suitable approximants $\mathcal{A}(\phi) \subset \mathcal{M}$ is defined by the relation

$$\forall \phi_{a,b} \in \mathcal{A}(\phi) \ : \quad \|P - P_{a+b}\|_1 = \min_{\lambda \in \mathbb{R}^+} \|P - P_\lambda\|_1 \tag{4.77}$$

whereby P is the (unknown!) exact solution corresponding to ϕ and P_{a+b} resp. P_λ is given by (4.42). The choice of $\|\cdot\|_1$ is natural because the associated metric sums up the differences between two functions. Furthermore, it is well defined for all probability densities because we restrict on the surface of the unit sphere $\|P\|_1 = 1$ while the 2-norm would yield divergences for some densities[17].

On the other hand, we could measure the quality by comparing the mass moments of exact and approximative distributions. If we restrict comparison to one moment only this can be done without difficulties. However, we face some problems if we want to take into account several (all) moments because this ansatz requires an appropriate weighting of the moments contributing to an adequately defined norm.

Concerning our approach we may not forget that the ARAP with state independent fraction density is a very gentle model. Based upon the fact that second order moments factorize mean field approximations always provide good data. For symmetric ϕ-functions even three point moments factorize which indicates vanishing three point correlations (at least in the infinite system) [9]. So mean field ansatzes yield even better results here. First in fourth order we obtain correlations for densities not belonging to $\mathcal{M}$.[18]

Finally, we would like to note that the approximants could also be used as initial configurations for fixed point algorithms, because solving the steady state master equation is nothing else then treating

$$P(m) = \mathcal{F}(P)(m) \tag{4.78}$$

with $\mathcal{F}$ defined in (2.13).

4.6.2. Mean Field Solutions vs. $\mathcal{M}$-Approximants

Here we consider an ARAP defined by

$$\phi(r) = (1-p)\delta(r) + p\delta(r - R) \tag{4.79}$$

with $p \in (0,1]$ and $R \in (0,1)$. With probability p the fraction R is transfered while the mass remains on its site with probability $1-p$. On the other hand, we can interpret

---

[17]e.g. for $P(m) \sim m^\alpha \mathrm{e}^{-\beta m}$ with $\alpha \in (-1, -\frac{1}{2})$

[18]Private conversation with Prof. van Leeuwen and Jacco Snoeijer.

(4.79) as an interpolation between parallel and random sequential update with density $\delta(r - R)$. For $p = 1$ we obtain the set of exact mean field solutions $\mathcal{M}_\delta$. Here we would like to focus on continuous time dynamics ($p \to 0$). Then the mean field equation (4.65) reads

$$2Q(s) = Q((1 - R)s) + Q(Rs)Q(s) .\tag{4.80}$$

By the ansatz (4.10) it is possible to give a recursively defined solution of (4.80) similar

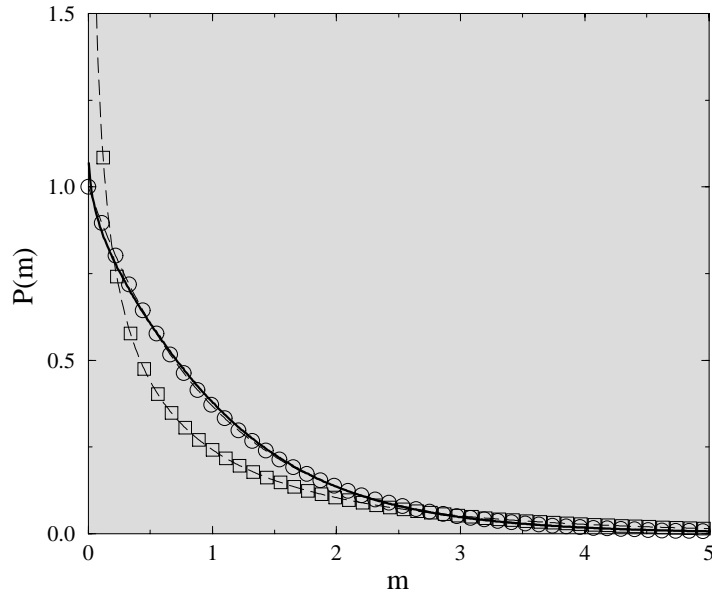
Figure 4.9.: Comparison between numerical data (bold line), mean field ansatz ($\circ$) and $\mathcal{M}$-approach ($\square$) for $\phi(r) = \delta(r - \frac{1}{2})$ and random sequential dynamics.

to (4.11). For the case $R = \frac{1}{2}$ this relation simplifies to

$$a_n = \frac{1}{1 - \left(\frac{1}{2}\right)^{n-1}} \sum_{k=1}^{n-1} \left(\frac{1}{2}\right)^k a_k a_{n-k} \tag{4.81}$$

with $a_0 = 1$ and $a_1 = -\rho$ as usual and the corresponding explicit representation reads $a_n = (-1)^n \rho^n$ which can be proved easily. So the mean field solution becomes

$$Q(s) = (1 + \rho s)^{-1} .\tag{4.82}$$

Interestingly the functional form is identical to a $\lambda = 1$ solution, see (4.41) or (4.42), although this is not valid in general as the mean field solutions for $R \neq \frac{1}{2}$ show. In appendix A.1 we enhance our considerations to the neighbourhood of $R = \frac{1}{2}$.

From (4.67) we see that (4.79) is not an element of the class of exact mean field solutions in the continuous time limit. Nevertheless, we find an $\mathcal{M}$-approximant by

determining $\lambda = \lambda^{(0)} = 1 - R$ and for $R = \frac{1}{2}$ the approximation $Q(s) = (1 + 2\rho s)^{-\frac{1}{2}}$ is obtained.

So $\mathcal{M}$-approach and mean field approximation yield different results and figure 4.9 proves that the $\mathcal{M}$-approach lacks of quality in case of random sequential dynamics while the mean field ansatz still yields very good results. Nevertheless, we have to study the failure of the $\mathcal{M}$-approximation into more detail.

Finally, we would like to add that a more general solution of (4.80) is of the form

$$Q(s) = \frac{1}{1 + sg(\ln s)} \tag{4.83}$$

with $g(s - \ln 2) = g(s)$. This can be verified by inserting. However, $g \circ \ln$ must be analytic in zero here. From periodicity we obtain the relation $g \circ \ln(s) = g \circ \ln\left(\frac{s}{2^n}\right)$ for all $n \in \mathbb{N}$ which yields by applying the "Identitätssatz" that $g \circ \ln$ has to be constant.

5. Nonsymmetric Ergodicity Breaking in an Ultralocal ARAP

In this chapter we focus on truncated random average processes. They are characterized by constraints on fundamental variables, e.g. the mass per site or the transfer per site. On the one hand, this subclass is closely related to physical problems and offers a lot of interesting phenomena, on the other hand, an analytical treatment is difficult and the results obtained are mainly based on simulations and approximative calculations.

We introduce truncated ARAPs in concern with transport problems of Internet and road traffic (section 5.1). By rewriting these examples in terms of ϕ-functions we obtain three different kind of truncated ARAPs:

❏ a fully truncated ARAP (F-TARAP) given by a local (two-site) state-dependent fraction density and bounded mass variables,

❏ a truncated ARAP (TARAP)[1] given by an ultralocal state-dependent fraction density and bounded absolute mass shift and

❏ a mean field version of the truncated ARAP (MF-TARAP) given by a state-independent fraction density and bounded fractional mass shift.

In the following we mainly focus on the investigation of the TARAP. Although equipped with short-range interaction this process shows the surprising behaviour of nonsymmetric ergodicity breaking which implies a state space decomposition into dynamically unconnected subsets not related by a symmetry. While examples of phase transitions [5] and spontaneous symmetry breaking [25, 44] are known for 1D nonequilibrium systems, this kind of phenomenon seems to be undiscussed and relevant for various applications.

We give a brief discussion of F-TARAP and MF-TARAP in section 5.2, point out relations to the TARAP and go on with intensive numerical (section 5.3) and analytical (section 5.4) studies to obtain the phase diagram of the TARAP in detail. Here the feature of nonsymmetric ergodicity breaking is also met.

---

[1]This name, reflecting the whole class, has been chosen due to the prime example function of this model.

In section 5.5 we work out the connections between the TARAP and the Krauss model, see also section 2.2.2, and show the similarities between both phase diagrams. Finally, we compare the TARAP with stochastic models showing related phenomena, e.g. spontaneous symmetry breaking or the occurrence of infinite aggregates, to classify the effect observed in the TARAP (section 5.6).

Please note that some of the results presented here can also be found in [37, 45].

5.1. Truncated ARAPs

As mentioned in the introduction (see section 2.2) the ARAP represents a comprehensive model for transport along linear chains. Here we would like to introduce two examples that are inspired from different areas of application (Internet and road traffic) but may be reduced to ARAPs with identical fraction densities (F-TARAP). We conclude by deriving the offsprings TARAP and MF-TARAP.

5.1.1. Internet Transport

The modelling of the Internet has recently become a research interest also for physicists, for example see [46, 47]. The World Wide Web can be considered as a network of routers that shuffle information among each other. So fundamental and crucial questions deal with an effective workflow and correspondingly an important task is given by the maximization of local and global data flows. Here we focus on a minimal representation of the problem in the framework of the ARAP: a ring of routers $\{i\}$ with actual storage m_i transfers data packages in a preferred direction. Multiple and uncorrelated requests ("pings") occurring on a smaller timescale than the unit time ΔT, and different sizes of the data packages to be transmitted are realized by transporting only random fractions $\Delta_i = r_i m_i$ to the next neighbour per unit timestep whereby the fraction density ϕ should be uniform to simplify matters. The underlying update is parallel reflecting the independence of the routers. Additionally, we would like to include a uniform maximum capacity B of the routers. Whenever the transfer of a data package Δ_i would exceed the free capacity of the successor, expressed by $B - m_{i+1}$, the shift is omitted.

5.1.2. Street with Traffic Lights

While modelling of highway traffic is well established and understood in theoretical physics (see [12] and references therein), the description of city traffic [48, 49] is still at the beginning due to a higher degree of complexity: streets form a network, cars move on different routes with individual destinations and external control tools like traffic rules, signs or lights intervene in dynamics. Here we focus on cars moving on a perodical closed one way street that is equidistantly divided by L traffic lights. Each section may contain B vehicles at a maximum and the number of cars in front of a traffic light i is

given by m_i. We assume all traffic lights to switch signals simultaneously and restrict the distance covered by a car in a green light phase to one segment. So cars can only hop from one traffic light to the next, but due to randomly distributed delays in accelerating the number of vehicles crossing per unit timestep ΔT (defined by the length of the green light phase) varies and is given by $\Delta_i = r_i m_i$. For simplicity we work with a uniform fraction density ϕ henceforth. If the number of moving cars Δ_i exceeds the free space $B - m_{i+1}$, only the amount $B - m_{i+1}$ is transferred.

This model could be considered as a simplified and one-dimensional version of the CHOWDHURY-SCHADSCHNEIDER (CS) model [49]: while in the CS model the movement of all cars is calculated individually according to the NaSch rules, here the vehicles per street are understood as a new entity with properties depending on the number of cars only and incorporated in the fraction density.

5.1.3. Abstraction

It is quite evident that both models are strongly related and under the following changes they can be identified with each other. First we assume the state variables in the traffic model to be continuous. This means no problematic variation - we shift from the number of cars per segment to the total length of the queue in front of the traffic light. Since vehicles are not of the same length in general this approach seems to be more appropriate than the discrete one. Secondly we mutate the traffic update rule: instead of transferring the maximal possible queue length, we refuse the move if the boundary B would be exceeded. Although this changes the underlying physics, we can now deal with one unified model given by the following formal definition.

The fully truncated ARAP (F-TARAP) is defined on the bounded local state space $[0, B]$ equipped with parallel dynamics given by

$$\phi(r_i, m_i, m_{i+1}) = [1 - R(m_i, m_{i+1})]\,\delta(r_i) + \theta\left(R(m_i, m_{i+1}) - r_i\right)\,. \tag{5.1}$$

Here the critical (= maximal allowed) fraction R depends on m_i and m_{i+1} via

$$R(m_i, m_{i+1}) \equiv \min\left(\frac{B - m_{i+1}}{m_i}, 1\right)\,. \tag{5.2}$$

A graphical visualization can be found in figure 5.1. We skip the argument of R whenever possible.

We see that for $m_i \leqslant B - m_{i+1}$ the local update procedure reduces to the free ARAP. For $m_i > B - m_{i+1}$ the case $\Delta_i > B - m_{i+1}$, i.e. $r_i > R$, occurs with probability $1 - R$ resulting in a no jump modelled by an appropriately weighted $\delta(r_i)$.[2]

So the F-TARAP is locally state-dependent. Furthermore, we assume $m_i \leqslant B$ yielding the condition $\rho \leqslant B$. In the following we reduce the degree of complexity and present two variations belonging to the class of ultralocal and state-independent ARAPs.

---

[2]Please note that the original traffic model is given by $\delta(R(m_i, m_{i+1}) - r_i)$ instead of $\delta(r_i)$ in (5.1), i.e. moves are not rejected.
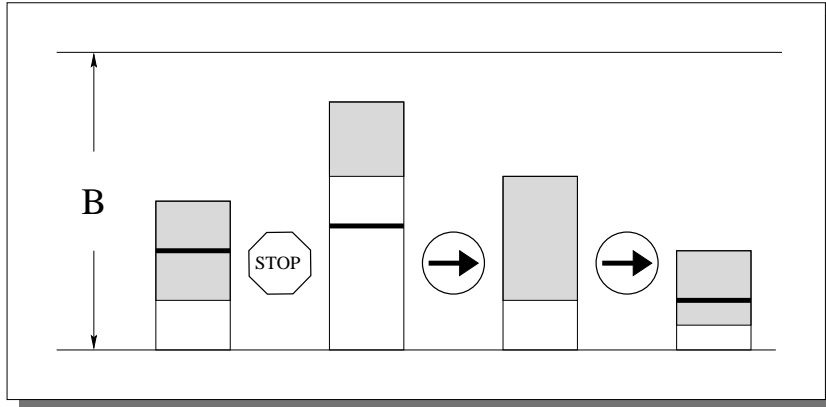
Figure 5.1.: Fully truncated ARAP (F-TARAP) as defined in (5.1) and (5.2). The thick lines determine the mass shift limit $B - m_{i+1}$ while the grey pieces assign the randomly chosen fragments Δ_i to transfer. Rejected or allowed moves are labelled by STOP or GO signs.

By the assumption $R(m_i) = R(m_i, \rho)$ we obtain an ultralocal ARAP. This ostensible simplification corresponds to a mean field like approximation reflecting $m_{i+1} \approx \langle m_{i+1} \rangle = \rho$. Introducing[3] $\Delta \equiv B - \rho > 0$ we obtain

$$R(m_i) = \min\left(\frac{\Delta}{m_i}, 1\right) . \tag{5.3}$$

This model simply denoted as truncated ARAP (TARAP) has no mass restricting dynamics anymore (see figure 5.2), so the corresponding local state space is $\mathbb{R}_0^+$ again.[4] Most important is the fact that in the TARAP the maximum transfer is restricted to Δ. Every time a chosen fragment exceeds Δ, the move is rejected.

This model fits to a lot of transport problems. In context of the Internet it corresponds to a router system where all routers have infinite storage capacity, but transfer is limited by a maximum band width Δ. Also the KRAUSS traffic model can be related to the TARAP which will be shown in section 5.5

Finally, we would like to present a state-independent version derived by the double mean field like ansatz $R = R(\rho, \rho)$. The resulting critical R reads now

$$R(K) = \min(1, K) \tag{5.4}$$

with $K = \frac{B-\rho}{\rho} > 0$. So for $K \geqslant 1$ we obtain the free ARAP while $K \in (0, 1)$ reproduces the model already presented in section 4.6.1, eq. (4.75), from now on called mean field TARAP (MF-TARAP).

---

[3]To avoid misunderstandings we neglect the fragment variable Δ_i from now on.

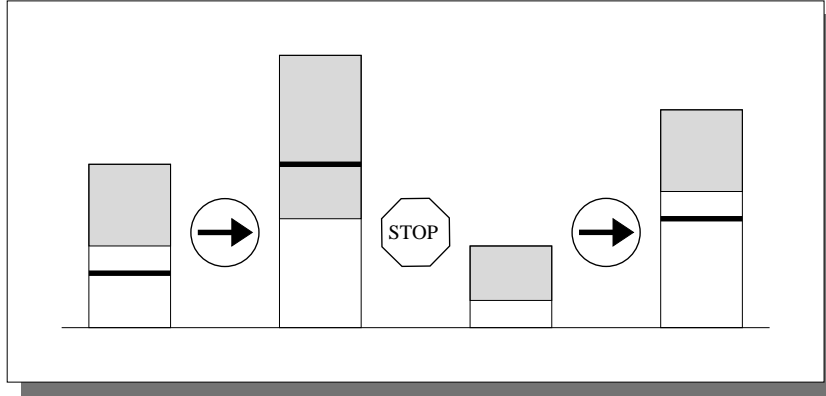[4]It is always possible to reduce the local state space to $[0, \rho L]$ for finite L.

Figure 5.2.: Truncated ARAP (TARAP) as defined in (5.1) and (5.3). Now the mass shift limits, illustrated by the thick lines, are constant ($= \Delta$) compared to the F-TARAP.

So all truncated models (F-TARAP, TARAP and MF-TARAP) are equipped with an additional cutoff parameter (beside the system parameters size L and density ρ) restricting the mass per site (B), the shifted mass (Δ) or the transferred fraction of mass (K).

5.2. MF-TARAP and F-TARAP

In this chapter we briefly discuss the MF-TARAP and the F-TARAP numerically and analytically. This is done mainly to provide a better understanding of the exceptional position of the TARAP compared to its direct relatives.

We begin with the calculation of the average current per site i generally defined by

$$J_i \equiv \langle r_i m_i \rangle_{P,\phi} \equiv \int_0^\infty dm_i \ldots dm_{i+k} \, P(m_i, \ldots, m_k) \underbrace{\int_0^1 dr_i \, \phi(r_i, m_i, \ldots, m_{i+k}) \, r_i m_i}_{\equiv J(m_i, \ldots, m_{i+k})} .$$

(5.5)

For translation invariant systems the relation $J_i = J$ is obtained. Here $J(m_i, \ldots, m_{i+k})$ describes the average mass transfer in dependence of the column heights $m_i, \ldots, m_{i+k}$. For state-independent fraction densities with translation invariant steady state (5.5) reduces to the simple relation

$$J = \mu_1 \rho .$$

(5.6)

So J is independent of the system size L and the current-density relation often called the fundamental diagram is simply linear. According to this we obtain the exact expression $J(K) = \frac{1}{2}\rho R(K)^2$ for the MF-TARAP (figure 5.3) which allows to identify two phases: For $K < 1$ the system is in a congested phase where moves are truncated and the flow

increases quadratically from zero to its maximum value

$$J^{\mathrm{max}} = \frac{1}{2}\rho \qquad (5.7)$$

corresponding to the free ARAP. For $K \geqslant 1$ the flow (and the dynamics) remain fixed and we refer to this parameter range as the free phase. Please note that the current-cutoff relation is continuous but not differentiable at $K = 1$. Adopting the theory of equilibrium systems we use discontinuities in macroscopic quantities or their derivatives to identify phase transitions [50].
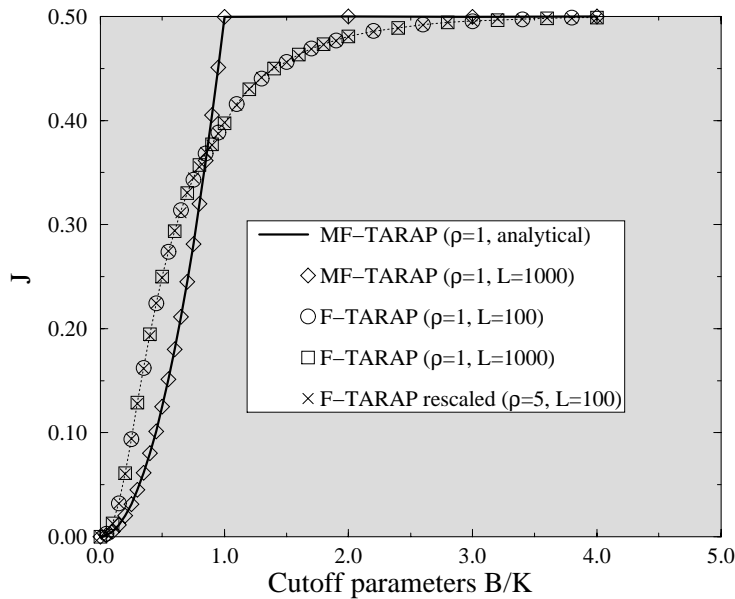

Figure 5.3.: Numerically determined current-cutoff relation of the MF-TARAP (J vs. K) and the F-TARAP (J vs. B). The F-TARAP for $\rho = 5$ has been rescaled according to (5.10). Measurement time is about 10^4 time steps.

Now we present a derivation of single-site mass moments of the MF-TARAP. In section 4.6.1 we have already calculated a suitable $\mathcal{M}$-approximant given by (4.76) and (4.42). It has been plotted in figure 4.8 showing excellent agreement with numerical results obtained by Monte-Carlo simulations. Of course we are able to calculate the single-site moments in the $\mathcal{M}$-calculation. Provided that the mass density is given by (4.42) we obtain

$$m_n^{(\lambda)} := \langle m^n \rangle_{P_\lambda} = (\lambda)_n \left(\frac{\rho}{\lambda}\right)^n . \qquad (5.8)$$

Here the so-called POCHHAMMER symbol $(a)_n$ is recursively defined via $(a)_0 := 1$ and $(a)_{n+1} := (a+n)(a)_n$. It can also be expressed by Γ-functions as done in chapter 4. So for the MF-TARAP the moments are given by (5.8) with (4.76). The special case $n = 2$ yields $m_2^{(\lambda)} = (1 + \lambda^{-1})\rho^2 = \frac{6-3R^2}{6-4R}\rho^2$.

Alternatively we derive the one-point moments in the mean field approximation (4.6) by the ansatz (4.10) together with (2.52) and obtain the recurrence relation[5]

$$m_n^{\mathrm{MF}} = \left[\overline{R}^{n+1} - R^{n+1} + (n+1)R - 1\right]^{-1} \sum_{k=1}^{n-1} \binom{n+1}{k+1} R^{k+1} \left\{\overline{R} + \frac{1 - \overline{R}^{n+1-k}}{n+1-k}\right\} m_k^{\mathrm{MF}} m_{n-k}^{\mathrm{MF}} \tag{5.9}$$

for $n \geqslant 2$ with $\overline{R} \equiv 1 - R$ and $R = R(K)$. In the special case $n = 2$ we obtain $m_2^{\mathrm{MF}} = \frac{6 - 3R^2}{6 - 4R}\rho^2$.

Finally, we can use the exact representation of the two-point moments given in (2.57). For the MF-TARAP the relation $m_2 = \frac{6 - 3R^2}{6 - 4R}\rho^2$ holds, i.e. both approximations reproduce the exact result!

In table 5.1 we compare the moments m_n^λ and m_n^{MF} with numerical data for $n = 2$ and $n = 4$. Even for $n = 4$ both approximations match very well but as shown in figure 4.9 this is not mandatory. The deviations from Monte Carlo data are rather based on poor numerics than related to inaccuracies from the approximations as can be seen from the $K = 1$ values where both approximations become exact but differ from numerics.

K	$m_2^{(\lambda)} = m_2^{\mathrm{MF}}$	m_2^{num}	$m_4^{(\lambda)}$	m_4^{MF}	m_4^{num}
0.2	1.1308	1.1303	1.9861	1.9867	1.9945
0.4	1.2546	1.2542	3.3390	3.3416	3.3882
0.6	1.3667	1.3656	4.9747	4.9780	5.0430
0.8	1.4571	1.4565	6.6148	6.6151	6.6647
1.0	1.5000	1.4988	7.5000	7.5000	7.4661

Table 5.1.: Second and fourth order mass moments derived by mean field and $\mathcal{M}$-approximation and Monte-Carlo simulations ($\rho = 1$, $L = 1000$ and 10^6 runs for measurement).

Now let us do a flying visit to the F-TARAP which has been studied numerically only because of the complex two-site-dependent ϕ-function. In figure 5.3 the current-cutoff relation is plotted which is independent of the system size (neglecting finite size effects) as in case of the MF-TARAP. However, the $J - B$ curve does not show any nonanalytic behaviour, so the F-TARAP is free of phase transitions in spite of truncation. In addition, we derive a scaling law from numerics given as

$$\rho^{-1} J_\rho(\rho B) = \tilde{\rho}^{-1} J_{\tilde{\rho}}(\tilde{\rho} B) . \tag{5.10}$$

Furthermore, the fundamental diagram becomes more complicated compared to the MF-TARAP due to the limited state space (figure 5.4). It is clear that $J_B(\rho = 0) = 0$ and $J_B(\rho = B) = 0$. The maximal current is achieved for half filling $\rho = \frac{B}{2}$ (for larger densities

---

[5]Note that $m_n = (-1)^n n! a_n$ holds.

frustration appears) and there is no particle-hole symmetry, i.e. $J_B(\rho) \neq J_B(B - \rho)$. For $\rho < B$ the current depends rather linearly on the density with slope $\frac{1}{2}$ which is in agreement with the free limit $B \to \infty$. Finally, we derive the scaling law

$$B^{-1} J_B (B\rho) = \tilde{B}^{-1} J_{\tilde{B}} \left(\tilde{B}\rho \right) \tag{5.11}$$

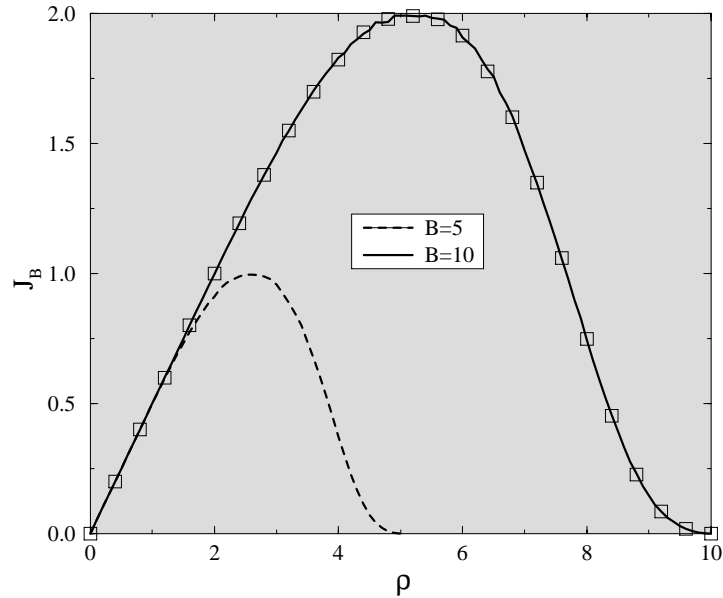with $\rho \in [0, 1]$, also from Monte-Carlo simulations, visualized in figure 5.4.

Figure 5.4.: Fundamental diagrams for different cutoff parameters B. In addition, we have plottet J_5 ($\square$) rescaled by (5.11). [$L = 100$, measurement time: 10^4]

The fundamental diagram of the F-TARAP is very similar to the behaviour of other asymmetric driven particle systems on a ring[6] like the ASEP or the NaSch model, whereby the most important commonness is given by a bounded local state space. So we may regard the F-TARAP as a continuous version of these systems.

5.3. TARAP - Numerics

Although one expects the TARAP to be an intermediate process between the full TARAP and the mean field TARAP, this model represents a fascinating system on its own. First we work out some important scaling relations. After that the numerically derived phase diagram is presented showing the surprising feature of nonsymmetric ergodicity breaking which is also defined, explained and compared to the well-known effect of spontaneous symmetry breaking.

---

[6]Although we have to keep in mind that the density ρ' in particle systems is given by ρ^{-1}.

5.3.1. Scaling Behaviour

In the following we study mainly the current-cutoff relation of the TARAP and without loss of generality we set $\rho = 1$ from now on. This is motivated by the scaling relation (5.11) which is also valid for the TARAP, i.e.

$$J_\rho(\Delta) = \rho J \left(\frac{\Delta}{\rho} \right) \tag{5.12}$$

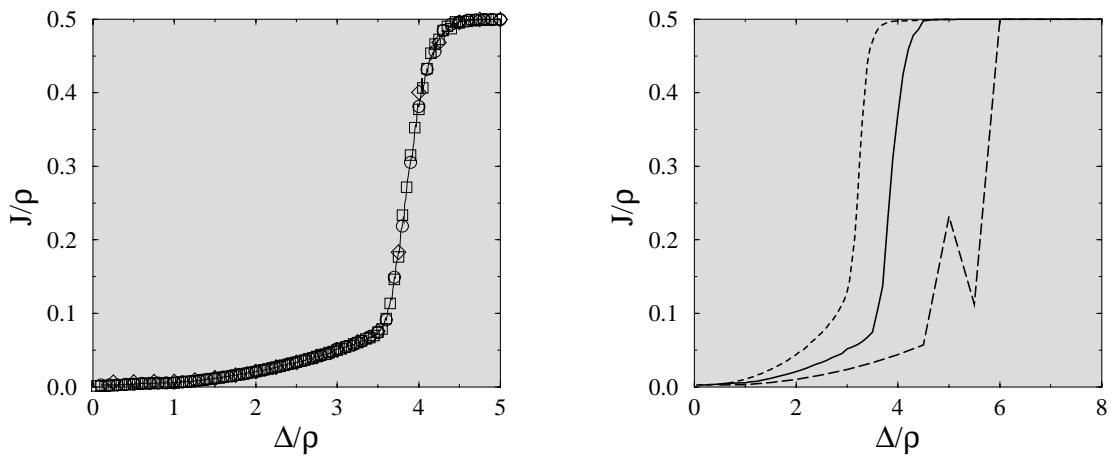with $J \equiv J_1$, as shown in figure 5.5 (left).[7]

Figure 5.5.: Current-cutoff diagrams for different densities $\rho = \frac{2}{5}, 1, 2$ ($\diamond$, $\circ$, $\square$) and fixed size $L = 100$ (left) resp. for different sizes $L = 50, 100, 200$ (dashed, solid, long dashed line) and fixed density $\rho = 1$ (right). Each flow value is obtained by 10^3 measurements over 10^3 samples with random initial configurations, except the $L = 200$ case which is simulated with 10^7 measurement time steps.

But in contrast to F-TARAP and MF-TARAP the current cutoff relation is not independent of L, see figure 5.5 (right). For larger L the curve stretches to the right which is understood easily: expanding the system increases the total mass M, so the occurrence probability of large sticks grows. However, the upper bound for mass shifts Δ is kept constant. Correspondingly the rejection rate also increases and the flux lowers. In addition, we also present an analytical derivation of the L behaviour in section 5.4.3. The outcome of this calculation and numerical simulations results in the introduction of the rescaled cutoff

$$\tilde{\Delta} = 2L^{-\frac{1}{2}}\Delta \ . \tag{5.13}$$

---

[7]Inserting (5.12) in (5.5) yields after some algebra the additional scaling relation $P_{\rho,\Delta}(m) = P_{1,\frac{\Delta}{\rho}}\left(\frac{m}{\rho} \right)$ for the single-site mass density.

This definition guarantees L-independence of the $J - \tilde{\Delta}$ diagram for $L \gg 1$ and makes it possible to derive a phase diagram for the TARAP. So from now on we work primarily with the rescaled cutoff $\tilde{\Delta} > 0$ representing the only parameter of the model. Nevertheless, we will fall back to the absolute notation Δ whenever necessary, e.g. for the discussion of numerical data.

5.3.2. Phases

The TARAP holds another interesting property. As figure 5.5 (right) shows the current-cutoff curve lacks of smoothness for large system sizes. While regimes of low (small Δ) and high (large Δ) total flow are simulated trouble-free, we have to increase the time of measurement enormously to obtain adequate results for the ascending branch of the current. This points to meta-stability and hysteresis which we will exemplify now.

We start by studying the flow J in dependence of time. While the $J - t$ curve does not show distinctive features for small or large cutoffs, see figure 5.6 (left), we observe an alternating behaviour in the ascending regime of the current-cutoff diagram $(0.7 < \tilde{\Delta} < 1)$, see figure 5.6 (right). Here the system decomposes into two well-defined substates with completely different properties. These substates are best characterized and distinguished by their associated flux and correspondingly we refer to them as low flow and high flow state. Both substates are briefly described in the following two paragraphs.
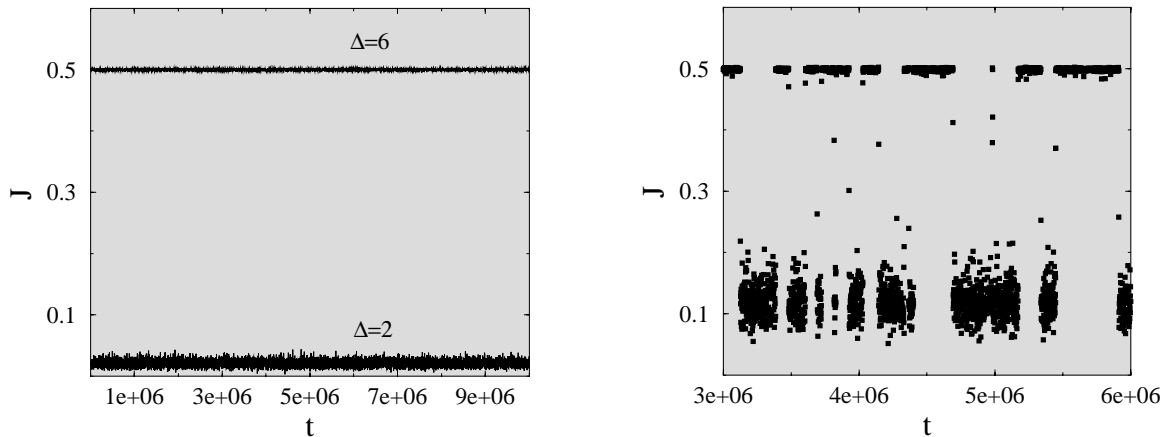

Figure 5.6.: Current-time diagrams of an $(L = 100)$-system for different cutoffs: low $(\tilde{\Delta} = 0.4)$ and high $(\tilde{\Delta} = 1.2)$ flow states (left) and coexisting $(\tilde{\Delta} = 0.846)$ state (right). Each current value is averaged over 10^3 time steps.

In the high flow state the mass distribution is nearly identical to the one of the free ARAP, i.e. it factorizes and the single-site distribution is approximately given by the exponential decaying distribution (2.49). In particular, we face a translation invariant

substate. The flow is independent of $\tilde{\Delta}$ and corresponds to the maximum current

$$J_{\text{high}} \equiv J^{\text{max}} = \frac{1}{2} \tag{5.14}$$

However, the low flow state, figure 5.7 (left), is given by a macroscopic condensate, i.e. nearly the total mass M is sharply located on one site and even in the thermodynamic limit those mega sticks hold a finite fraction of the total mass. The remaining mass is distributed equally in the system with an algebraically decaying mass distribution $P(m) \sim m^{-\kappa}$. For small system sizes κ depends weakly on L due to finite size effects.[8] In addition, κ depends monotonously on $\tilde{\Delta}$, see figure 5.7 (right), i.e. large cutoffs produce rapidly falling off mass distributions on sites not holding the condensate. Assuming the $L = 500$ system to be a good representative for the thermodynamic limit we obtain $\kappa(\tilde{\Delta}) \sim 1.23\tilde{\Delta} + 3.87$ by a linear fit.
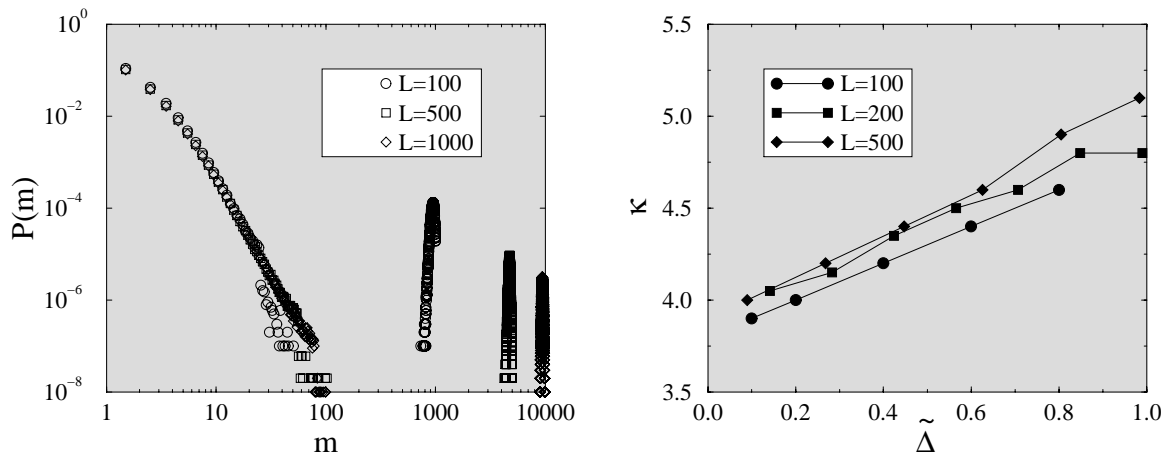

Figure 5.7.: Mass distributions in the low flow state for fixed rescaled cutoff $\tilde{\Delta} = 0.5$ and different system sizes (left). Exponents κ describing the algebraic mass decay $P(m) \sim m^{-\kappa}$ in the low flow state for different rescaled cutoffs and system sizes (right).

So translation invariance is broken in the low flow state. Furthermore, numerics show that the low flow current tends upwards with $\tilde{\Delta}$ but does not exceed

$$J_{\text{low}}^{\text{max}} \equiv \frac{1}{4} \ . \tag{5.15}$$

By numerics we find that for $\tilde{\Delta} > \tilde{\Delta}_c$ the TARAP resides in the high flow state only. Here the transition point $\tilde{\Delta}_c$ is given by

$$\tilde{\Delta}_c \equiv 1 \ . \tag{5.16}$$

---

[8]Figure 5.7 (left) shows that the algebraic tail declines stronger for large masses which is a result of poor statistics combined with a logarithmic representation. But this impact levels off for increasing L.

So this cutoff parameter range is labeled as high flow phase.

Correspondingly alternating current-time relations are obtained for $\tilde{\Delta} < \tilde{\Delta}_c$ denoted mixed phase from now on. Numerically we also derive an additional regime for small cutoffs where the system exclusively stays in the low flow state. Although the picture of a phase space divided into three sections sounds very feasible, we argue that the cutoff area of the low flow phase shrinks and finally disappears for increasing L. In section 5.4.2 and 5.4.3 we also give analytical evidence for the nonexistence of a pure low flow phase.

In a finite system the transition probabilities between low and high flow states, denoted by $p_{\nearrow}$ (low to high) and $p_{\searrow}$ (high to low), are small but nonzero in the mixed phase. According to this the average life times of the substates $\tau_{\text{low}} = (p_{\searrow})^{-1}$ and $\tau_{\text{high}} = (p_{\nearrow})^{-1}$ are very large but finite.[9] Here we have assumed the transition probabilities to be defined per timestep. Although the switching process between two states takes more than one time step (usually $\sim L$), it acts on a timescale much smaller than the lifetimes, see figure 5.6 (right) again. Accordingly the transition possibilities can be defined per switching time or per unit time. A comprehensive and intuitive picture of the mixed phase is presented in figure 5.8. For $L < \infty$ every arbitrary chosen configuration m can be transferred into a configuration m' in a finite number of time steps. So the system is ergodic. Correspondingly the steady state is unique and can be written as

$$|P\rangle = p_{\text{low}} |P_{\text{low}}\rangle + p_{\text{high}} |P_{\text{high}}\rangle \tag{5.17}$$

whereby $|P_x\rangle = \int_{\mathcal{C}(x)} \mathrm{d}^L m P(m) |m\rangle$ with $x = $ low,high. The associate configuration subsets $\mathcal{C}(x)$ fulfill $\mathcal{C}(\text{low}) \bigcap \mathcal{C}(\text{high}) = \varnothing$. Of course the separation of the state vector (5.17) is quite formal and can always be achieved.[10] For a comprehensive overview regarding properties of stationary states we refer to [51, 52].

5.3.3. Lifetime Analysis

To complete analysis of the mixed phase we measure lifetimes τ_{low} and τ_{high} in dependence of the system size L and the rescaled cutoff $\tilde{\Delta}$. Monte-Carlo simulations are difficult in the mixed phase since the lifetimes of the substates are very large. Correspondingly we have to restrict numerics to small systems ($L \leqslant 600$) and a small cutoff parameter range. Nevertheless, it is safe to say that both the average lifetimes of low and high flow states diverge in the thermodynamic limit, see figure 5.10. This implies that the steady state of the mixed phase is not unique in the thermodynamic limit. Ergodicity is broken and the steady state can either be in the high flow phase $|P\rangle = |P_{\text{low}}\rangle$ or the low flow phase $|P\rangle = |P_{\text{low}}\rangle$ depending on the initial condition. This behaviour is very similar to systems with spontaneously broken symmetry. However, it is most remarkable that in our case

---

[9]The lifetimes are simply calculated by evaluating the sum $\tau = \sum_{T=1}^{\infty} T p (1-p)^{T-1}$ (indices skipped).

[10]For completeness the conditions $\sum_x \mathcal{C}(x) = \otimes_L \mathbb{R}_0^+$ or $P(\otimes_L R_0^+ \backslash [\mathcal{C}(\text{low}) \bigcup \mathcal{C}(\text{high})]) = \{0\}$ are necessary.
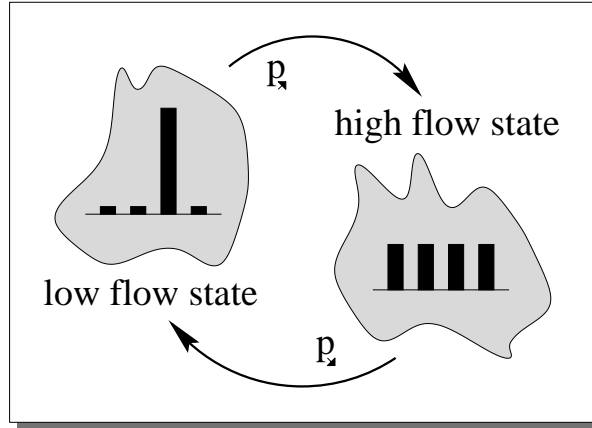
Figure 5.8.: In the mixed phase the system decomposes into two separated substates both occupying disjunctive subsets of configuration space (indicated by a representative configuration in each case). For finite systems there are non-zero transition probabilities $p_\nearrow$ and $p_\searrow$, whereas in the thermodynamic limit the substates decouple completely and the dynamics is frozen either in the high flow or the low flow state.

both phases are obviously not related by symmetry. Furthermore, the lifetimes of the substates do not scale both exponentially with size L (see next paragraph). This is also a strong indication that the observed scenario is different from spontaneous symmetry breaking. We therefore call this effect nonsymmetric ergodicity breaking. For a detailed classification of this new phenomenon we refer to section 5.6.

Figure 5.10 (left) indicates that τ_{high} increases exponentially for all $\tilde{\Delta} < \tilde{\Delta}_c$. Correspondingly numerics only work for small system sizes. Assuming $\tau_{\text{high}} \sim \exp[\alpha(\tilde{\Delta})L]$ we obtain α as an increasing function of $\tilde{\Delta}$, see figure 5.9. This behaviour is expected while approaching the pure high flow phase where the relation $\tau_{\text{high}} = \infty$ holds. Nevertheless, we are not able to predict the functional form of $\alpha(\tilde{\Delta})$ (algebraic or exponential) numerically while approaching $\tilde{\Delta}_c$.[11]

$\tilde{\Delta}$	$\alpha\left(\tilde{\Delta}\right)$
0.76	0.079
0.80	0.091
0.84	0.102
0.88	0.113

Figure 5.9.: Numerically determined scaling factor α.

The corresponding data for τ_{low} in the low flow state are better fitted algebraically than exponentially, refer to figure 5.10 (right). We see that the exponents obtained by the assumption $\tau_{\text{low}} \sim L^{\beta(\tilde{\Delta})}$ increase while moving into the mixed phase, i.e. for $\tilde{\Delta}$ tending to zero.

Although both transitions are driven by fluctuations, the above scaling behaviour

---

[11]Based on the numerical data in figure 5.9 a linear relation $\alpha \sim \overline{\alpha}L$ with $\overline{\alpha} = 0.28$ is obtained. Nevertheless, this result has to be treated with care in case of poor statistics caused by an insufficient set of reading points. In particular, a linear relation would lead to a finite α for $\tilde{\Delta} \nearrow \tilde{\Delta}_c$.

reflects different switching mechanisms. While the high $\rightarrow$ low transition is based on a collective effect which involves all sites of the lattice, the opposite transition involves only the lattice site where the macroscopic condensate is located. This is different to spontaneous symmetry breaking where both transitions obey the same purely fluctuation driven mechanism. Correspondingly the same exponential behaviour of the lifetimes is obtained.
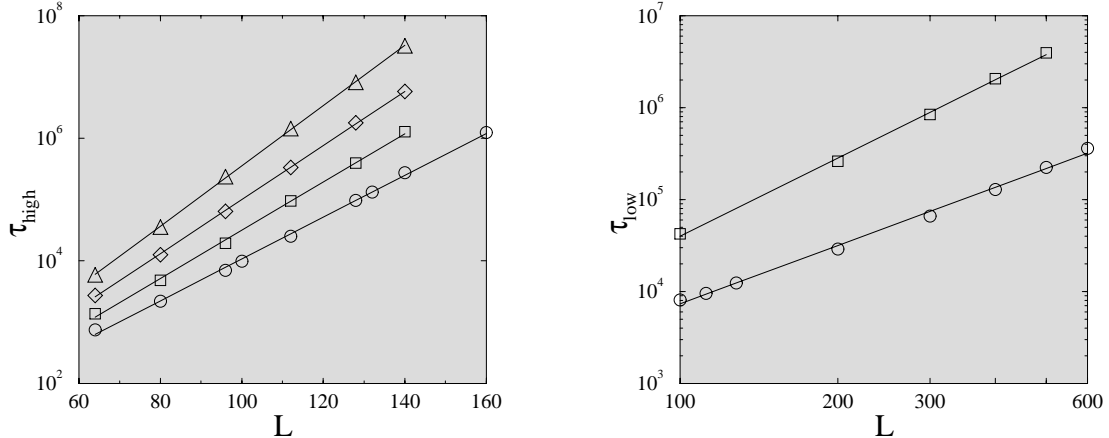

Figure 5.10.: Lifetimes of the mixed phase substates in dependence of the system size L for several rescaled cutoffs $\tilde{\Delta}$. Linear-logarithmic plot of τ_{high} for $\tilde{\Delta} = 0.76(\circ)$, $0.80(\square)$, $0.84(\diamond)$ and $0.88(\triangle)$ (left) and log-log plot of τ_{low} for $\tilde{\Delta} = 0.92(\circ)$ and $0.88(\square)$ (right).

Finally, we would like to mention that the long average lifetimes $\tau_{\text{low/high}}$ can be interpreted as the occurrence of meta-stable states. If the underlying time scales, i.e. the measurement times, do not allow the system to evolve into the stationary state - or more precise: are smaller than the lifetimes, hysteresis can be observed: in figure 5.11 we start with an one-stick initial configuration (total mass is located on one site) at $\Delta = 0$ and increase the cutoff until the system turns into the high flow branch. Subsequently we decrease the cutoff towards zero again. As expected the resulting J-Δ relations are different for rising and falling cutoff since the system is pinned to the corresponding substates.

Furthermore, we see in 5.11 that the regime of hysteresis shrinks for increasing measurement time. For measurement times $\gg \tau_{\text{low/high}}$ the current-cutoff relation would be unique for finite systems since the steady state is pictured completely by the simulation.

5.4. TARAP - Analytics and Heuristics

The results derived so far are mainly based on Monte-Carlo simulations. Now we continue by presenting a few analytical results which support the numerical findings and
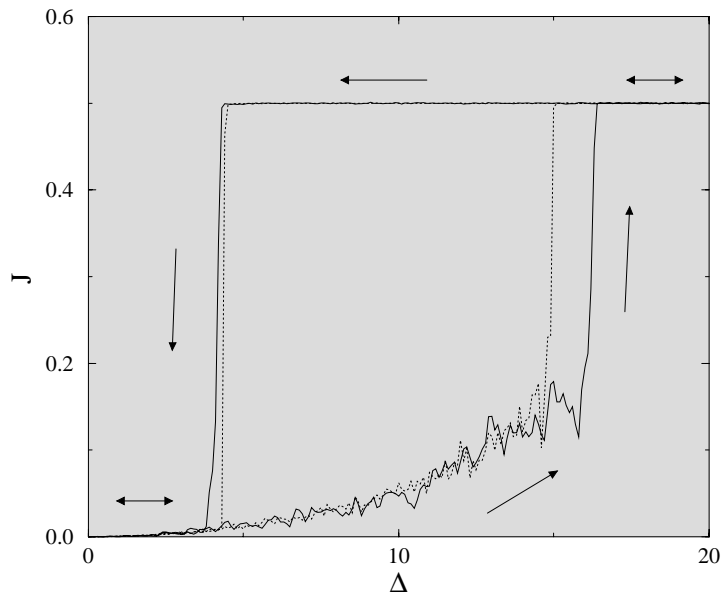
Figure 5.11.: Hysteresis for a system of size $L = 1000$ ($\rho=1$). In-/decrement of Δ in steps of 0.1. For each data point the flux has been averaged over 10^3 (solid line) resp. 10^4 (dotted line) time steps.

deepen the understanding of the underlying physics.

Starting point is a closer look at the average mass transfer per site (5.5) given as

$$J(m) = \begin{cases} \frac{1}{2}m & \text{for} \ \ 0 \leqslant m < \Delta \\ \frac{\Delta^2}{2m} & \text{for} \ \ \Delta \leqslant m < \infty \end{cases} . \tag{5.18}$$

This shows that the average mass shift $J(m)$ tends to zero for $m \to \infty$ and $m \to 0$. So high (low) columns shrink (grow) very slowly and accordingly low flow states, resp. one stick configurations, are very stable. On the other hand, homogeneous configurations maximize the current. We will exemplify this in the following paragraphs.

5.4.1. Low Flow State

We study the low flow state using the approximation

$$\langle J(m) \rangle_{P_i} = J\left(\langle m \rangle_{P_i} \right) . \tag{5.19}$$

Here P_i denotes the steady state single-site distribution of site i.[12] Equation (5.19) holds for stable distributions $P_i(m) \sim \delta(m - \overline{m}_i)$ which we assume here motivated by

---

[12]Equation (5.19) is equivalent to $\langle J(m_i) \rangle_P = J\left(\langle m_i \rangle_P \right)$.

the numerical results. Introducing the nomenclature $\overline{m}_i \equiv \langle m \rangle_{P_i}$ we obtain in the steady state from the continuity equation the condition

$$J_{\text{low}} \equiv J(\overline{m}_i) = J(\overline{m}_{i+1}) \tag{5.20}$$

for all i. Restricting now to the case where only one high column exists at site j (one-stick approximation), i.e. $m_+ \equiv \overline{m}_j > \Delta$, the remaining columns are all of the same mass (see (5.20)), i.e. $m_- \equiv \overline{m}_i < \Delta$ with $i \neq j$. Due to (5.18) and (5.20), the quantities $m_\pm$ are related by $m_+ m_- = \Delta^2$ and the mass conservation law yields the condition $\rho L = (L-1)m_- + m_+$.

Equipped with these relations we are able to compute $m_\pm$ and finally the current in the low flow state J_{low}. Assuming $L \gg 1$ our calculations lead to the formulas

$$m_+ = \frac{1}{2}\rho L \left\{ 1 + \sqrt{1 - \tilde{\Delta}^2} \right\} , \quad m_- = \frac{1}{2}\rho \left\{ 1 - \sqrt{1 - \tilde{\Delta}^2} \right\} \tag{5.21}$$

and

$$J_{\text{low}} = J_{\text{low}}^{\text{max}} \left\{ 1 - \sqrt{1 - \tilde{\Delta}^2} \right\} . \tag{5.22}$$

So the current of the low flow state increases from zero to $J_{\text{low}}^{\text{max}}$ for $0 < \tilde{\Delta} \leqslant \tilde{\Delta}_c$. For rescaled cutoffs larger than $\tilde{\Delta}_c$ relation (5.22) is not defined and the one-stick approximation is not valid anymore. Thus, we have derived an upper bound for the occurrence of the low flow state in accordance with the simulations. As figure 5.12 (left) shows the analytical result agrees very well with Monte-Carlo data.
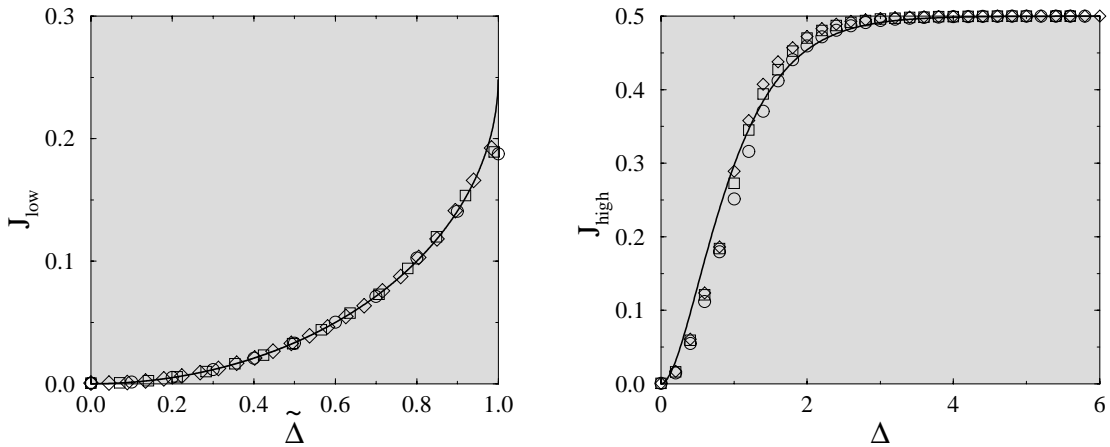

Figure 5.12.: Analytically (solid line) and numerically derived currents in dependence of low and high flow substate for different system sizes and density $\rho = 1$. Monte-Carlo parameters: $L = 100(\circ), 200(\square), 500(\diamond)$ (left) and $L = 100(\circ), 500(\square), 1000(\diamond)$ (right).

In addition, we give evidence that the condensate holds a finite fraction of mass even in the thermodynamic limit (5.21). Therefore, we also speak of an infinite aggregate,

e.g. [18]. The mass stored in a mega stick reaches from total mass M ($\tilde{\Delta} = 0$) to half total mass $\frac{1}{2}M$ ($\tilde{\Delta} = \tilde{\Delta}_c$) and collapses by passing the transition point.

By extending the calculations above to N_+ mass aggregates the validity range of the corresponding flow and mass equations shrinks in terms of $\tilde{\Delta}$ and we obtain smaller critical cutoffs given by $\tilde{\Delta}_c = N_+^{-\frac{1}{2}}$. Furthermore the flux increases. For the detailed expressions we refer to appendix A.3. These results indicate that the mixed phase is described best by the one-stick approximation, see numerical data in figure 5.12 (left) again, especially in the vicinity of the critical point because higher approximations do not reach this area. The one-condensate picture is also confirmed by numerical investigations that have shown that configurations with two or more aggregates are not stable.

5.4.2. High Flow State

Focussing on the high flow state, every site carries the same mass ρ on average. Motivated by the numerical results we approximate the mass distribution by the product measure solution of the free ARAP (2.49) for large L and calculate by the help of (5.18) the high flow state current

$$J_{\text{high}} = J_{\text{high}}^{\max} \left\{ 1 - (1 + L^{\frac{1}{2}}\tilde{\Delta})\, \mathrm{e}^{-L^{\frac{1}{2}}\tilde{\Delta}} \right\} \xrightarrow[L\to\infty]{} J_{\text{high}}^{\max} \tag{5.23}$$

defined for all rescaled cutoffs. So the high flow state exists both in the mixed phase and in the high flow phase whereby the associated flux $J_{\text{high}}^{\max}$ is independent of the rescaled cutoff in the limit $L \to \infty$.

Equation (5.23) also predicts that the current in the high flow state differs from $J_{\text{high}}^{\max}$ for small absolute cutoffs $\Delta \leqslant 5$ only. However, this area is mapped to zero for $L \to \infty$ in the $\tilde{\Delta}$ representation.[13] We have verified the behaviour for small absolute cutoffs by Monte-Carlo simulations, see figure 5.12 (right), although it is no longer possible to distinguish the states by their flows which are nearly identical in this parameter range. So we used the appearance of a macroscopic condensate as a criterion. The collapse of the total current for small cutoffs is also demonstrated in figure 5.11.

In addition, the failure of identifying the substates by their currents may mislead to the assumption that a third "pure" low flow phase exists for small absolute cutoffs. In particular, for small systems $L < 1000$, on which we can focus by numerics only, the regime of $J_{\text{high}} < J_{\text{high}}^{\max}$ covers a substantial part of the mixed phase[14] and accordingly high flow states are wrongly regarded as low flow states.

5.4.3. Lifetime Approximations and Phase Diagram

We start by giving a lower bound for the lifetime τ_{low}. As presented in section 5.4.1 the low flow state can be approximated by one-stick configurations very well. Using (5.5) we

---

[13]We only concentrate on positive $\tilde{\Delta}$.
[14]E.g. for $L = 100$ the transition point is given by $\Delta_c = 5$.

obtain the following deterministic evolution equation in time for the mass condensate m_+:

$$m_+(t+1) = m_+(t) + J\left(m_-(t)\right) - J\left(m_+(t)\right) = m_+(t) + \frac{1}{2}m_-(t) - \frac{1}{2}\frac{\Delta^2}{m_+(t)} \ . \quad (5.24)$$

For (5.21) the system is in a stationary state with respect to (5.24), i.e. $m_+(t+1) = m_+(t)$, because $m_\pm$ have been calculated by using (5.20) where inflow equals outflow.

We have several possibilities to modify (5.24) in order to estimate τ_low. First we neglect the inflow from the left and calculate τ_switch given by the time required to reduce the condensate to zero.[15] Although this corresponds to the transition time (from low to high state) rather than to the lifetime it represents a lower bound, i.e. $\tau_\text{low} \geqslant \tau_\text{switch}$.

By $m_+(t+1) - m_+(t) \cong \dot{m}_+(t)$ the recurrence relation (5.24) without inflow rereads as an ordinary differential equation with solution $m_+(t) = \sqrt{m_+(0)^2 - \Delta^2 t}$. Under use of $m_+(0) = \rho L$ – the most extreme one-stick configuration – we derive

$$\tau_\text{switch} = 4L^\beta \left(\frac{\rho}{\tilde{\Delta}}\right)^2 \quad \text{with} \quad \beta = 1 \ . \quad (5.25)$$

This relation qualitatively reflects the dependence on $\tilde{\Delta}$ and L: τ_low decreases with $\tilde{\Delta}$ and increases with L. Additionally, the relation between τ_low (or more accurately τ_switch) and L is algebraical which is also in agreement with numerical results. Nevertheless, the according exponent β is too small and Monte-Carlo data point at an additional dependence on $\tilde{\Delta}$. For example we give the exponents derived from the graphs in figure 5.10: $\beta = 2.8$ for $\tilde{\Delta} = 0.88$ and $\beta = 2.1$ for $\tilde{\Delta} = 0.92$. Otherwise, these values indicate that $\tau_\text{low} \to \tau_\text{switch}$ for $\tilde{\Delta} \to \tilde{\Delta}_c$. Correspondingly the low flow state becomes unstable in vicinity of the transition point $\tilde{\Delta}_c$, i.e. it collapses before being established.

In appendix A.4 another approach is presented taking into account the inflow. We obtain

$$\tau_\text{low} \gtrsim L^\beta \left(\frac{\rho}{\tilde{\Delta}}\right)^2 \ln\left(L^\beta \left(\frac{\rho}{\tilde{\Delta}}\right)^2\right) \sim \tau_\text{switch} \ln \tau_\text{switch} \quad (5.26)$$

with $\beta = 1$. So the improved calculations produce logarithmic corrections yielding longer lifetimes. However, the algebraic behaviour is still weak and independent of $\tilde{\Delta}$.

The average lifetime τ_high is determined by starting with the high flow state and calculating the probability (per unit time step) for switching into the low flow state. So the system can be described by the single-site mass distribution of the free ARAP (2.55) and assuming product measure. Accordingly all sites carry the mass ρ on average. The

---

[15]In general one would ask for the time needed to reduce a mega stick to m_- or mass 1 $(= \rho)$ corresponding to the average mass in the high flow phase. But these approaches only yield marginal corrections, especially because we assume equation (5.24) to be valid for all $m_+(t)$ although it is strictly spoken only available for $m_+(t) \geqslant \Delta$. However, this ansatz is justified because the largest period of time is used to remove mass from the top layer of a mega stick.

deterministic flow equation – based on (5.18) and the introduction of $\dot{m}$ – rereads for an arbitrary site:

$$\dot{m}(t) = J(\rho) - J(m(t)) \ . \tag{5.27}$$

Here the inflow is not neglected – as done in the previous paragraph – but set to a constant value (comparable to appendix A.4). We have to take into account that J takes different forms for $\rho \leqslant \Delta$ or $\rho \geqslant \Delta$. According to this (5.27) possesses two fixed points ρ and $\frac{\Delta^2}{\rho}$. The corresponding dynamic scenarios are visualized in figure 5.13.
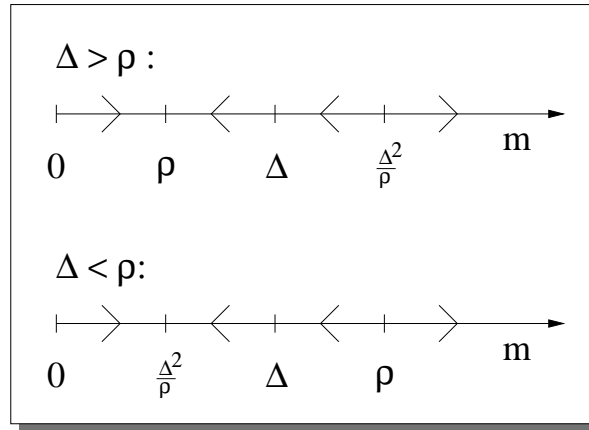

Figure 5.13.: Fixed points and flows of $\dot{m} = J(\rho) - J(m)$ in dependence of Δ.

For $\Delta \leqslant \rho$ sticks either shrink to small piles $\frac{\Delta^2}{\rho} \leqslant \rho$, or their mass diverge. This constellation can be identified with a low flow state, so for $\Delta \leqslant \rho$ the probability of being in the low flow phase will be set to one. However, Δ scales with $\sqrt{L}$ (5.13), so this case is irrelevant for further considerations.

For $\Delta > \rho$ things become more complicated. Here ρ is an attractor and corresponds to a free ARAP distribution. The fixed point $\frac{\Delta^2}{\rho}$ is repulsive and only sticks with $m > \frac{\Delta^2}{\rho}$ will develop to mega sticks. Finally, a high current constellation may evolve into a one-stick configuration if and only if at least one stick is bigger than $\frac{\Delta^2}{\rho}$. But this probability is easy to calculate and we obtain

$$p_{\searrow} = 1 - (1 - w)^L \tag{5.28}$$

with

$$w = \int_{\frac{\Delta^2}{\rho}}^{\infty} \mathrm{d}m P(m) = \left(1 + 2 \left(\frac{\Delta}{\rho} \right)^2 \right) \mathrm{e}^{-2 \left(\frac{\Delta}{\rho} \right)^2} \ . \tag{5.29}$$

For $L \gg 1$ we have $\Delta \gg \rho$ and correspondingly $w \ll 1$ yielding[16]

---

[16]Please note that τ_{high} has been derived under the assumption $L\tilde{\Delta}^2 \nrightarrow 0$. In the exact derivation of (5.30) the algebraic term is replaced by $\frac{1}{L} \left[1 + \frac{1}{2} L \left(\frac{\tilde{\Delta}}{\rho} \right)^2 \right]^{-1}$ being convergent even for $\tilde{\Delta} \to 0$.

$$\tau_{\text{high}} \sim \left(L\frac{\tilde{\Delta}}{\rho}\right)^{-2} \exp\left\{\alpha\left(\frac{\tilde{\Delta}}{\rho}\right)L\right\} \quad \text{with} \quad \alpha(x) = \frac{1}{2}x^2 . \tag{5.30}$$

The dependence of $\tilde{\Delta}$ and L is qualitatively reproduced: the average lifetime τ_{high} increases exponentially with $\tilde{\Delta}$ and L, supplemented by algebraic corrections which are irrelevant in the thermodynamic limit. Furthermore, the scaling function α depends monotonously on $\tilde{\Delta}$ as derived numerically (fig. 5.9) but does not fit quantitatively, and neither does J_{high}.

In addition, we notice that the lifetimes derived by (5.30) are very small for $L < 200$ and $\tilde{\Delta} \lesssim 0.5$. Furthermore, the formula (5.30) overestimates the lifetimes obtained numerically (refer to figure 5.10). According to this we conclude that the high flow state is unstable for small cutoffs in the regime of numerically relevant L (while the low flow state becomes more stable while tending to zero with respect to $\tilde{\Delta}$) misguiding to the conjecture that a pure low flow state would exist.

In appendix A.5 we present a simple deterministic approach for determining the transition time from high to low flow state yielding $\tau_{switch} \sim L$. So switching between the substates is of order L in both directions while the lifetimes diverge either algebraically (stronger than linear) or exponentially in system length.

The results derived so far lead us to the following phase diagram presented in figure 5.14 consistent with numerical simulations and analytical calculations.
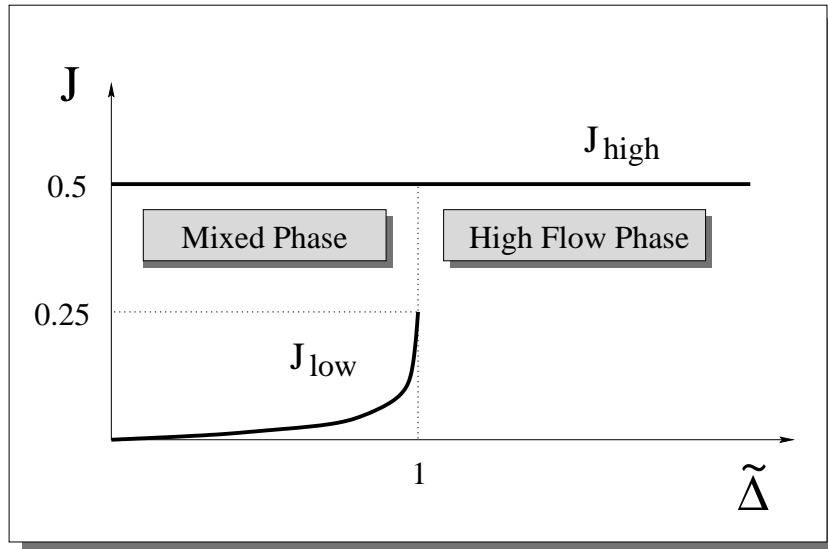

Figure 5.14.: Phase Diagram of the TARAP with $\rho = 1$.

5.5. TARAP meets Krauss Model

While the Krauss model has already been embedded into the framework of the ARAP (subsection 2.2.2) we now show that the physics behind this traffic model can be explained by means of the TARAP.

In [16] the occurrence of a new regime in the phase space of the Krauss model has been proposed[17], and based on numerical data the schematic fundamental diagram given in figure 5.15 (left) has been derived. The authors argue that a new phase exists between the stable free flow branch (corresponding to the high flow phase of the TARAP) and the area of congested flow (related to the low flow phase of the TARAP). So in addition to well-known domains of pure phases or meta-stability, we obtain a sector where both, jammed and free states, are stable! In other words, the Krauss model exhibits nonsymmetric ergodicity breaking.
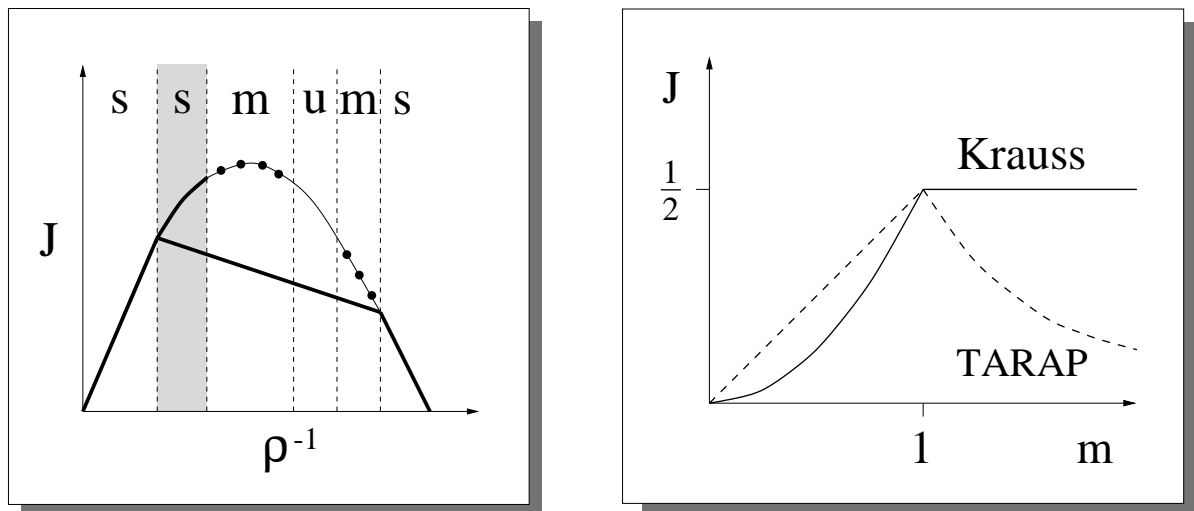

Figure 5.15.: Fundamental diagram of the Krauss model, excerpted from [16]. The shortcuts s,m,u stand for stable, meta-stable, unstable and are related to the free flow phase. The new phase is highlighted. Note that the inverse mass density ρ^{-1} corresponds to the density of particles (left). The average mass transfer per site in the Krauss model and the TARAP for $\Delta = v_{\max} = 1$ (right).

In the following the similarities between TARAP and Krauss model are worked out. First we derive the average mass transfer per site (5.5) for the traffic model by the use

---

[17]The existence of this additional phase was also emphasized in the original work [14].

of (2.37), i.e. we calculate[18] $J(m) = \int_0^m \mathrm{d}\Delta f(\Delta, m)\Delta$, and obtain for $\sigma \geqslant v_{\max}$

$$J^K(m) = \begin{cases} \frac{1}{2\sigma}m^2 & 0 \leqslant m < v_{\max} \\ \frac{1}{2\sigma}v_{\max}^2 & v_{\max} \leqslant m < \infty \end{cases} \tag{5.31}$$

and for $\sigma < v_{\max}$

$$J^K(m) = \begin{cases} \frac{1}{2\sigma}m^2 & 0 \leqslant m < \sigma \\ m - \frac{1}{2}\sigma & \sigma \leqslant m < v_{\max} \\ v_{\max} - \frac{1}{2}\sigma & v_{\max} \leqslant m < \infty \end{cases} . \tag{5.32}$$

In both cases we notice a common property: while the shifted mass is proportional to m for sticks smaller than $v_{\max}$, the transferred mass is constant for $m > v_{\max}$. So we are confronted with the phenomenon of truncation also in the KRAUSS model! The transfered mass is bounded by $v_{\max}$ which can be evaluated directly from (2.36) while the maximal deceleration σ has only marginal impact on the dynamics.

From now on we restrict on $\sigma = v_{\max}$. This is justified because the functional shape of J^K depends only weakly on σ. Furthermore, this ansatz is in line with the approach $a_{\max} = v_{\max}$. To compare TARAP and KRAUSS model we equate $v_{\max}$ and cutoff Δ, the effective truncation parameters of both models. According to this set of parameters both processes generate even quantitatively coequal average mass transfers as figure 5.15 (right) illustrates. Note that the different behaviour for $m \to \infty$ is negligible because it does not matter for an infinite aggregate if the broken off mass is constant or zero.

Finally, we would like to rewrite the KRAUSS model by its fraction density ϕ^K. By the use of simple tricks regarding δ-, θ- and min/max-functions the ultralocal representation

$$\phi^K(r, m) = \left(1 - \frac{m}{\Delta}R(m)\right)\delta(r) + \frac{m}{\Delta}\theta\left(R(m) - r\right) \tag{5.33}$$

is derived from (2.37) with $R(m)$ defined in (5.3). So formally the only difference between KRAUSS model (5.33) and TARAP (5.1) is given by the additional factors $\frac{m}{\Delta}$. In figure 5.16 both fraction densities are visualized in dependence of m:

❑ $m < \Delta$: Here both models represent free ARAPs with uniform distributions and without truncations, However, they differ in dynamics: while the TARAP is updated strictly parallel, the ARAP formulation of the KRAUSS model is equipped with mixed dynamics, i.e. discrete parallel and continuous time updates are superposed! This is nothing else than the interpolated update given in (2.20). For $m \to \Delta$ the update is purely parallel while it is random sequential for $m \to 0$.

❑ $m \geqslant \Delta$: Both models are truncated and prohibit transfers larger than Δ, However, they differ in the implementation of the cutoff. In the TARAP moves are rejected if the chosen fragment exceeds the cutoff,[19] while in the KRAUSS model only suitable fragments are generated by ϕ^K.[20]

---

[18]Here Δ does not represent the cutoff!

[19]This is possible because the fraction r is still determined from a uniform distribution.

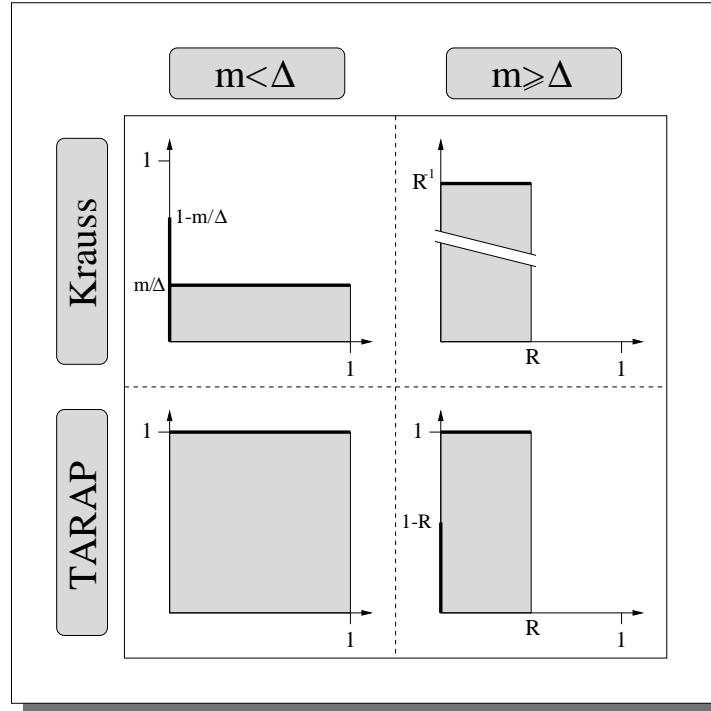[20]This is achieved by renormalization of the relevant domain of fractions.

Figure 5.16.: Ultralocal ϕ-functions of Krauss model and TARAP in dependence of the mass m. Here R is defined according to (5.3) and $v_{\max} = \Delta$. Furthermore, δ-functions are visualized by upright bars whereby their height is given by the associated prefactors.

So the fraction densities of Krauss model and TARAP rest upon the same physical mechanism. Therefore, both models show universal behaviour like the phenomenon of nonsymmetric ergodicity breaking.

Since the TARAP is defined by simpler dynamics, we fall back onto this process whenever fundamental properties like nonsymmetric ergodicity breaking are studied. In addition, the TARAP can be viewed as a toy model that catches some of the physics behind the Krauss model. On the other hand, the Krauss model should be treated as a process focussing on reproducing phenomena of traffic.

We conclude with two final remarks:

❏ In [16] it is pointed out that jam formation, corresponding to the high → low transition in the TARAP, and jam dissolution, corresponding to the low → high transition, are driven by different mechanisms. While the first is a bulk effect (a jam can emerge everywhere in the system), the latter is an interface effect (a jam can be reduced at the top only). This perspective is in accordance with our approach presented in the previous sections.

❏ In figure 5.15 (left) also an additional congested phase is observed while we have argued that there is no pure low flow phase in case of the TARAP - at least in the

thermodynamic limit (subsection 5.4.3). Nevertheless, there is no strict proof for this conclusion. Are the KRAUSS model and the TARAP related with respect to this problem? And if this is the case: is the congested phase of the KRAUSS model a mixed phase in disguise? Or is it even possible to find evidence for a pure low flow phase in the TARAP?

5.6. Relations to other Models

In this concluding section the TARAP and its physics are compared with related models and phenomena, emphasizing and explaining differences and similarities. On the one hand, we focus on the occurrence of infinite aggregates, on the other hand, we look for systems with ergodicity breaking. Both effects are still interesting on its own, but occur even simultaneously in case of the TARAP! In particular, we have not found a model in literature that was able to reproduce both phenomena.

5.6.1. Infinite Aggregates

As shown before the TARAP is equipped with a condensed (low flow) phase where one lattice site holds a finite fraction of the total mass, i.e. the mass of that infinite aggregate scales with L (5.21). This behaviour is very similar to the equilibrium BOSE-EINSTEIN condensation (BEC) in an ideal BOSE gas [53]: for temperatures lower than T_c a finite fraction of particles occupies the lowest energy level (condensate phase), while the remaining bosons are distributed asymptotically thin over the energy scale (gas phase). The difference is that the infinite mass stick forms in real space as opposed to the BOSE gas where the condensation takes place in momentum space. In addition, the transition to the low flow phase occurs even in one dimension as opposed to the BOSE gas where the condensation takes place in two or higher dimensions [19]. Finally, the analogy is only formal as mass sticks are no non-interacting quantum particles.

But there exist also some nonequilibrium systems with condensate effects. So the ASEP with quenched randomness in the hopping rates [22,54] shows a condensed phase given by totally jammed configurations, i.e. all particles stuck together forming a mega jam with small fluctuating gaps (masses) only. Therefore, the headway of the leading car is infinite, corresponding to the macroscopic mass condensate. The quenched disorder is realized by an assignment of different hopping rates to cars yielding unequal effective maximum speeds v_{max}. According to this the slowest particle will give rise to a platoon of particles behind it.[21] Nevertheless, there is a significant difference between quenched ASEP and TARAP: in the case of quenched disorder the fragment probabilities are site-dependent because particles correspond to sites in the stick representation, while in case of the TARAP the fragment density is translation invariant. So the BEC phenomenon occurs in absence of explicit disorder in the TARAP.

---

[21]Similar effects of blockage can be achieved by introducing site-dependent hopping rates [12].

In section 2.2.3 we have studied models of aggregation and fragmentation, namely a chipping model (CM) (2.39) and a truncated zero-range process (2.45). Both show the phenomenon of BOSE-EINSTEIN like condensation. In case of the CM the asymptotic mass densities have also been derived [17, 18].

❑ Condensed (low flow) phase: the non-aggregated mass is distributed algebraically due to $P(m) \sim m^{-5/2}$ for the CM. Although the spread mass also shows power-law behaviour in the TARAP, the decaying exponent is larger and cutoff dependent (section 5.3.2).

❑ Homogeneous (high flow) phase: both models show exponential behaviour with algebraic corrections, but differ quantitatively.

Nevertheless, there are some important differences between CM and TARAP. Due to diffusion the infinite stick is moving through the system in CM, while in the TARAP it is pinned at a fixed but randomly chosen site. Anyway, the process of the condensate formation is different in both systems. In the CM aggregates may emerge at several sites and coalesce at last (coarsening). In the TARAP aggregates are formed at several sites, too, but stay at their origins. These aspirants for infinite condensates struggle for masses until only one stick is left (competing).

Furthermore, the model of aggregation and fragmentation does not show the feature of nonsymmetric ergodicity breaking and the same applies to the zero-range process (2.45). However, the latter shares some properties with the TARAP. The fragment density (2.45) is ultralocal state-dependent with built-in cutoff C: for sticks equal to or larger than C the rate of transfers is reduced (in case of the TARAP those move are rejected). In addition, phase separation between condensed and homogeneous phase occurs in the limit $C \to \infty$ only. This is very similar to the TARAP where the phase transition takes place at $\tilde{\Delta}_c = 1$ corresponding to $\Delta \to \infty$.

Finally, we would like to mention the so-called bus-route model [55] also showing a condensate transition in a somewhat special limit of the underlying dynamics: a hopping rate must tend to zero and approximative calculations imply a special L dependence, similar to the cutoff rescaling (5.13) in the TARAP.

So effects of BOSE-EINSTEIN like condensation are observed in equilibrium and nonequilibrium systems. But while the original BEC is derived in case of non-interacting quantum particles, the nonequilibrium offsprings are generated by interacting stochastic models with perturbed dynamics. This means the infinite aggregates are formed in consequence of perturbations like quenched randomness or truncation.

5.6.2. Ergodicity Breaking

Both TARAP and the chipping model (2.39) exist in low flow (condensed) and free flow (homogeneous) phases. Furthermore, in both systems a pure homogeneous phase is

present. But while in case of the chipping model (CM) the condensed phase is clearly separated from the homogeneous phase by a nonequilibrium phase transition, the low flow phase coexists with the high flow phase in a non-ergodic steady state for the TARAP.[22] Why is the CM free of ergodicity breaking?

In the following paragraph we argue that the CM is free of ergodicity breaking because the model is defined on integer space. By discretization of continuous ARAPs an intrinsic mass scale is introduced, given by the smallest mass unit 1. Although the underlying dynamics can formally be mapped onto the discrete system, we obtain artefacts of discretization with strong impact on the dynamics in the low density regime. To exemplify this we consider the free continuous ARAP under parallel dynamics with fraction density (2.48). Here the exact mass distribution (2.49) is obtained. Discretization yields the fragment density (2.54) and the according discrete ARAP can also be solved exactly (2.55). Furthermore, it is possible to regain the continuous ARAP (2.49) from (2.55) by assuming $m \gg 1$ and $\rho \gg 1$ with $\frac{m}{\rho} = $ const. But what happens for $\rho \ll 1$? We assume the free continuous ARAP again. In addition, we ask for finite L. Let the system be in the initial state $m_1 = 1$ and $m_i = 0$ for $i \neq 1$. The steady state is of product measure form and exactly described by (2.49), renormalized according to (4.62). However, the discrete ARAP reduces to an one-particle ASEP with hopping probability $p = \frac{1}{2}$, solved by $P(0) = \rho$ and $P(1) = 1 - \rho$. Furthermore, there is no way back to the solution of the continuous form. So in case of the discrete ARAP the distribution of the free ARAP is obtained only for large densities, while we are confronted with a one-stick configuration for small densities. However, in case of the continuous ARAP the structure of the steady state is conserved for the complete density spectrum.

Although this example cannot be mapped onto the CM and TARAP directly, it clarifies the influence of state space discretization. And it offers a heuristic argument why the high flow state may exist over the whole cutoff regime in the TARAP and therefore coexists with the low density state for $\tilde{\Delta} < \tilde{\Delta}_c$.

The heuristic statement above is also in agreement with numerical investigations done for the discrete ARAP where we have failed to spot the mixed phase for any cutoff [45].

Finally, we would like to address systems exhibiting spontaneous symmetry breaking (SSB). It is well-known that effects like phase transitions and SSB cannot occur in one-dimensional equilibrium systems with short range interactions and bounded state variables. However, when the local state space is not restricted to a finite set of values, the phenomena quoted above may take place [56].[23] On the other hand, systems far from equilibrium are less restrictive and it has been shown that they are capable of exhibiting SSB even when the local state variables are restricted to a finite number of values [25, 44]. This is not surprising since one-dimensional stochastic systems can be mapped onto two-dimensional quantum systems where above mentioned theorem does

---

[22]Please note that the phase space is spanned by the density in the CM whereas the cutoff is fixed (chipping of one particle). So for comparison one should also parameterize the phase space in the TARAP by the density instead of the cutoff. This is possible due to the scaling relations (section 5.3.1).

[23]In the particle picture this case corresponds to bounded state space and arbitrary interaction range.

not apply and SSB may occur.

For example in [25] an ASEP with two types of charges moving in opposite directions on an open chain is introduced. For a certain set of parameters it exhibits spontaneous symmetry breaking, i.e. the system may be in either one of two states related by charge conjugation and space inversion. Here also oscillations between these two substates can be observed. However, in contrast to the TARAP, these states are connected by a symmetry. Therefore, the lifetimes of the substates, which also diverge in the thermodynamic limit, are identical.

Furthermore, SSB is always fluctuation driven, resulting in lifetimes that are growing exponentially with the system size. A more fundamental explanation of SSB is given in [52]: for random sequential dynamics[24] the approach to stationarity is governed by the eigenvalue ϵ of the stochastic Hamiltonian H with the lowest positive real part.[25] By evaluating the expectation value $\langle F(t) \rangle_{P(0)} = \langle s \,|F|\, P(t) \rangle_{P(0)}$ with $|P(t)\rangle = \exp(-Ht)\,|P(0)\rangle$ (section 2.1.3) we obtain for large t:

$$\langle F(t) \rangle_{P(0)} \approx \langle F(t) \rangle_{P(\infty)} + \langle s\,|F|\,\epsilon \rangle \, \langle \epsilon\,|P(0) \rangle \, \exp(-\epsilon\, t) \;. \qquad (5.34)$$

Here ϵ determines the longest relaxation time $\tau = |\epsilon|^{-1}$. Then a typical signature of SSB is given by an energy gap exponentially small in system size, i.e. $|\epsilon| \sim \exp(-\alpha L)$. So the state $|\epsilon\rangle$ is also stable in the thermodynamic limit in addition to $|P(\infty)\rangle$ and the system becomes non-ergodic. According to this we face two (or more) stationary distributions and the symmetry is broken.

Here the expression 'symmetry' does not inevitably apply to a symmetry relation between these multiple stationary states. However, this is in general the case [25]. Furthermore, exponential lifetime behaviour is associated with SSB. Therefore, we call the ergodicity breaking in the TARAP nonsymmetric to emphasize its different and exceptional position.

The process in [25] exhibits exponentially diverging lifetimes, exceeding the flipping times between the substates by several orders of magnitude. In [57] it has been found that the model even exhibits nonsymmetric ergodicity breaking. By Monte-Carlo simulations and analytical calculations three types of asymmetric phases are identified. This is very similar to the TARAP. But here asymmetry is achieved by an asymmetric choice of input and output rates, i.e. the rates associated with particle species 1 disagree with the rates associated with particle species 2, whereas the TARAP is defined on a ring with homogeneous (site-independent) dynamics. Actually the particles are not distinguishable in the TARAP.

A flipping mechanism between two alternating symmetric substates that is not purely driven by fluctuations is studied in [58]. Here a condensate moves on a ring either to the right or to the left with lifetimes that diverge only logarithmically with L. This

---

[24]The extension to discrete dynamics is canonical.

[25]All eigenvalues of stochastic Hamiltonians have a non-negative real part. Furthermore, zero is always an eigenvalue.

non-exponential behaviour implies that spontaneous symmetry breaking does not occur. Furthermore, the condensates gradually spread out, becoming more diffuse at the front than at the back, before reversing again. According to this there is a permanent change in the condensate (state) until flipping and moving into the other direction. So the lifetimes are rather defined by the switching times in this model.

Thus, the ergodicity breaking observed in the TARAP differs from SSB because the underlying flipping mechanisms are totally unequal (sections 5.3.3 and 5.4.3). While the high $\rightarrow$ low transition features SSB characteristics (collective phenomenon, fluctuation driven, exponential behaviour), the low $\rightarrow$ high transition is of a quite different nature (single-site effect, algebraic behaviour). Nevertheless, the latter one is also fluctuation driven: the low flow state, approximated by (5.21), must be kicked out of its 'equilibrium' by the random based dynamics. By the way, for $\tilde{\Delta} \rightarrow \tilde{\Delta}_c$ the pure lifetimes of the low flow state decrease and tend to the transition times. So in this regime the low $\rightarrow$ high transition is similar to the alternate flocking in [58].

6. Summary and Conclusions

In this work we have studied the asymmetric random average process (ARAP). The model is related to the class of driven lattice gases and equipped with a stochastic nearest neighbour interaction. Its characteristics are continuous and unbounded state variables called masses. The local dynamics is given by asymmetric shifts of masses whereby the transferred mass fragments are determined by a fraction density ϕ.

We have shown that problems from granular media, traffic flow theory and other fields of physics can be formulated in terms of the ARAP (section 2.2) which justifies a fundamental discussion of this interesting model. In addition, the ARAP represents some kind of toy because its simplicity makes it still analytical tractable. So it may take the position of a standard model for stochastic hopping processes on continuous space, similar to the ASEP for models on discrete space.

Here we have focused on the ARAP with discrete parallel update mainly, although we have given definitions and master equations of ARAPs with random sequential dynamics or integer masses as well. Furthermore, we have presented a classification scheme related to ϕ-functions (section 2.1).

In case of state-independent fraction densities $\phi = \phi(r)$ we have analytically determined the set of ARAPs with exact product measure solutions (chapter 4). In general mean field approaches provide poor results in low dimensions. But for the ARAP this is different. Since two-point (in case of symmetric ϕ-functions even three-point) mass correlations vanish, mean field ansatzes yield excellent results as proven by numerics. According to this, we have calculated the two-parametric set $\mathcal{M}$ of fraction densities yielding exact product measure solutions. The class $\mathcal{M}$ covers a wide range of models including almost critical fraction densities. On the one hand, this feature allows us to find appropriate approximants in $\mathcal{M}$ for arbitrary given ARAPs (section 4.6), on the other hand, we may restrict to $\mathcal{M}$ as a set of representatives when studying further properties of the ARAP.

Our results have been derived for arbitrary system sizes and formally transferred to continuous time dynamics as well. However, in the latter case an explicit representation in terms of ϕ-functions does not exist and we are equipped with a moment representation only. It would be nice to clarify if this sequence of moments is defined free of contradictions.

Furthermore, the calculation of $\mathcal{M}$ can be applied to some related problems. In [9] exact product measure solutions have been determined for the q-model. Although this

model is defined slightly different (the local dynamics is symmetric but contain N-site interactions), the calculations are very similar to the derivation presented in this work. It is even possible to enhance the considerations to an asymmetric q-model which contains the ARAP as a special case (section 4.2.5). In addition, one could try to adopt our approach to discrete ARAPs. Nevertheless, we are dealing with ultralocal fraction densities there, offering a richer spectrum of solutions, e.g. the class of zero-range processes should be part of the complete set of solutions. Therefore, we could also look for exact mean field solutions in case of the continuous ARAP with ultralocal densities.

Finally, one is also interested in exact solutions where product measures are not exact. Here one should focus on the simplest model first, the free continuous ARAP with continuous time dynamics. Up to now there is no explicit solution!

In this work we have also adopted the matrix product ansatz (MPA) to the ARAP (chapter 3). Although this technique represents a well-established tool for stochastic processes, it has mainly been applied to systems with discrete and bounded state variables so far. However, we have shown that this method also works with unbounded and even continuous local state spaces. Furthermore, in case of continuous ARAPs functional equations are obtained. So combined with powerful tools of functional analysis, the matrix product technique could represent the appropriate instrument for continuous ARAPs and we believe that the solution of the free continuous ARAP with random sequential update could be possible by using MPA.

So far we have concentrated on fundamental and analytical treatable properties of the ARAP. In chapter 5, however, the truncated ARAP (TARAP) is introduced and studied. It is motivated by Internet transport and single-lane traffic with traffic lights. Its mass transfer is bounded by a cutoff $\tilde{\Delta}$. The TARAP is investigated by Monte-Carlo simulations, supplemented by analytical considerations. It represents an interesting model due to several facets:

❏ The TARAP may exist in a homogeneous high flow phase and a condensed low flow phase. The phase space, spanned by $\tilde{\Delta}$, is divided twofoldly: for $\tilde{\Delta} > 1$ only the high flow phase occurs, whereas in the other regime ergodicity is broken and the system resides either in the high or the low flow phase. Although condensation effects and ergodicity breaking in nonsymmetric substates have been observed in several stochastic models, it is remarkable that they occur simultaneously here. In section 5.6 we have argued that the high flow phase coexists with the low flow phase due to continuous state space. However, this question has to be studied into detail in the future.

❏ The interesting phase space behaviour is achieved in a closed system with translation invariant dynamics. Furthermore, the model deals with one particle species only.

❏ A simplified version of the KRAUSS traffic model can be represented as an ARAP

with a dynamics very similar to that of the TARAP. This confirms the recently published assumption [16] that the KRAUSS model would offer a density regime with both stable low flow and stable high flow.

❏ A simplified version of the TARAP has been successfully studied by using an $\mathcal{M}$-approximant instead. So our analytical work in chapter 4 comes directly into operation.

However, there are some points for further work. First it would be interesting to solve the mean field equation of the TARAP exactly. This could give information about the transition point $\tilde{\Delta}_c$ and the asymptotic behaviour of the mass distributions. So far the introduction of the rescaled cutoff and the derivation of the transition point $\tilde{\Delta}_c = 1$ base on approximative calculations and numerics only. Furthermore, the analytical lifetime estimations have to be improved. It would also be interesting to enhance the considerations to related systems, e.g. equipped with different updates or given by symmetric dynamics.

Finally, the influence of continuous state spaces has to be clarified. This problem is not TARAP specific, but of general interest in stochastic processes. We know from other fields of physics, e.g. quantum field theory, that continuous systems offer more freedoms than discrete ones. By discretizing continuous theories we loose some information that we cannot get back by performing continuous limits. But in case of the ARAP we should formulate the problem vice versa: which phenomena incorporated in continuous models cannot be found in discrete systems?

So the ARAP still seems to hold some interesting properties.

A. Appendices

A.1. $\phi(r) = \delta(r - R)$ with Continuous Dynamics

Here we would like to enhance our calculations for the state-independent fraction density (4.80) in the random sequential update limit $p \to 0$. Initial point is the mean field equation (4.80) which is exactly solveable for $\bar{R} \equiv \frac{1}{2}$, see (4.82) - although the result does not represent an exact solution. In the following we denote the R-dependence of the solutions explicitly, so $Q(s) \to Q(R, s)$. The underlying idea is a TAYLOR expansion in the model parameter R, i.e. we apply[1]

$$Q(R, s) = \sum_n \frac{1}{n!} \left(\partial_1^n Q\right) \left(\bar{R}, s\right) (R - \bar{R})^n . \tag{A.1}$$

For small deviations around $\bar{R}$ we neglect quadratic contributions. $Q(\bar{R}, s)$ has been already determined (4.82), so we only focus on the calculation of $(\partial_1 Q) \left(\bar{R}, s\right)$. We start by partial derivation of (4.80) according to R and derive for $R = \bar{R}$

$$\left[Q(\bar{R}, \bar{R}s) - 2\right] (\partial_1 Q)(\bar{R}, s) + \left[Q(\bar{R}, s) + 1\right] (\partial_1 Q)(\bar{R}, \bar{R}s) + s \left[Q(\bar{R}, s) - 1\right] (\partial_2 Q)(\bar{R}, \bar{R}s) = 0. \tag{A.2}$$

By use of[2] $(\partial_2 Q) \left(\bar{R}, s\right) = -\rho(1 + \rho s)^{-2}$ the result

$$\begin{aligned}
(\partial_1 Q)(\bar{R}, s) &= \frac{1}{2} \left(\frac{2 + \rho s}{1 + \rho s}\right)^2 (\partial_1 Q) \left(\bar{R}, \frac{s}{2}\right) + \frac{s(3 - \rho s)}{8(1 + \rho s)^2 (2 + \rho s)} \\
&\equiv \mu(s)(\partial_1 Q) \left(\bar{R}, \frac{s}{2}\right) + \nu(s)
\end{aligned} \tag{A.3}$$

is obtained. For $s = 0$ we obtain $(\partial_1 Q) \left(\bar{R}, 0\right) = 0$ which is in accordance with $Q(\bar{R}, 0) = 1$. Finally, the general but formal solution of (A.3)

$$(\partial_1 Q)(\bar{R}, s) = \sum_{n=0}^{\infty} \nu \left(\frac{s}{2^n}\right) \prod_{k=0}^{n-1} \mu \left(\frac{s}{2^k}\right) \tag{A.4}$$

is constructed via reinserting.

---

[1]We write $(\partial_i Q)$ for a partial derivative according to the ith argument instead of $(\partial_R Q)$ or $(\partial_s Q)$. By this we avoid terms like $\partial_R Q(R, Rs)$.

[2]We assume Q to be a $\mathcal{C}^\infty$ function, so the relation $\frac{\mathrm{d}}{\mathrm{d}s} \left[Q(\bar{R}, s)\right] = (\partial_1 Q)(\bar{R}, s)$ holds.

A.2. Calculation of the Partition Sum Z

We present a proof of the relation

$$Z(\lambda, L, \rho, M) \equiv \int_{F_L(M)} d^L m \prod_{i=1}^{L} P_\lambda^\rho(m_i) = \frac{1}{M\,\Gamma(\lambda L)} \left(\lambda \frac{M}{\rho}\right)^{\lambda L} e^{-\lambda \frac{M}{\rho}}. \tag{A.5}$$

The superscript in P_λ^ρ reminds of the ρ dependence. The following lines use the FOURIER representation of the δ-function and the relation between (4.41) and (4.42), i.e. the principles of LAPLACE transformation:

$$
\begin{aligned}
Z(\lambda, L, \rho, M) &= \int_0^\infty d^L m \prod_j P_\lambda^\rho(m_j)\delta\!\left(M - \sum_j m_j\right) \\
&= \frac{1}{2\pi} \int_{-\infty}^\infty dp\, e^{ipM} \prod_j Q_\lambda^\rho(ip) \\
&= \frac{1}{2\pi} \int_{-\infty}^\infty dp\, e^{ipM} Q_{\lambda L}^{\rho L}(ip) \\
&\overset{s=ip}{=} P_{\lambda L}^{\rho L}(M)
\end{aligned}
$$

So the r.h.s. of (A.5) is nothing else than a single site mass density (4.42) at M that is rescaled according to $\rho \to \rho L$ and $\lambda \to \lambda L$.

A.3. N-Stick Approximation

We assume a state given by a sharp mass distribution supporting N_+ sticks of mass m_+ and $N_- = L - N_+$ sticks of mass m_-. From mass conservation $N_+ m_+ + N_- m_- = \rho L$ and the continuity equation $m_+ m_- = \Delta^2$ (see section 5.4.1 for a brief derivation) we obtain

$$m_\pm = \frac{\rho L}{2 N_\pm}(1 \pm \xi) \quad \text{with} \quad \xi = \sqrt{1 - \frac{N_+ N_-}{L}\left(\frac{\tilde{\Delta}}{\rho}\right)^2} \tag{A.6}$$

For the assumption $m_+ > m_-$ a further condition is derived after some fundamental calculus: system states with N_+ sticks exist if and only if

$$\tilde{\Delta} \leqslant \begin{cases} \left(\frac{L}{N_+ N_-}\right)^{\frac{1}{2}} \rho & \text{for } \frac{N_+}{L} \in \left[0, \frac{1}{2}\right] \\ 2 L^{-\frac{1}{2}} \rho & \text{for } \frac{N_+}{L} \in \left[\frac{1}{2}, 1\right] \end{cases} . \tag{A.7}$$

So in the thermodynamic limit only configurations with a finite number N_+ lead to a nonzero upper bound for the rescaled cutoff[3] given by

$$\tilde{\Delta}_c = N_+^{-\frac{1}{2}} \rho . \tag{A.8}$$

According to (5.18) the current is given by

$$J_{\text{low}} = \frac{1}{2} m_- = \frac{1}{4} \rho \left\{ 1 - \sqrt{1 - \left(\frac{\tilde{\Delta}}{\tilde{\Delta}_c}\right)^2} \right\} \tag{A.9}$$

in the N-stick approximation for $L \to \infty$.

---

[3]In the limit $L \to \infty$ nonzero mega stick densities $\frac{N_+}{L}$ yield $\tilde{\Delta} = 0$.

A.4. Calculation of τ_{low}

Origin of the forthcoming calculations is the evolution equation (5.24). While we have neglected the inflow term in section 5.4.3, now the ansatz

$$J(m_-(t)) = \gamma = \text{constant} \tag{A.10}$$

is made. Here we choose $\gamma = J(m_-)$ with m_- defined as in (5.21) because the assumption that $L - 1$ sticks of height m_- are placed in front of a mega stick, shifting half of their mass per update step (5.18), yields a constant inflow γ for at least $L - 1$ timesteps (see also appendix A.5). So by $\sigma = \frac{1}{2}\Delta^2$ and introducing the continuous time derivative as done in 5.4.3, the ODE

$$\dot{m}_+(t) = \gamma - \sigma m_+^{-1}(t) \tag{A.11}$$

is constructed. For constant $m_+(t) = \frac{\sigma}{\gamma} = m_+$, see (5.21) for a definition, the system is stable. Here we are interested in the case $m_+(0) < \frac{\sigma}{\gamma}$ resulting in a complete reduction. From (A.11) we get (by integration) the time $t(m_+(0))$ associated with the total annihilation (to zero) of an aggregate $m_+(0)$:

$$t(m_+(0)) = - \left[\frac{m_+(0)}{\gamma} + \frac{\sigma}{\gamma^2} \ln \left(1 - \frac{\gamma}{\sigma} m_+(0) \right) \right] . \tag{A.12}$$

However, this explicit formula entails an inconvenience because there is no criterion which initial value $m_+(0)$ to use (for $m_+(0) \to \frac{\sigma}{\gamma}$ the lifetime diverges). So the calculation of τ_{low} is divided into two parts: we determine the time τ_1 for transferring the primary brick and use (A.12) to determine τ_2 for the remaining condensate.

According to the ϕ-function of the TARAP (5.1) and (5.3) with respect to the property $m_+(0) > \Delta$ we see that mass is transferred with probability $\frac{\Delta}{m_+(0)}$. From this follows

$$\tau_1 = \frac{m_+(0)}{\Delta} = \frac{m_+}{\Delta} \tag{A.13}$$

whereby the inflow has been neglected. Note that this approach disrupts the sensitive random based interplay between in- and outflow leading to long lived low flow states. So a gross amount of time generally contributing to τ_{low} is lost by this approximative step.

The calculation of τ_2 is straightforward. By using $m_+(0) = m_+$ we obtain

$$\tau_2 = \frac{m_+}{\Delta} \int_0^{\frac{\Delta}{m_+}} t\left(m_+ - r m_+\right) \mathrm{d}r = \frac{m_+}{\Delta} + \left(\frac{m_+}{\Delta} \right)^2 \ln \left(\frac{m_+}{\Delta} \right)^2 . \tag{A.14}$$

Note that (A.14) is well defined although it contains contributions from $t(m_+(0))$ with $m_+(0) \to m_+$. Assuming $m_+ = \rho L$ yields for $L \gg 1$ the relation[4]

---

[4]Using m_+ as defined in (5.21) would yield even smaller lifetimes.

$$\tau_{\text{low}} \sim L^{\beta} \left(\frac{\rho}{\tilde{\Delta}} \right)^2 \ln \left(L^{\beta} \left(\frac{\rho}{\tilde{\Delta}} \right)^2 \right) \sim \tau_{\text{switch}} \ln \tau_{\text{switch}} \qquad (A.15)$$

with $\beta = 1$ and τ_{switch} given in (5.25).

A.5. Formation of Mega Sticks

In this chapter we present a simplified model to calculate the time for building up a mega stick. We assume the system to exist in the high flow state so all sites initially carry the weight $m_i(0) = \rho = 1$. Furthermore the average mass transfer per site is given by $\frac{1}{2}m_i(t)$. This can be seen from (5.18) by using $\rho \ll \Delta$ (which is valid here because Δ scales with $L^{\frac{1}{2}}$). In other words: the TARAP in the high flow state simply behaves like a free ARAP. We obtain the deterministic dynamics

$$m_{i+1}(t+1) = \frac{1}{2}m_i(t) + \frac{1}{2}m_{i+1}(t) \tag{A.16}$$

under which the periodic system is invariant. Now we consider the ARAP defined on a one sided closed lattice $\mathbb{N}_0$. Table A.1 gives a first impression of the dynamics: a shockwave propagates through the system. By extracting the geometric factor 2^{-t} the problem reduces to integer sequences $N(i,t)$. Consulting [59] gives a first guess and finally, we make the ansatz

$$m_i(t) = \frac{1}{2^t}N(i,t) \quad \text{with} \quad N(i,t) = \sum_{j=0}^{i}\binom{t}{j}. \tag{A.17}$$

It is easy to show by inserting that (A.17) fulfills (A.16). Furthermore (A.17) matches the boundary conditions $m_i(0) = 1$ and $m_0(t) = \frac{1}{2^t}$ which completes the proof. A few additional remarks:

- ❏ There is an alternative approach to obtain (A.17): the configurations in A.1 correspond to a superposition of PASCAL's triangles (rescaled by 2^{-t}). According to this the numbers $N(i,t)$ represent partial sums of binomial coefficients.

- ❏ The numbers $N(i,t)$ also represent the maximal number of regions which i dimensional space can be divided into by t hyperplanes [59]. For $i = 3$ this reduces to the so called "cake cutting" problem and the associated series is formed by the "cake numbers".

$t\backslash i$	0	1	2	3
0	1	1	1	1
1	$\frac{1}{2}$	1	1	1
2	$\frac{1}{4}$	$\frac{3}{4}$	1	1
3	$\frac{1}{8}$	$\frac{4}{8}$	$\frac{7}{8}$	1
4	$\frac{1}{16}$	$\frac{5}{16}$	$\frac{11}{16}$	$\frac{15}{16}$
5	$\frac{1}{32}$	$\frac{6}{32}$	$\frac{16}{32}$	$\frac{26}{32}$
6	$\frac{1}{64}$	$\frac{7}{64}$	$\frac{22}{64}$	$\frac{42}{64}$

Table A.1.: Configurations $m_k(t)$ for $k = 0, 1, 2, 3$ and $t = 0, \ldots, 6$.

❑ Although for $t \leqslant i$ the solution $N(i, t) = 2^t$ is derived and for small i explicit formulas can be given, there is no closed form for $t > i$ [60].

Now we assume the system to be finite, i.e. the mass is accumulated in the last site. This approximation is based on the fact that the average outflow shrinks if the level Δ is exceeded (5.18). Nevertheless the main amount of time is spent for reaching this level. So we neglect an essential mechanism stabilizing the high flow state. According to this our calculations lead to transition times rather than lifetimes, which also happened in section 5.4.3. So we obtain

$$m_{L-1}(t+1) = \frac{1}{2} m_{L-2}(t) + m_{L-1}(t) = 1 + \sum_{k=0}^{t} \sum_{j=0}^{L-2} \frac{1}{2^{k+1}} \binom{k}{j} . \qquad (A.18)$$

Finally, we derive by numerical evaluation of (A.18) that $m_{L-1}(t) \sim L$ is solved approximately by $t \sim L$.

B. Deutsche Zusammenfassungen

B.1. Kurze Zusammenfassung

In der vorliegenden Arbeit wird der „asymmetric random average process" (ARAP) untersucht. Dieses stochastische Modell ist auf einem eindimensionalen periodischen Gitter definiert. Seine Zustandsvariablen m_i, genannt Massen, sind unbeschränkt und kontinuierlich, d.h. $m_i \in \mathbb{R}_0^+$. Die lokale Dynamik transferiert zufällig ausgewählte Bruchteile r_i der Masse m_i auf Platz i nach rechts, wobei die Zufallsvariable r_i gemäß einer beliebigen Wahrscheinlichkeitsdichte ϕ bestimmt wird.

Wir beginnen mit einer formalen Definition des ARAPs und zeigen, dass viele stochastische Modelle durch die Wahl einer geeigneten ϕ-Funktion als ARAP interpretiert werden können.

Ferner wird gezeigt, dass der ARAP mit konstanter ϕ-Funktion und paralleler Dynamik mit Hilfe des Matrixprodukt-Ansatzes gelöst werden kann. Dies stellt eine Erweiterung des Anwendungsspektrums dieser erfolgreichen Methode auf Systeme mit unbeschränkten diskreten und unbeschränkten kontinuierlichen Zustandsvariablen dar. Im Falle kontinuierlicher Massen erhalten wir eine ungewöhnliche Matrixalgebra, die durch eine Integralgleichung mit zwei zu bestimmenden Funktionen gegeben ist.

Des weiteren bestimmen wir analytisch die Menge aller ARAPs, deren Massenverteilungen faktorisieren. Dabei beschränken wir uns auf ϕ-Funktionen, die nicht vom aktuellen Zustand des Systems abhängen, also $\phi = \phi(r_i)$. Wir übertragen unsere Ergebnisse auf endliche Systeme und Systeme mit kontinuierlicher Dynamik. Auch die Verbindung zum q-Modell wird genauer untersucht und eine Approximationsmethode zur Bestimmung von Massenverteilung für beliebige ARAPs vorgestellt.

Schließlich wird der trunkierte ARAP (TARAP) eingeführt, dessen Massentransfer durch einen Cutoff begrenzt ist. Mit Hilfe von Monte-Carlo Simulationen und analytischen Näherungen leiten wir das Phasendiagramm her. In diesem tritt eine Phase auf, in der die Ergodizität des Systems gebrochen ist: der TARAP befindet sich entweder in einer translationsinvarianten Hochflussphase oder in einer Phase, in der ein nichtverschwindender Bruchteil der Gesamtmasse auf genau einem Gitterplatz fixiert ist – vergleichbar mit dem Effekt der BOSE-EINSTEIN Kondensation. Wir entschlüsseln die Verbindung zum Verkehrsmodell von KRAUSS und präsentieren abschließend einen Vergleich mit anderen Modellen, die ein dem TARAP ähnliches Verhalten aufweisen.

B.2. Ausführliche Zusammenfassung

Das Studium des Nichtgleichgewichts (NGG) hat sich in der modernen statistischen Physik zu einem attraktiven und wichtigen Forschungszweig entwickelt. Insbesondere interdisziplinäre Probleme basieren häufig auf NGG-Prozessen, wie die Proteinsynthese in biologischen Systemen, die Modellierung des Straßenverkehrs, Diffusionsprozesse in Polymernetzwerken oder das Oberflächenwachstum von Kristallen. Aber es gibt auch physikalische Anwendungen, die auf NGG-Dynamiken beruhen, z.B. das Relaxationsverhalten von Spin-Gläsern oder dissipativer Transport in dünnen supraleitenden Drähten.

Für Systeme im thermischen Gleichgewicht existiert eine abgeschlossene Theorie, die sowohl im Fall klassischer als auch quantenmechanischer Prozesse greift. Solange man in der Lage ist, den Hamiltonian eines Problems zu formulieren, kann zumindest formal das BOLTZMANN-Gewicht einer jeden Systemkonfiguration, also der Gleichgewichtszustand, angegeben werden. NGG-Prozesse hingegen lassen sich im Allgemeinen nicht in Form hermitescher HAMILTON-Funktionen oder -Operatoren beschreiben, sondern sind stattdessen durch eine mikroskopische Dynamik definiert. Dies bedeutet nicht, dass die NGG-Physik die Gesetze NEWTONs oder der Quantenmechanik verletzt. Aufgrund fehlender Informationen über die zugrunde liegenden physikalischen Abläufe werden die NGG-Modelle jedoch häufig auf phänomenologischer Basis erstellt, sind weniger restriktiv und im Allgemeinen zufallsbasiert.

Generell kann man zwei Arten von NGG-Prozessen unterscheiden: Systeme, die in das thermische Gleichgewicht relaxieren und Systeme fernab vom thermischen Gleichgewicht, die z.B. durch ein externes Feld daran gehindert werden, den Gleichgewichtszustand anzunehmen. Der Fokus der vorliegenden Arbeit liegt auf Modellen, die zur zweiten Klasse gehören. Sie sind dadurch ausgezeichnet, dass ihre mikroskopische Dynamik nicht den Bedingungen des detaillierten Gleichgewichts genügt.

In den letzten Jahrzehnten wurden im Bereich der NGG-Physik wesentliche Fortschritte erzielt. Mit dem „asymmetric simple exclusion process" (ASEP) wurde ein sehr flexibles und dennoch einfaches Standardmodell eingeführt. Viele Methoden aus der Gleichgewichtsphysik, insbesondere für eindimensionale Quantenspin-Systeme, wurden auf dieses Modell und seine Varianten übertragen, wie der Quantenformalismus, der BETHE-Ansatz oder der Matrixprodukt-Ansatz. Nichtsdestotrotz befinden wir uns im Falle von Systemen fernab vom Gleichgewicht auch noch fernab einer wohl elaborierten Theorie, was nicht zuletzt daran liegt, dass NGG-Systeme ein viel größeres Spektrum an Phänomenen bieten als klassische oder Quantensysteme gleicher Dimension. Des weiteren existieren aufgrund des breiten Anwendungsgebietes eine Vielzahl von NGG-Modellen, die erst einmal für sich verstanden werden müssen, bevor man grundlegende Gemeinsamkeiten herausarbeiten kann.

Die meisten Modelle der NGG sind eng verwandt mit dem ASEP. Dieser stellt ein getriebenes stochastisches System dar, das auf einem eindimensionalen Gitter definiert ist. Die Gitterplätze können frei oder von genau einem Teilchen besetzt sein. Der ASEP is somit diskret im Ortsraum und in seinen Zustandsvariablen. Des weiteren ist sein

lokaler Zustandsraum {leer,besetzt} beschränkt. Diese Eigenschaften sind den meisten Modellen zu Eigen.

In der vorliegenden Arbeit wollen wir uns aus diesem Grund mit einer Modellklasse beschäftigen, die zwar immer noch auf einem Gitter definiert ist, deren Zustandsvariablen jedoch kontinuierlich und unbeschränkt sind, d.h. $m_i \in \mathbb{R}_0^+$ (wobei i den Gitterplatz beschreibt). Im Folgenden bezeichnen wir die Zustandsvariablen auch als Massen. Des weiteren sei eine stochastische lokale Nächste-Nachbar-Wechselwirkung gegeben, die zufällig bestimme Bruchteile r_i einer Masse nach rechts transferiert. Hierbei werde die Zufallsvariable r_i gemäß einer Wahrscheinlichkeitsdichte ϕ bestimmt. Dieses Modell ist in der Literatur auch bekannt als „asymmetric random average process" (ARAP).

In dieser Arbeit konzentrieren wir uns auf zwei wesentliche Aspekte. Zum einen erarbeiten wir allgemeine Eigenschaften des ARAPs für beliebige ϕ-Funktionen, um das fundamentale Verständnis für stochastische Systeme mit kontinuierlichen Zustandsvariablen zu vertiefen. Zum anderen konzentrieren wir uns auf ARAPs mit speziellen ϕ-Funktionen, die interessantes physikalisches Verhalten zeigen, das in diskreten Systemen bisher nicht beobachtet wurde.

Wir beginnen mit einer formalen und umfassenden Definition des ARAPs. Diese beinhaltet die Master-Gleichungen für diskrete (parallele Dynamik) und kontinuierliche Zeiten. Es wird auch der ARAP mit diskreten Zustandsvariablen, d.h. $m_i \in \mathbb{N}_0$, abgeleitet. Des weiteren wird gezeigt, dass viele Modelle aus dem Bereich der getriebenen NGG-Systeme nichts anderes sind als ARAPs oder zumindest auf diese projiziert werden können. So formulieren wir das q-Modell aus dem Bereich der granularen Materie, das Verkehrsmodell von KRAUSS und einige diskrete Systeme wie den ASEP exemplarisch im Gewande des ARAPs. Damit unterstreichen wir auch die praktische Relevanz dieser Modellklasse für die Physik.

Kurz zeigen wir, dass der ARAP mit konstanter ϕ-Funktion und paralleler Dynamik mit Hilfe des Matrixprodukt-Ansatzes gelöst werden kann. Dies stellt eine Erweiterung des Anwendungsspektrums dieser erfolgreichen Methode auf Systeme mit unbeschränkten diskreten bzw. kontinuierlichen Zustandsvariablen dar. Im Falle diskreter Massen erhalten wir eine „Algebra" mit unendlich vielen algebraischen Objekten und Bedingungen, während wir im kontinuierlichen Fall genau eine Integralgleichung mit zwei zu bestimmenden Funktionen erhalten. In beiden Fällen ist ein mean field-Ansatz exakt und die Darstellungen der Objekte bzw. Funktionen sind somit eindimensional.

In ARAPs mit beliebigen ϕ-Funktionen, die nicht vom aktuellen Zustand des Systems abhängen, also $\phi = \phi(r_i)$, verschwinden bei paralleler Dynamik im thermodynamischen Limes alle Massenkorrelationen. Im Falle symmetrischer ϕ-Funktionen, d.h. $\phi(r_i) = \phi(1 - r_i)$, faktorisieren gar die 3-Punkt Massenmomente. Folglich stellen mean field-Approximationen sehr gute Näherungen im ARAP dar. Aus diesem Grunde haben wir analytisch die Menge $\mathcal{M}$ aller $\phi(r)$ bestimmt, deren assoziierte Massenverteilungen faktorisieren. Es zeigt sich, dass $\mathcal{M}$ ein breites Spektrum von ϕ-Funktionen abdeckt. Somit bildet die Menge der ARAPs mit exakten Produktzuständen eine repräsentative Untermenge im Raum der ARAPs mit beliebigen ϕ-Funktionen. Basierend auf dieser

Eigenschaft konstruieren wir eine Approximationsmethode zur Bestimmung von Massenverteilung für beliebige ARAPs. Des weiteren übertragen wir unsere Ergebnisse auf endliche Systeme und Systeme mit kontinuierlicher Dynamik. Auch die Verbindung zum q-Modell wird genauer untersucht.

Wir konzentrieren uns aber auch, wie oben erwähnt, auf einen speziellen ARAP. Basierend auf Überlegungen zum Transport im Internet und Straßenverkehr konstruieren wir einen trunkierten ARAP (TARAP). Er ist dadurch ausgezeichnet, dass Massentransfers, die eine bestimmte Obergrenze, den Cutoff, überschreiten, zurückgewiesen werden. Mit Hilfe von Monte-Carlo Simulationen und analytischen Näherungen leiten wir das Phasendiagramm her. In diesem tritt eine Phase auf, in der die Ergodizität des Systems gebrochen ist: der TARAP befindet sich somit entweder in einer translationsinvarianten Hochflussphase, die sich approximativ durch einen Produktzustand beschreiben lässt, oder in einer Niedrigflussphase, in der ein nichtverschwindender Bruchteil der Gesamtmasse (auch im thermodynamischen Limes) auf genau einem Gitterplatz fixiert ist – vergleichbar mit dem Effekt der BOSE-EINSTEIN Kondensation. Basierend auf dieser Erkenntnis gelingt es auch, einige Ergebnisse, die im Rahmen des Verkehrsmodells von KRAUSS formuliert wurden, zu bestätigen. Abschließend präsentieren wir einen Vergleich mit anderen Modellen, die ein dem TARAP ähnliches Verhalten aufweisen.

Bibliography

[1] J. Krug and J. Garcia. Asymmetric particle systems on $\mathbb{R}$. *J. Stat. Phys.*, 99:31–55, 2000.

[2] R. Rajesh and S.N. Majumdar. Conserved mass models and particle systems in one dimension. *J. Stat. Phys.*, 99:943–965, 2000.

[3] F.C. Alcaraz, M. Droz, M. Henkel, and V. Rittenberg. Reaction-diffusion processes, critical dynamics, and quantum chains. *Ann. Phys.*, 230:250, 1994.

[4] J. Keizer. *Statistical Thermodynamics of Nonequilibrium Processes.* Springer-Verlag, 1987.

[5] J. Krug. Boundary-induced phase transitions in driven diffusive systems. *Phys. Rev. Lett.*, 67:1882, 1991.

[6] N. Rajewsky, L. Santen, A. Schadschneider, and M. Schreckenberg. The asymmetric exclusion process: Comparison of update procedures. *J. Stat. Phys.*, page 151, 1998.

[7] C.-H. Liu, S.R. Nagel, D.A. Schecter, S.N. Coppersmith, S. Majumdar, O. Narayan, and T.A. Witten. Force fluctuations in bead packs. *Science*, 269:513, 1995.

[8] S.N. Coppersmith, C.-H. Liu, S. Majumdar, O. Narayan, and T.A. Witten. Model for force fluctuations in bead packs. *Phys. Rev. E*, 53:4673, 1996.

[9] J.H. Snoeijer and J.M.J. van Leeuwen. Force correlations in the q-model for general q-distributions. cond-mat/0202120.

[10] R. Rajesh and S.N. Majumdar. Exact calculation of the spatiotemporal correlations in the takayasu model and in the q model of force fluctuations in bead packs. *Phys. Rev. E*, 62:3186, 2000.

[11] J.H. Snoeijer and J.M.J. van Leeuwen. Force relaxation in the q model for granular media. cond-mat/0110230.

[12] D. Chowdhury, L. Santen, and A. Schadschneider. Statistical physics of vehicular traffic and some related systems. *Phys. Rep.*, 329:199, 2000.

[13] K. Nagel and M. Schreckenberg. A cellular automaton model for freeway traffic. *J. Physique I*, 2:2221, 1992.

[14] S. Krauss, P. Wagner, and C. Gawron. Continuous limit of the nagel-schreckenberg model. *Phys. Rev. E*, 54:3707, 1996.

[15] S. Krauß. *Microscopic Modeling of Traffic Flow: Investigation of Collision Free Vehicle Dynamics*. PhD thesis, Universität zu Köln, 1998.

[16] K. Nagel, C. Kayatz, and P. Wagner. Breakdown and recovery in traffic flow models. In Y. Sugiyama et al., editor, *Traffic and Granular Flow '01*. Springer, 2002.

[17] S.N. Majumdar, S. Krishnamurthy, and M. Barma. Nonequilibrium phase transition in models of aggregation, adsorption, and dissociation. *Phys. Rev. Lett.*, 81:3691, 1998.

[18] S.N. Majumdar, S. Krishnamurthy, and M. Barma. Nonequilibrium phase transition in a model of diffusion, aggregation and fragmentation. *J. Stat. Phys.*, 99:1, 2000.

[19] R. Rajesh and S.N. Majumdar. Exact phase diagram of a model with aggregation and chipping. *Phys. Rev. E*, 63:036114–1, 2001.

[20] F. Spitzer. Interaction of markov processes. *Advances in Math.*, 5:246, 1970.

[21] M.R. Evans. Phase transitions in one-dimensional nonequilibrium systems. *Braz. J. Phys.*, 30:42, 2000.

[22] M.R. Evans. Exact steady states of disordered hopping particle models with parallel and ordered sequential dynamics. *J. Phys. A*, 30:5669, 1997.

[23] T.M. Liggett. *Interacting Particle Systems*. Springer-Verlag, New York, 1985.

[24] B. Derrida and M.R. Evans. The asymmetric exclusion model: exact results through a matrix product approach. In Vladimir Privman, editor, *Nonequilibrium Statistical Mechanics in One Dimension*, page 277. Cambridge University Press, 1997.

[25] M.R. Evans, D.P. Foster, C. Godrèche, and D. Mukamel. Spontaneous symmetry breaking in a one dimensional driven diffusive system. *Phys. Rev. Lett.*, 74:208, 1995.

[26] B. Derrida, M.R. Evans, V. Hakim, and V. Pasquier. Exact solution of a 1d asymmetric exclusion model using a matrix formulation. *J. Phys. A*, 26:1493, 1993.

[27] G.M. Schütz. Exact solution of the master equation for the asymmetric exclusion process. *J. Stat. Phys.*, 88:427, 1997.

[28] G.M. Schütz. Exact tracer diffusion coefficient in the asymmetric random average process. *J. Stat. Phys.*, 99:1045–1049, 2000.

[29] R. Rajesh and S.N. Majumdar. Exact tagged particle correlations in the random average process. *Phys. Rev. E*, 64:036103, 2001.

[30] A. Klümper, A. Schadschneider, and J. Zittartz. Equivalence and solution of anisotropic spin-1 models and generalized t-j fermion models in one dimension. *J. Phys. A*, 24:L955, 1991.

[31] A. Klümper, A. Schadschneider, and J. Zittartz. Groundstate properties of a generalized vbs-model. *Z. Phys. B*, 87:281, 1992.

[32] K. Klauck and A. Schadschneider. On the ubiquity of matrix-product states in one-dimensional stochastic processes with boundary interactions. *Physica A*, 271:102, 1999.

[33] H. Hinrichsen. Nonequilibrium critical phenomena and phase transitions into absorbing states. *Adv. Phys.*, 49:815, 2000.

[34] V. Karimipour. A multi-species asymmetric exclusion process, steady state and correlation functions on a periodic lattice. *Europhys. Lett.*, 47:304, 1999.

[35] A. Schadschneider. MPA for ASEP with parallel dynamics. unpublished.

[36] F. Zielen and A. Schadschneider. Exact mean-field solutions of the asymmetric random average process. *J. Stat. Phys.*, 106:173, 2002.

[37] F. Zielen and A. Schadschneider. Asymmetric random average process: Aggregation and fragmentation on continuous state space. In Y. Sugiyama et al., editor, *Traffic and Granular Flow '01*. Springer, 2002.

[38] H.S. Wilf. *generatingfunctionology*. Academic Press, Inc., 1990.

[39] M. Abramowitz and I. Stegun. *Handbook of Mathematical Functions*, chapter 13. New York: Dover, 1964.

[40] J. Zinn-Justin. *Quantum Field Theory and Critical Phenomena*, chapter 11, page 235. Clarendon Press, Oxford, 1996.

[41] F. Haussdorf. Summationsmethoden und Momentfolgen. I. and II. *Math. Z.*, 9:74 and 288, 1921.

[42] D.D. Ang, R. Gorenflo, and D.D. Trong. A multi-dimensional haussdorff moment problem: Regularization by finite moments. *Journal for Analysis and its Applications*, 18:13, 1999.

[43] M.-D. Choi. Tricks or treats with the hilbert matrix. *Amer. Math. Monthly*, 90:301, 1983.

[44] P.F. Arndt, T. Heinzel, and V. Rittenberg. Spontaneous breaking of translational invariance and spatial condensation in stationary states on a ring. I. The neutral system. *J. Stat. Phys.*, 97:1, 1999.

[45] F. Zielen and A. Schadschneider. Nonsymmetric ergodicity breaking in a stochastic model on continuous state space. cond-mat/0112066.

[46] M. Takayasu, A.Y. Tretyakov, K. Fukuda, and H. Takayasu. Phase transition and 1/f noise in the internet packet transport. In Schreckenberg, M. and Wolf, D.E., editors, *Traffic and Granular Flow '97*. Springer.

[47] T. Huisinga, R. Barlovic, W. Knospe, A. Schadschneider, and M. Schreckenberg. A microscopic model for packet transport in the internet. *Physica A*, 294:249, 2001.

[48] O. Biham, A.A. Middleton, and D. Levine. Self organization and a dynamical transition in traffic flow models. *Phys. Rev. A*, 46:6124, 1992.

[49] D. Chowdhury and A. Schadschneider. Self organisation of traffic jams in cities: effects of stochastic dynamics and signal periods. *Phys. Rev. E*, 59:1311, 1999.

[50] M.R. Evans and R.A. Blythe. Nonequilibrium dynamics in low dimensional systems. Preparatory notes, International Summer School, Fundamental Problems in Statistical Physics X, Altenberg, Germany, 2001.

[51] N.G. van Kampen. *Stochastic Processes in Physics and Chemistry*. Elsevier, 1992.

[52] G.M. Schütz. Exactly solvable models for many-body systems far from equilibrium. In C. Domb and J. Lebowitz, editors, *Phase Transitions and Critical Phenomena*, volume 19. Academic Press, Inc., 2000.

[53] W. Nolting. *Grundkurs: Theoretische Physik*, volume 6. Verlag Zimmermann-Neufang, 1994.

[54] J. Krug and P.A. Ferrari. Phase transitions in diffusive systems with random rates. *J. Phys. A*, 29:465, 1996.

[55] O.J. O'Loan, M.R. Evans, and M.E. Cates. Jamming transition in a homogeneous one-dimensional system: The bus route model. *Phys. Rev. E*, 58:1404, 1998.

[56] J.M.J. van Leeuwen and H.J. Hilhorst. *Physica (Amsterdam)*, 107A:319, 1981.

[57] M.R. Evans, D.P. Foster, C. Godrèche, and D.Mukamel. Asymetric exclusion model with two species: Spontaneous symmetry breaking. *J. Stat. Phys.*, 80:69, 1995.

[58] O.J. O'Loan and M.R. Evans. Alternating steady state in one-dimensional flocking. *J. Phys. A*, 32:L99, 1999.

[59] AT&T Integer Sequences Research. The on-line encyclopedia of integer sequences. http://www.research.att.com/~njas/sequences/index.html.

[60] R.L. Graham, D.E. Knuth, and O. Patashnik. *Concrete Mathematics: a foundation for computer science*, chapter 5, page 165. Addison-Wesley Publishing Company, 1990.

Erklärung

Ich versichere, daß ich die von mir vorgelegte Dissertation selbständig angefertigt, die benutzten Quellen und Hilfsmittel vollständig angegeben und die Stellen der Arbeit – einschließlich Tabellen, Karten und Abbildungen –, die anderen Werken im Wortlaut oder dem Sinn nach entnommen sind, in jedem Einzelfall als Entlehnung kenntlich gemacht habe; daß diese Dissertation noch keiner anderen Fakultät oder Universität zur Prüfung vorgelegen hat; daß sie – abgesehen von unten angegebenen Teilpublikationen – noch nicht veröffentlicht worden ist sowie, daß ich eine solche Veröffentlichung vor Abschluß des Promotionsverfahrens nicht vornehmen werde. Die Bestimmungen dieser Promotionsordnung sind mir bekannt. Die von mir vorgelegte Dissertation ist von Herrn Priv.-Doz. Dr. A. Schadschneider betreut worden.

Köln, den 17. Mai 2002

Teilpublikationen:

F. Zielen, A. Schadschneider, *Exact Mean-Field Solutions of the Asymmetric Random Average Process*, J. Stat. Phys. **106**, Seite 173 (2002)

F. Zielen, A. Schadschneider, *Asymmetric Random Average Process: Aggregation and Fragmentation on Continuous State Space*, akzeptiert für die Veröffentlichung in Traffic and Granular Flow '01, Herausgeber Y. Sugiyama et al. (Springer Verlag)

F. Zielen, A. Schadschneider, *Nonsymmetric Ergodicity Breaking in a Stochastic Model on Continuous State Space*, erschienen als e-print cond-mat/0112066

Danke!

Lebenslauf

Persönliche Daten

Name:	Frank Zielen
Geburtsdatum:	1. April 1973
Geburtsort:	Oelde
Familienstand:	ledig
Staatsangehörigkeit:	deutsch
Adresse:	Wiesenstr. 20
	59302 Oelde

Schulbildung und Zivildienst

1979 – 1983	Karl-Wagenfeld-Grundschule in Stromberg
1983 – 1992	Priv. Gymnasium Johanneum Wadersloh
1992 – 1993	Zivildienst im Marienhospital Oelde

Hochschulstudium und Promotion

10/1993	Studium der Physik an der Westfälischen Wilhelms-Universität Münster
10/1995	Vordiplom in Physik
04/1997 – 10/1998	Diplomarbeit am Institut für Theoretische Physik der Westfälischen Wilhelms-Universität Münster über die „Rigorose und Perturbative Konstruktion von ϕ^4-Trajektorien"
11/1998	Diplom in Physik
seit 03/2000	Doktorarbeit am Institut für Theoretische Physik der Universität zu Köln über „Asymmetric Random Average Processes"

Arbeitsverhältnisse

04/1997 – 10/1998	Studentische Hilfskraft am Mathematischen Institut der Westfälischen Wilhelms-Universität Münster
01/1999 – 02/2000	Berater für strategische Unternehmensfragen bei Deloitte Consulting Germany
seit 03/2000	Wissenschaftlicher Mitarbeiter am Institut für Theoretische Physik der Universität zu Köln